EVALUATION OF AN ELASTOMER CUSHION

FOR TOTAL KNEE REPLACEMENT

TO MY PARENTS

MECHANICAL EVALUATION OF AN ELASTOMER

CUSHION FOR TOTAL KNEE REPLACEMENT

By

BRIAN P. KELLY, B.ENG.

A Thesis

Submitted to the School of Graduate Studies

in Partial Fulfilment of the Requirements

for the Degree

Master of Engineering

McMaster University

MASTER OF ENGINEERING (1992)
(Mechanical)

MCMASTER UNIVERSITY
Hamilton, Ontario

TITLE: Mechanical Evaluation of an Elastomeric Cushion For Total Knee Replacement

AUTHOR: Brian P. Kelly, B.Eng (McMaster University)

SUPERVISORS: Prof. W. R. Newcombe

Dr. R. U. Repo

NUMBER OF PAGES: xii, 207

ABSTRACT

Mechanical factors have been cited as a primary cause of total knee replacement failure. A hypothesis has been formulated stating that the introduction of a compliant interface into a total knee prosthesis would moderate excessive stresses and strains, thereby, extending joint life. A biocompatable elastomer developed by the Dow Corning Corporation was selected for mechanical evaluation as a cushioning material. Force-strain, impact, and fatigue tests were conducted on several specially designed and fabricated elastomer test shapes.

Test results demonstrate that a suitably stiff and dynamically responsive elastomer cushion can be designed to handle repeated physiological knee joint loads. Physiological impacts with cadaver tibias demonstrated significant shock reduction benefits, including peak force reductions of up to 70%, with the addition of different elastomer shapes. Compressive fatigue evaluation of elastomer samples was inconclusive owing to extensive sample wear. As a result configurations or applications where the elastomer can move relative to a rigid surface are not recommended. A new, mechanically contained elastomer shape was designed and tested which greatly reduced wear. Bonding of this new shape to prosthetic joint materials is recommended for further experimental evaluation.

ACKNOWLEDGEMENTS

I would like to express my appreciation to Professor W.R. Newcombe and to Dr. R.U. Repo for their time, patience and guidance throughout the course of this study.

Special thanks are extended to IBM Canada for donating use of their shock test laboratory. I would especially like to thank R.G. Gibson of the packaging engineering department for his generous donation of time and expertise towards the shock testing portion of this study.

I would like to thank the staff and technicians of the Mechanical Engineering department at McMaster for their invaluable advice and assistance.

I would also like to thank my fellow graduate students whose continued friendship and advice have contributed greatly to this work.

Last but not least, I would like to thank my parents for their unconditional support throughout my entire education.

TABLE OF CONTENTS

LIST OF FIGURES

LIST OF TABLES

CHAPTER ONE

INTRODUCTION

The surgical technique of total knee joint replacement using artificial components has been in practice for about 20 years. This technique has brought pain relief and restored joint function to thousands of individuals suffering from severe joint diseases. Intense and ongoing research has focused on improving function, durability, and longevity of artificial knee joints, as these implants remain undesirably limited in potential service life.

1.1 General Objective

The objective of the work described herein is based on the idea of introducing a compliant, shock absorbing interface between the rigid metal and polyethylene tibial components of a total knee replacement. It is believed that the improved distribution of forces and reduction of shock loads across the knee joint will greatly prolong artificial joint life.

The idea of introducing compliancy into prosthetic knee joints is not new. However, a novel approach has been undertaken in this study. Very little research has been conducted in this area, and the authors are aware of little published material addressing the introduction of compliant, biocompatible, elastomeric materials into prosthetic knee implants.

As the reader may not be familiar with the technique of total knee replacement, the remainder of this chapter provides some background information on knee joint anatomy, total knee arthroplasty, and its limitations.

1.2 Anatomy Of The Knee Joint

The knee joint is one of the most complex and highly loaded joints in the human body. Referring to figure 1.1, the two major bones which comprise this joint are the femur and the tibia. The ends of these long bones which meet to form the knee joint are enlarged, irregular shaped and composed of cancellous bone surrounded by a thin supporting shell of cortical bone. Cancellous bone* having a porous, three dimensional lattice structure, is a soft type of bone suited to distributing loads and absorbing energy, while cortical bone is much denser and harder providing compressive strength. The very distal end of the femur terminates with two irregular curved projections on either side known as the medial and lateral condyles. The proximal end of the tibia forms two relatively flat or level areas known as the tibial plateaux which are separated by a small raised area of bone. Load bearing capacity and articulating movement of the joint are provided by

---

* also referred to as subchondral or trabecular bone.

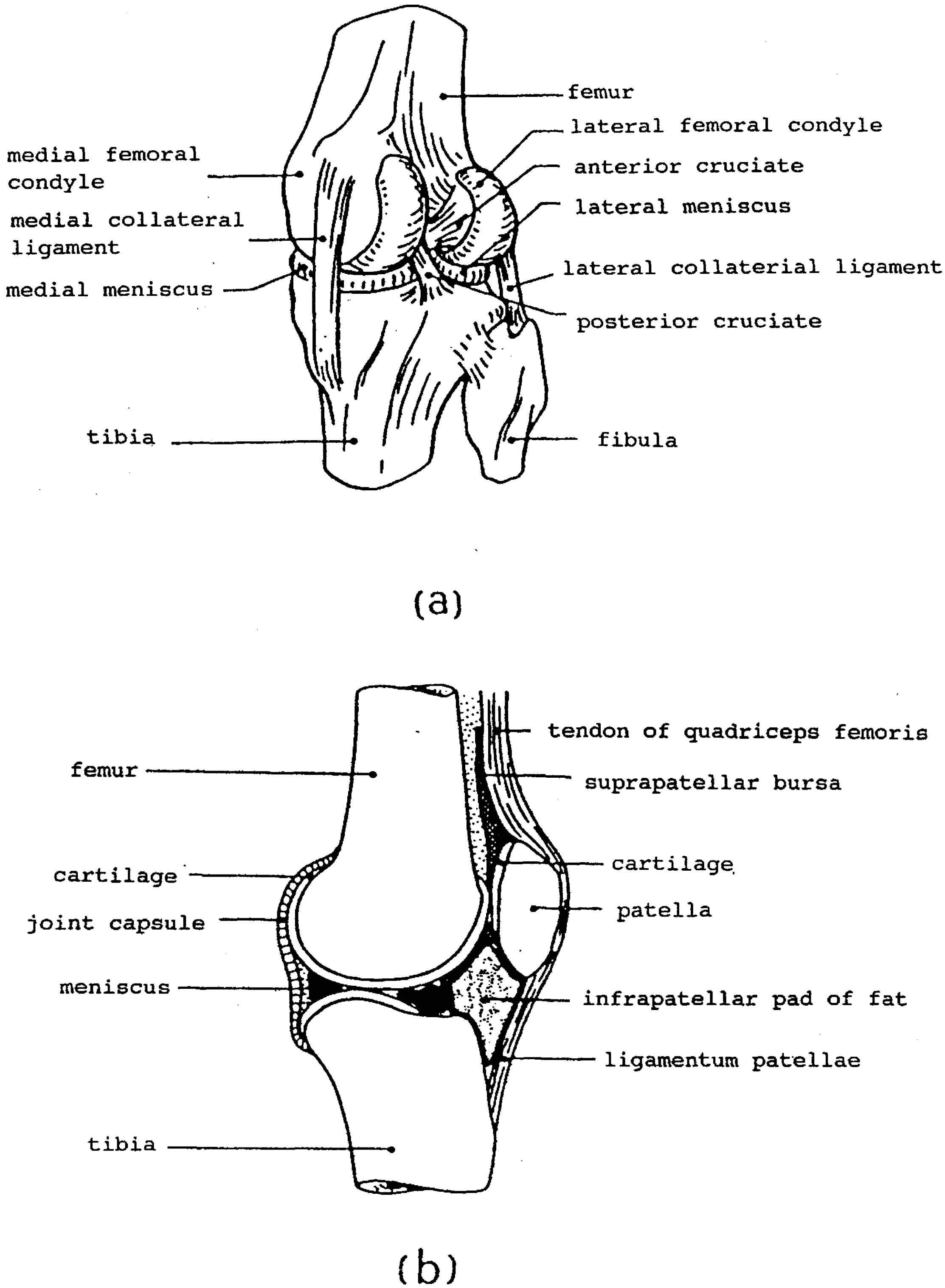

Figure 1.1 The human knee joint (a) viewed postero-medially without muscles, (b) viewed in a sagittal plane (from Biomechanics of Normal and Pathological Human Articulating Joints 1985).

the mating of the femoral condylar surfaces with the tibial plateaux.

The articulating surfaces of the knee joint are covered in a glossy rubber-like tissue called articular cartilage. Articular cartilage creates smooth and compliant contact surfaces on both the femur and the tibia preventing bone on bone contact. Interposing between the articulating surfaces are further soft tissue structures known as the menisci. On top of each tibial plateau a semicircular or c-shaped meniscus covers about two thirds of the surface area leaving the central region exposed. Each meniscus has a wedge shaped cross section being thicker at the outer edge where there is greatest incongruity. The menisci protect and fill joint space, and serve as load distributing agents, maintaining intimate contact between the femur and tibia. The tibia is directly attached to the femur by four other tissue structures known as ligaments which strongly resist tension. Two of these are located in the joint space between the femoral condyles and are called the cruciate ligaments. The other two, located externally on the medial and lateral sides, are known as the collateral ligaments. These tissue structures maintain normal joint movement stability and integrity by preventing the joint surfaces from shearing, separating and over rotating [1].

1.2.1 Knee Joint Pathology : Arthritis

While many types of injuries and diseases exist which can afflict articulating joints, by far the most prevalent cause of joint destruction is arthritis. Rheumatoid arthritis afflicts about one quarter of all arthritis patients and is the greatest crippler from a standpoint of severity and prolonged disability [4]. Rheumatoid arthritis characteristically causes inflammation which leads to pain, swelling and damage to supporting soft tissue structures of the joint. Osteoarthritis is present in one to two individuals out of three in any population over 35 years of age, and incapacitates approximately two to six people out of every thousand in the general population. In intermediate and late stages, osteoarthritis results in progressive destruction of articular cartilage leading to exposure of bone at a site where it will then be subject to possible bone on bone contact, abrasion and other damage [3].

Although arthritis has many sited clinical causes, the exact nature of its morphologic event is not understood and no cure exists. Arthritis is considered as the second greatest cause of chronic limitation of major activity following heart disease, and continues to be a major cause of pain, economic loss and social disadvantage.

1.3 Total Knee Arthroplasty

Following the development of total hip arthroplasty, total knee arthroplasty was first developed in the early 1970's. Using polyethylene and metal components bonded directly to bone with a hard cement known as polymethylmethacrylate, articulating surfaces of the knee joint can be replaced. Figure 1.2 shows a general schematic of an

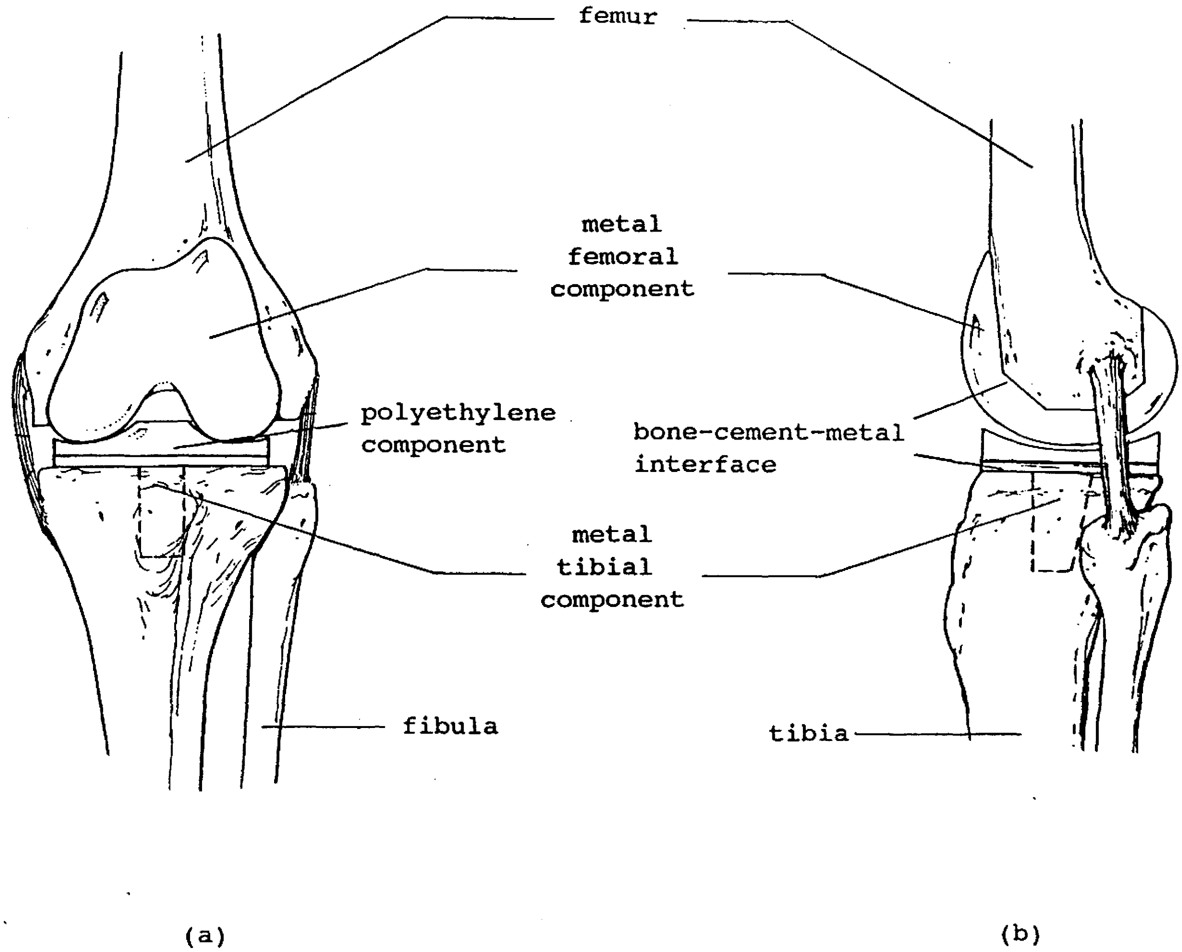

Figure 1.2 Schematic diagram of an implanted total knee prosthesis. (a) anterior view (b) lateral view

implanted total knee prosthesis. During surgery the proximal surface of the tibia, including the plateaux, is cut away leaving a flat surface of exposed cancellous bone. A metal tibial component, usually a flat thin metal tray with some type of central post or peg underneath, is bonded directly to the cut surface using polymethylmethacrylate cement. On top of the metal tibial tray a polyethylene component is seated securely and remains fixed. In a similar manner the distal surfaces of the femur, including the condyles, are removed using a series of beveled cuts. A single contoured metal femoral component is then cemented in place. The distal surface of the femoral component is very smooth and polished while the proximal surface of the polyethylene component is also smoothly contoured. These two surfaces mate to form the new articulating joint surfaces.

Removal of the natural articulating surfaces and underlying bone during total knee surgery provides space for artificial components, as well as removal of damaged or diseased joint regions, thus providing significant pain relief. The surgeon can also treat the artificial components as mechanical spacers to restore proper ligament tension and joint alignment. For severly disabled and elderly patients the speed and certainty of pain relief along with restored joint function provided by this single procedure can mean a dramatic increase in quality and standard of life.

The implant type illustrated in figure 1.2 is known as an unlinked implant, as the tibial and femoral components are not mechanically connected. Knee implants come in many different types offering various degrees of stability. Unlinked, unconstrained versions rely on preservation of the ligaments for joint stability, while semiconstrained implants require removal of the cruciate ligaments having mechanical constraint and stability incorporated into their design. Unicompartmental designs which allow resurfacing of only one condyle and plateau, as well as mechanically linked implants, exist but are not used frequently.

Although early total knee replacement designs were not highly successful, intensive research and clinical evaluation have improved component design and cementing techniques considerably. While many types of total knee replacements exist, most have evolved to a basically similar design. Figure 1.3 shows an example of a modern total knee replacement. Current designs have metal tibial trays which employ some type of central or peripheral peg design. The pegs act to resist tilting moments when the metal tray is compression loaded eccentrically, and provide torsional resistance about the vertical axis. Metal tibial and femoral components have been commonly made from stainless steel, cobalt-chrome-molybdenum and titanium alloys. Plastic tibial components are made from ultra high molecular weight polyethylene, which currently remains the best suited material for combined strength, resistance to wear and cold flow properties. Modern

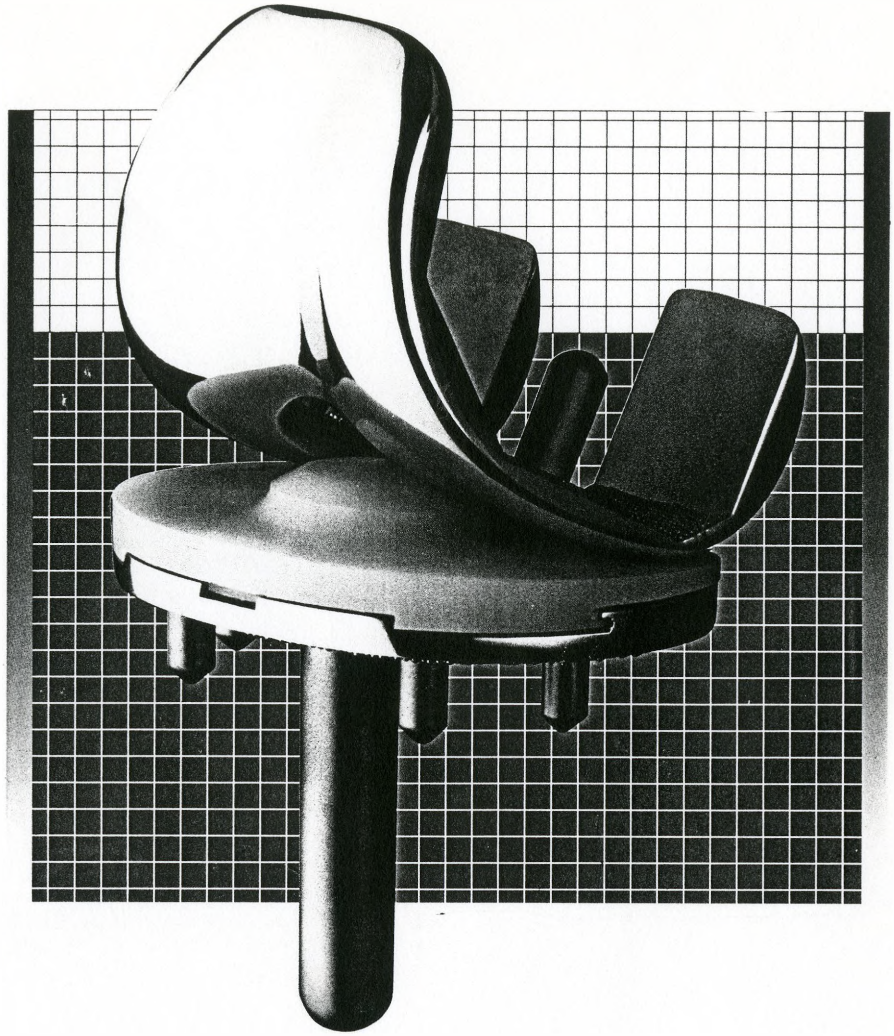

Figure 1.3 Example of a modern total knee prosthesis. The implant shown has a thin snapfit polyethylene component, and no rotational constraint about the vertical axis (Whiteside Ortholoc II, Dow Corning Wright 1987).

prosthesis designs have polycentric anatomically shaped components, available in a variety of sizes and thicknesses to better fit the individual patient.

More recently, a new method of fixation for implants has been developed which relies on bone ingrowth into small pores on the underside of metal implants for long term fixation. Tibial components are initially secured into place using bone screws. This method requires longer periods of inactivity following implantation to minimize relative movements between the bone and prosthesis, thus allowing bone to grow into the pores. While porous implants have been used increasingly, they are only successful where there is adequate healthy bone stock. Subsequently, cement still remains the most common form of fixation.

1.4 Limitations Of Total Knee Arthroplasty

Total knee replacement has become the procedure of choice for cases of severe arthritis and deformities of the knee not amenable to lesser procedures. As many as 40,000 total knee replacements per year are performed in the United States alone [3]. This procedure however, is not without significant limitations. The most predominant mode of failure of knee replacements has been and continues to be, failure of the bone-cement-metal interface and subsequent loosening of the tibial component. Because of the probable failure of this interface in an undesirably short time period, durability of knee replacements is considered finite, with successive revisions becoming less satisfactory. This limited durability imposes constraints on patients receiving implants. Activities producing high forces across the knee such as heavy work, unlevel walking, and sporting activities should be avoided. Higher failure rates in younger, more active or obese patients have meant that knee replacement is primarily performed on senior patients who are less likely to place large, repetitive force loads on a prosthesis. An elderly, somewhat frail individual with other afflicted joints, who is not presumed to outlive the service life of the prosthesis, constitutes an ideal candidate for knee arthroplasty. There are, however, no precise rules for knee replacement. The surgeon must be a good observer and decide on the basis of a number of factors including age, quality of life, general condition, symptoms, and clinical and radiological state of the joint, whether or not arthroplasty should be done [2]. Other treatment options are always considered first. Failing these, replacement surgery is usually left until the joint is in an intermediate to severly degenerated state. The unfortunate result is that patients are often already at a stage of severe pain and disability when surgery is performed. Further, surgeons must be careful to minimize the amount of bone removal necessary to implant a prosthesis. It is desireable to have as much bone stock left as possible should the implant fail and repair surgery be required to reseat prosthetic components. Thus, as a result of current limitations in prosthetic service life, the surgeons' options also remain undesireably limited.

CHAPTER TWO

PROBLEM REVIEW

2.1 Some Aspects Of Gait

Normal level walking is a cyclic activity in which each limb spends about 60 % of the total cycle time in a stance (weight bearing) phase, beginning with heel strike and ending with toe off. During the remaining 40 % of the cycle time, swing phase, the limb is bent or flexed and swung under the body to advance forward. The two main progressional forces in walking are momentum added by the forward swinging limb and, more importantly, forward fall of the body over the single weight bearing limb [6]. Adult walking normally has a step length of about 70 cm with average natural cadences reported in the literature from 101 to 122 steps per minute [7]. Using the above approximation of each leg spending 60 % of its cycle time in stance phase, these rates translate to stance times of 0.71 to 0.59 seconds respectively for each leg.

2.2 Tibio-Femoral Contact Forces During Gait

Level walking is the most common and highly repetitive of our daily activities, and subsequently has been the focus of much research including efforts to determine contact forces at the knee joint. For obvious ethical reasons direct in vivo (internal) measurements of forces across the knee cannot be taken, leaving only external or in vitro methods. In order to evaluate mechanical loads acting at the knee joint, the interaction of a number of simultaneaous forces occuring during gait must be considered; they are as follows:

i) forces due to gravity which act downward through the centre of mass of each lower limb segment.

ii) inertial forces due to angular and linear accelerations of lower limb segments.

iii) external ground reaction forces on the foot during stance phase.

iv) net muscle and ligament forces acting across the joint.

Bresler and Frankel [8] provided the first significant attempt to determine forces at the knee joint during gait. In this work a link segment model was developed which treated the foot and shank as simply connected members. Using free body diagrams, equations of motion for the foot and shank were written with the unknowns of interest being the three coordinate force and moment components acting at the knee. Using anthropormetric data, a floor mounted piezoelectric force plate, and simultaneous high speed filming, ground reaction forces and linear and angular accelerations of body segments could be determined from actual subjects. With this data the equations of motion were reduced to a determinant system enabling calculation of external knee joint forces and moments for an instant of gait. Bresler and Frankel calculated force values for four normal subjects during level walking. Among their results it was determined that the largest force acting at the knee was the vertical or z component, varying from about 600 to 1000 N through stance phase, while horizontal components remained much smaller reaching a maximum of about 100 N.

The work of Bresler and Frankel was extended by Morrison [9] to include the contribution of muscle and ligament forces acting internally across the knee joint. Using a similar technique to that of Bresler and Frankel, Morrison first determined external joint reaction forces. An anatomically based model of the knee joint was then created which included the locations and lines of action of major muscle and ligament groups. External moments were broken down to the appropriate muscle force in action, times the moment arm from the line of action to the joint centre. Total compressive tibio-femoral contact forces were determined by summing all of the vertical or z components of muscle and ligament forces acting to stabilize the knee, as well as external joint forces for an instant of gait. The results of Morrison's work showed peak tibio-femoral contact forces generated during level walking in the range of two to four times body weight, with an average of 3.03 times body weight over twelve subjects. A plot of the vertical component of knee joint force with time is shown in figure 2.1. Three distinct peaks in this plot are noted, the first peak just after heel strike (HS) being the highest and of the shortest duration. Medio-lateral shear forces were determined to be small in comparison, with a mean maximum of 0.26 times body weight. In another study using the same technique Morrison [10] determined forces at the knee for a variety of activities. Results showed maximum knee joint forces of 3.97, 3.95, 3.83 and 4.25 times body weight for upramp walking, downramp walking and descending and ascending stairs respectively.

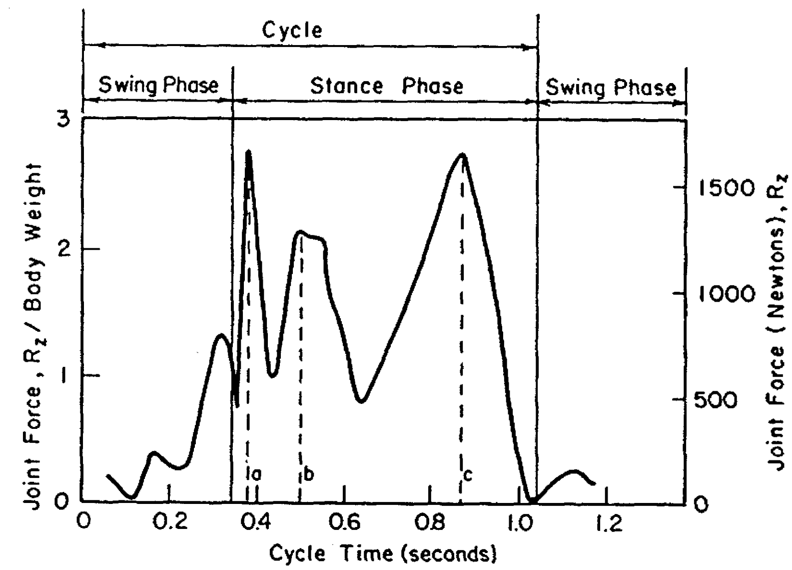

Figure 2.1 Vertical Rz component of knee joint contact force as a function of time (drawn with SI units from Morrison 1968).

Subsequent researchers have obtained similar results for normal level walking. Harrington [12] found peak knee joint contact forces to be in the range of 2 to 4.8 times body weight, with an average of 3.5 times body weight. Rohrle et al [11] also found average peak contact forces in the range of 3 to 4 times body weight. Using a more elaborate model of muscle action allowing for antagonistic muscle activity, Seirig and Arvikar [13] have reported knee joint contact forces as high as 7 times body weight during normal gait.

With prosthetic tibial components such mechanical loads are often eccentrically applied. This is due to anatomical shaping of the knee joint which causes contact of the femur with the tibia to move posteriorly as the joint is flexed, and to uneven loading of the medial and lateral compartments. Eccentrically applied compressive loads to the tibial component tend to compress the loaded side while the opposing side tends to lift or separate from the bone. This tilting or loosening moment is well recognized [37] and, coupled with the torsional resistance built into most knee protheses, creates combined stresses which tend to work the bone-cement-metal interface.

2.3 Transient Shock Pulses in Gait

During heel strike in normal gait, the forward extended limb is subjected to a jarring effect as it acts to deccelerate and smoothen the pathway of the forward falling body center of mass. Several investigators have identified high frequency shock or impulse type loads generated at heel strike during gait [14,15,16,17,18]. Impulse loads have been shown to have peak values in the range of 0.5 to 1.5 times body weight, and are typically 5 milliseconds, up to 25 milliseconds in duration. Resulting accelerations of up to 9 g's (g=acceleration of gravity) have been recorded at the knee joint with frequency components as high as 100 Hz. Examples of vertical ground reaction force profiles illustrating impact between the foot and ground

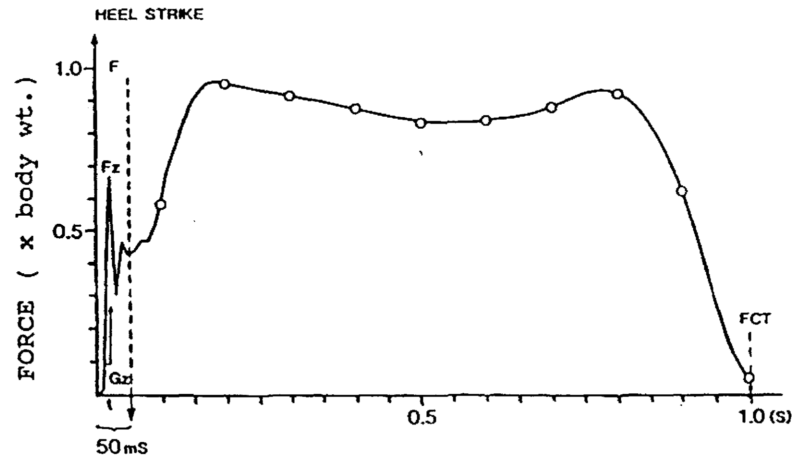

Vertical ground reaction force during a step on the force plate.

Fz = maximal impact force during the first 50 ms;
Gz = maximal impact loading rate;
t = time from heel contact to Fz;
FCT = foot contact time.

(a)

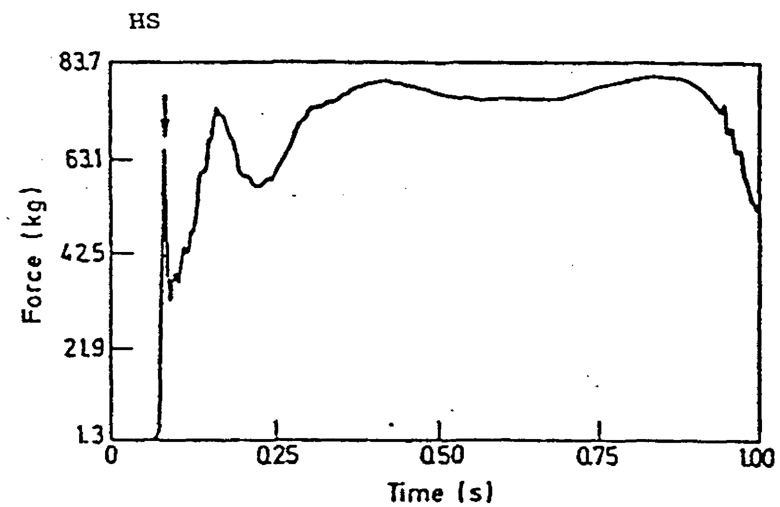

(b)

Figure 2.2 Examples of vertical ground reaction force profiles illustrating sharp impact loads generated at heel strike ((a) from Jorgensen and Bojsen-Moller 1989, (b) from Folman et al 1986).

at heel strike are shown in figure 2.2. These impulse loads have not been reported by many researchers as they require special high resonant frequency force plates or accelerometric techniques to be measured, and may have previously been filtered or dismissed as artifact. Impact pulses generated at heel strike propogate upwards through the entire muscoskeletal system to the skull, and are significantly attenuated along the way. Several structures such as the heel pad [20], subchondral bone [23], and soft tissues of the knee joint have been shown to significantly contribute to shock reduction. Studies have shown that healthy knee joints attenuate transient waves by about 30 % [30], and that excision of the meniscus leads to a 20 % loss in attenuational capacity of the joint [19].

While the full implications of these transients are not yet understood, they have been linked to several types of damage in the healthy muscoskeletal system including back pain, soft tissue injuries [21], and loss of attenuational capacity [16]. A causal relationship between repetitive impulsive loads and morphological and mechanical changes in subchondral bone and articular cartilage has also been demonstrated. These changes, which include subchondral bone stiffening, trabecular microfracture, and cartilage fatigue failure are consistent with clinical observations of degenerative joint disease, and show strong evidence for the role of mechanical factors in the onset of osteoarthritis [14,15,22,24]. Shock loads can also be particularly detrimental to mechanical structures due to sudden energy transfer and high strain rates imposed. If the structure is unable to absorb or dissipate this energy, damage or breakage can result. Several investigators have cited the potential role of shock transients in contributing to failure of the cement interface , however no research has directly addressed this issue. A further point worth noting is that the speed of propogation of these transients is faster than the speed of afferent nerve conduction and the reaction time of muscle [14,17]. This fact precludes any damping effects by reactive adjustment of muscle.

2.4 Forces Transmitted Through Knee Implants

Relatively little work has been conducted to measure forces through prosthetic knee implants. In a study by Chu et al [25] cadaver tibias and femurs, with knee joints intact, were instrumented with accelerometers in a special holding rig. Impacts to the distal end of the tibia, simulating heel strike during gait, were provided by a vibration shaker for three knee conditions; fully intact, menisci and cartilage abrasively removed, and prosthetically replaced. Results showed that the normal knee was able to attenuate 59% of the peak force transient generated by the shaker, while the abraded joint was 92% as effective, a loss in attenuational capacity of 8%. The prosthetically replaced joint showed a loss in attenuational capacity of 14%, and increased average tibial and femoral accelerations by 31 and 55% respectively over the normal knee condition. In another study by Hoshino and Wallace [26], 20 cadaveric knees were impacted vertically using a drop tower apparatus designed to produce an artificial load similar to that of a healthy person descending one step onto a force plate. Knee joints were impacted in a variety of conditions ranging from fully intact to artificially replaced with a conventional total knee replacement. Overall results showed that addition of a prosthesis increased the mean peak force transmitted through the joint by 180%. Figure 2.3 shows a comparison plot of forces for the intact and prosthetic cases. Note that in the prosthetic curve pulse duration is smaller while peak force and loading rate (and hence, strain rate) are increased.

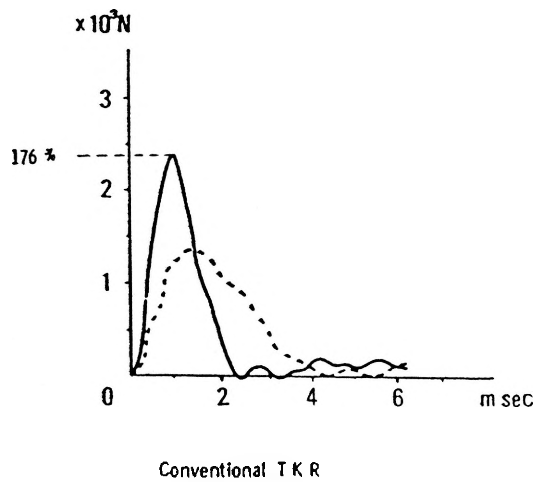

Figure 2.3 Force-time waveforms of impact forces transmitted through the human knee. Dashed line - joint intact; solid line - joint replaced with a conventional prosthesis (from Hoshino and Wallace, 1987).

The results of these two studies demonstrate that prosthetic knee replacements result in an increase in forces transmitted across the knee joint and thus act as 'stress risers'. Further, since natural attenuational capacity is lost, peak accelerations and forces all along the transient path are increased, placing other healthy joints in danger of overloading. This data is not surprising given the rigid nature of prosthetic components as illustrated in table 2.1 by the relative moduli of elasticity of various component materials and bone [31]. Chu et al sited in their work a clear need for research for the inclusion of shock absorbing materials in prosthetic implants.

Material	Modulus E (MPa)	Relative Ratio
Co-Cr-Mo Alloy	2.1×10^5	2000
Cortical Bone	1.55×10^4	150
Acrylic Cement	1.28×10^3	12
Polyethylene	2.27×10^2	2
Cancellous Bone	1.1×10^2	1

Table 2.1 Elastic Moduli of Bone and Various Prosthetic Materials.

2.5 Surface Damage to Polyethylene Components

Polyethylene tibial components used in total knee replacements are subjected to pitting, wear, abrasion and other forms of surface damage. In an analysis of retrieved implants, Wright and Bartel [27] found significant positive correlations between weight of the patient and time of implantation, to the amount of surface damage observed. Retrieval specimens that had been implanted for the longest durations (5 to 10 years) were in the worst condition. These results clearly indicate that mechanisms responsible for surface damage depend largely on mechanical factors such as applied load and number of loading cycles.

In an experiement to determine the wear rate of ultra-high molecular weight polyethylene tibial components, Rose et al [28] used a specially constructed apparatus to simulate gait movements and loads on knee prostheses. Their results revealed high wear rates as compared to those for hip replacements, which were dominated by high tibio femoral contact stresses. In measuring tibio femoral contact stresses of prosthetic knee replacements using simulated static loads, Wright and Bartel [27] also found high contact stresses which often exceeded the strength of polyethylene. Subsequent experimental and analytical analyses by Wright and Bartel [27,36] have revealed that tibio femoral contact stresses increase dramatically with decreasing polyethylene component thickness. Clinical examination of retrieved implants showed that thinner polyethylene components sustained more surface damage than thicker components, supporting this result. These authors have recommended that polyethylene components less than 8mm in thickness not be used in total knee replacement. There is currently significant probability that 6mm components will be withdrawn from use voluntarily by some or all orthopaedic manufacturers. Further, both Rose et al and Wright and Bartel also found strong evidence for the fatigue of polyethylene, which can lead to superficial cracking and complete fracture of the component.

In addition to mechanical factors, small debris particles released from wear of polyethylene elicit a biological response in surrounding tissues. This response has been strongly linked to long term problems such as infection and tibial component loosening via bone resorption and deterioration of the bone implant interface [29,55].

These mechanical and biological factors have created significant concern in the orthopaedic community over the long term fate of polyethylene tibial components and their contribution to loosening. The trend for thicker polyethylene components illustrates the need for more durable prosthetic components. This problem also supports the need for better stress distribution, force reduction and compliancy in prosthetic knees.

2.6 Stress Distribution in Bone Beneath Implants

It is well recognized that bone needs to be stressed in a normal physiological range in order to maintain a healthy state. Radin and coworkers have illustrated the detrimental effects of mechanical overloading on bone in healthy joints [22,24]. Of particular interest are stress distributions in bone adjacent to prosthetic knee implants.

Using a finite element analysis Garg and Walker [32] have studied the effect of prosthetic interfacing on bone stresses beneath tibial components. They found that for rigid interfaces the surface contact between the bone and prosthesis could be irregular, leading to areas of over and understressing. Typical prosthesis designs investigated had the effect of shifting the centre of pressure such that anterior bone became loaded much more than is normal. A further result was that a cemented interface produced stresses identical to direct metal on bone. This somewhat surprising result indicates that cemented interfaces may not necessarily provide more even or normal stress distributions than do metal porous coated implants. These authors also found that the addition of a 1 mm thick unbonded compliant interface to the prosthesis bone combination had a significant effect on stresses in the initial layer of bone, serving to generally smooth out stresses with large reductions seen in regions of high elastic modulus gradients (regions of abnormally low bone density surrounded by high density regions seen in arthritic bone). Walker et al [34] have also investigated the use of dacron velour (sheets of texturized pile 1 mm thick made from pure dacron yarn) as a compliant interface for total knee replacement. Experiments demonstrated that placement of a velour sheet between a rigid block and a flat exposed surface of subchondral bone increased the number of contact areas by 59 %. In vivo testing in sheep in which velour was interposed directly between tibial implants and underlying bone for 2 to 4 month periods was also conducted. Bone and fibrous ingrowth into the velour indicated that the velour had an effect of preventing overstressed conditions, and isolated bone from micromovements against the implant. A similar study of a compliant interface was conducted by Repo et al [53], in which canine total hip replacements were coated with a 1.5mm thick layer of silicone elastomer and implanted directly against bone in adult mongrel dogs. In comparison with standard metal implants used as controls the elastomeric stems promoted dense trabecular growth through the entire proximal femur, again indicating that underlying bone responds positively to a more compliant implant.

The effects of controlled loads on trabecular bone remodelling in femurs of large mongrel dogs was studied by Goldstein et al, using a special porous coated titanium implant fitted with a microprocessor controlled pumping system [33]. It was found that square wave form loading (fast rise time of 25 milliseconds) had the most significant and detrimental effect on trabecular bone remodelling, inducing a dramatic subchondral plate like structure to form at the bone implant interface with resorption of bone at the centre. A significant loss in bone density 6 mm below the interface was also observed. In contrast ramp wave type loads (slow rise time of 250 milliseconds) resulted in a more even distribution of trabecular bone structure and preservation of the bone distally. These results indicate that a further problem with rigid prosthetic implants is due to the abnormally rapid and high peak loads generated (refer to figure 2.3), which tend to adversely stress underlying bone, creating the risk of resorption.

Small relative movements are also known to occur at the bone-implant interface. This problem is compounded by high loads and large differences in elastic modui between prosthetic materials and bone. In the case of cemented implants such micromovements may contribute to cracking, trabecular failure and mechanical fatigue of the bone-cement-metal interface. For porous coated implants it has been shown that large micromovements of approximately 150 μ or more prevent bone formation into the porous surface [35]. Thus with porous implants initial periods of patient inactivity to promote bone ingrowth, initial stability of fixation, and minimal micromotion are essential to long term success.

In a recent ten year follow up study of eighty total condylar knee replacements in patients with rheumatiod arthritis, a prosthesis survival rate of 75% was reported with tibial component loosening being a main cause of failure [38]. In addition, 85% of the tibial components X-rayed showed radiolucency in one or more zones at the bone-cement-metal interface, revealing breakdown and withdrawl of bone away from the interface in these regions. These results, as well as those above, indicate that current rigid implants through non uniform coverage, increased stress tendencies, and relative micromotion, act only to impair the ability of underlying bone to adapt and provide long term component fixation. In recognition of these problems some researchers have attempted to develop more compliant prosthetic joints with the general aim of restoring natural compliancy and protecting the bone-prosthesis interface from overloading [49,50,51,52,53,54]. Work in this area however has been very limited with little to moderate success. To date compliant materials have not been successfully incorporated in total knee replacement and rigid prosthetic implants continue to be used.

2.7 Review Summary

Several investigations have shown that high contact forces are rapidly transmitted across the articulating surfaces of the knee joint during normal walking, which are accepted to be in the range of 3 to 4 times body weight. In addition, transient shock waves up to 1.5 times body weight in magnitude are generated during heel strike, and progress through the entire muscoskeletal system. These sudden and repetitive loads have been experimentally linked to fatigue and degenerative changes in healthy joints, and create a demanding environment for prosthetic replacements which must resist high stresses and strain rates, resulting micromotion, and fatigue, to provide long term fixation. The current technique of knee replacement involves excision of tissues known to provide natural compliancy, and replacement with rigid artificial materials. This procedure results in a significant increase in overall forces and accelerations transmitted through the knee joint mechanically aggravating the situation. High tibio femoral contact stresses inherent to prosthetic knee joints create high wear rates. This results in the release of debris which, in turn, poses risk to the cement interface through biological response. Through high and abnormal loading, underlying bone is also likely to become over stressed, creating the risk of resorption and failure of the bone-cement-metal interface as a whole.

All of these factors indicate mechanical loading as a main determinant of prosthetic longevity. Currently, prosthetic replacements are limited to the less active senior population, and a recent ten year follow up study of total condylar knee replacements reported a less than satisfactory prosthesis survival rate of 75%. Although the role of mechanical factors in prosthetic loosening are generally acknowledged, very limited research to date has been conducted on the potential effects of compliant interfacing in total knee replacement.

2.8 Hypothesis

The problems and finite service life associated with total knee arthroplasty outlined in the previous sections, demonstrate that current rigid prosthetic replacements poorly resist repetitive impulse loads, and are simply too overloaded to provide long term fixation and durability. It is hypothesized that the introduction of a compliant, shock absorbing material into a total knee prosthesis would serve to moderate high stresses and strain rates, protecting the bone-cement-metal interface, and thereby, extending joint life. Many of the mechanical and biological problems discussed in the previous sections might be significantly alleviated if a compliant material capable of providing peak load reductions and more normal stress distributions, were successfully incorporated into knee implants. The resulting extension of prosthetic service life would expand patient eligibility to include younger more active individuals in need of treatment.

CHAPTER THREE

BACKGROUND DISCUSSION ON MATERIAL SELECTION

3.1 Material Requirements For A Compliant Interface

To begin assessment of any compliant implant material as a shock absorbing interface for total knee replacement, the candidate material must be shown to possess the following essential properties before any further design stages can be considered:

i) Biocompatibility

For obvious health reasons, any biologically implanted material must be shown to have no toxic or adverse effects on the host, nor should it breakdown or degrade when exposed for an extended length of time to a physiological environment. Hence, chronic biocompatibility and biodurability are imperative required qualities.

ii) Fatigue Resistance

Everyday activities, such as normal walking, impose numerous and repetitive loads on the joints of the lower extremity. A compliant material in a total knee replacement would endure one compressive loading cycle every two steps. To significantly enhance the life of current knee prostheses it would be required that an interface material be able to withstand a large number of compressive cycles over several years of implantation, without significant abrasion, loss of mechanical properties, or fatigue cracking. Thus, the application requires high resistance to fatigue and flaw propogation.

iii) Shock Attenuation

One of the primary reasons for introducing a compliant material into a total knee prosthesis would be to serve as a shock absorbing interface. Therefore, a candidate material must itself be inherently able to lessen the severity of loads experienced at the knee joint. By deforming under impact, the material should serve to significantly slow the rate of application, and reduce peak force values of physiological impacts, thereby protecting cement interfaces and joint components from damaging stresses and strains.

iv) Elasticity

A compliant candidate must also possess appropriate stiffness and elasticity. If the material is too soft, it will be over strained when loaded, leading to early fatigue failure and potentially short service life. If the material is too stiff, it may prove durable, but may not provide the necessary shock reduction benefits. Further, as walking is repetitive, the material must be elastic enough to recover to its undeformed state after each step, so as to be able to cushion impact loads from subsequent steps. A material exhibiting a large amount of compression set after an initial loading cycle would not be useful in this role.

These four described properties form prerequisites for any compliant material for total knee replacement. If a given material were shown to possess all of these properties, design and implementation of a compliant interface into a knee prosthesis would be the next considered step.

Proving the biocompatibility of a material involves long term biological implant studies which go beyond the focus of the current investigation. For this reason, the approach undertaken was to select a candidate material with established biocompatibility and whose known mechanical properties best complied with the remaining three prerequisites. Such a selection would then constitute a best suited, or most eligible candidate material for investigation.

3.2 Polysiloxane Elastomers

Introduction

Polysiloxanes exist in a variety of material types such as elastomers, gel consistency materials, fluids, lubricants, adhesives, and are used widely as biomedical materials. Beginning with elemental silicone, polydimethyl siloxane prepolymer is formed and repolymerized or copolymerized with other polysiloxanes to form a variety of end products. Polysiloxane materials are typically stable and unreactive with most drugs and biological substances. They are also unchanged by clinical ultrasound and radiation, and can be sterilized by steam autoclave, ethelyene oxide or radiation [39]. Silicone based elastomers basically consist of cross linkable polysiloxanes, reinforcing filler (generally fumed silica) and an appropriate catalyst to initiate cross links. Devices fabricated from these elastomers are used in many medical specialities including orthopaedic surgery, plastic surgery and opthamology [39].

3.2.1 Biocompatibility

Various studies have been conducted to evaluate chronic biocompatibility and biodurability of implant grade silicone elastomers. These have included both two and three year implant studies with dogs as well as two year studies using albino rats. Results of these investigations have shown that the host reaction is typically limited to a mild foreign body reaction, resulting in encapsulation of the implant by fibrous tissue. No evidence of biodegration, or loss of physical properties of the elastomer specimens were found. Results from these and other shorter term laboratory tests, as well as over 15 years of human clinical implant use, have demonstrated the excellent biocompatibility and biodurability of these elastomers [39,40].

3.2.2 High Performance Silastic Brand Elastomers

Over the last twenty years flexible elastomer implants have been developed by Swanson and coworkers for use in reconstruction of various joints of extremities including the finger, wrist, elbow and toe [4,40]. These implants consist of specially shaped pieces of elastomer which must bend and flex to allow for controlled joint movement and restored function. For use in flexible hinge implants, the Dow Corning Corporation of Midland, Michigan has developed implant grade high performance elastomers. These elastomers have been developed especially to have a high resistance to both fatigue and flaw propogation.

3.3 Material Selection And Experimental Focus

Based on the four essential material requirements for a compliant interface outlined in section 3.1, it was evident that a high performance, implant grade silicone elastomer was an ideal candidate for investigation. The first and most difficult of the four requirements is immediately satisfied; the biocompatibility and biodurability of these materials have been well documented. A second advantage of high performance elastomers is that they have been developed especially for flexible application, and possess high resistance to fatigue and flaw propogation. These materials also have a very compliant rubber-like consistency appearing capable of providing shock reduction benefits. As they can be fabricated in a range of hardnesses, and to almost any desired shape, a variety of shapes and sizes of elastomer specimens should provide ranges of elasticity and shock absorbancy within which to experiment. In addition, silicone elastomers have excellent resistance to compression set, and their dynamic absorption characteristics do not change with aging or large temperature variations [44]. For the current study, Dow

Corning's most recently developed high performance elastomer, Silastic brand HP100 was selected. When tested in accordance with the American Standard ASTM D813 "Standard Method of Test for Crack Growth of Rubber", this material has typical crack growth of only 0.25 mm per 10^6 flexion cycles. The test is essentially one of pure bending. A few other properties of the selected material are listed here:

Tensile strength (psi)	1100
Die B Tear Strength (psi)	250
Elongation (%)	500
Durometer Hardness Shore A	52 ± 4

With a test material selected, the focus of the current work was broken down to experimental evaluation of the material for:

1) compressive fatigue resistance
2) attenuational capacity
3) material stiffness and elasticity

While many different methods of material evaluation exist, tests herein were chosen so as to give a direct and basic evaluation of the candidate material for knee joint application. From a design point of view, each of the above three areas will be interrelated. Design for performance in one area will likely affect performance in another, creating trade offs. Thus, data from testing in each of these areas should determine the overall feasibility of the selected material.

3.4 Preliminary Investigation

Prior to the current study, a preliminary investigation on Silastic HP100, was conducted by the current authors as an undergraduate engineering thesis project at McMaster Univeristy [41,42]. This project was identical in focus to the work presented here, however, the scope of this preliminary work allowed only limited fatigue, shock, and elasticity tests to be conducted. A brief summary of tests conducted and results are presented here.

Test Specimens

All test specimens were circular, one half inch diameter HP100 elastomer discs, ranging from 0.104 to 0.114 inches thick.

Fatigue Testing

i) <u>Method</u>

Disc samples were mounted flat in a compression fatigue test machine unconstrained so as to deform freely. Samples were compressed between two flat, parallel, metal faces to 20% strain at a rate of 150 to 180 cycles per minute. During testing, samples were removed at various intervals and inspected under a microscope for damage and signs of fatigue failure. It was later decided that a more severe compression strain of 30 % also be tested.

ii) <u>Results</u>

Because the fatigue test apparatus could accomodate only one sample at a time, testing proved extremely time consuming. As a result, only two elastomer samples were tested. The first of these samples was cycled at 20 % compression strain up to 18 million cycles, at which point no clear evidence of fatigue failure or fatigue cracking was found. However, this sample did show signs of abrasive wear and measurements revealed a 4 % reduction in overall thickness. The second sample was cycled at 30 % strain for up to 5 million compression cycles. At this point, the sample showed no signs of fatigue failure, however, testing was discontinued due to excessive abrasive wear on the sample. The wear problem was attributed to the roughness of finish of the top compression face, combined with relative radial movement and migration of the sample on compression.

Force Strain Testing

i) Method

Samples were placed on a smooth steel plate and manually loaded into an Instron test machine. Forces were charted as individual samples were first compressed to 30 % strain, and then immediately unloaded, both at a fixed speed of 0.05 inches per minute.

ii) Results

Force versus strain curves generated were all nonlinear with a significant amount of hysteresis. Unloading curves always fell well to the right of the loading curves, thus enclosing a sizable area. This area indicated that elastomer samples were not purely elastic in nature but possessed damping characteristics; the larger the area, the greater the damping ability. Also, unloading curves typically did not return exactly to the origin indicating a small amount of set or slowness to complete recovery in the compressed specimen.

At the given compression rate, an individual sample required from 45 to 55 pounds force to achieve 30 % compression strain. If it is considered that up to three square inches of surface area are available in a conventional total knee replacement, an equivalent area of discs would require between 690 to 840 pounds force to acheive 30 % strain. These estimated force values meet or exceed physiological knee joint loading values reported in the literature for normal walking [9,11,13], and indicated that a suitably stiff elastomer pad might be designed for knee joint application. Compression tests on fatigue cycled samples were inconclusive.

Shock Testing

i) Method

Because of a lack of availability of fresh bone plugs, one half inch diameter nylon plugs were substituted and placed directly on top of a piezoelectric force cell. Each plug was impacted bare, and with one, two and three elastomer disc samples placed directly on top, using a bar shaped impact pendulum as shown in figure 3.1. Peak force and time duration values were recorded for each impact. Pendulum drop height was kept constant at a value of 4.66 mm which generated impact stress values well within physiological ranges reported in the literature. Neither strain nor strain rate of the elastomer specimens was

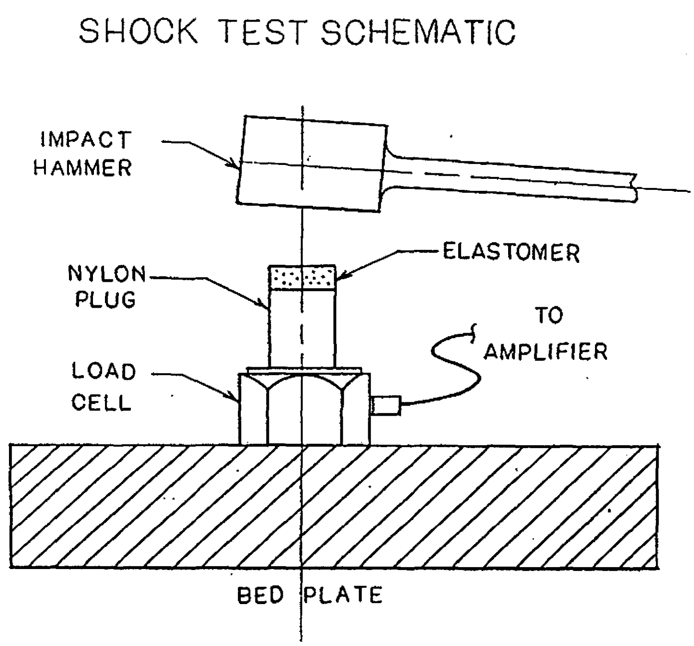

Figure 3.1 Shock test apparatus.

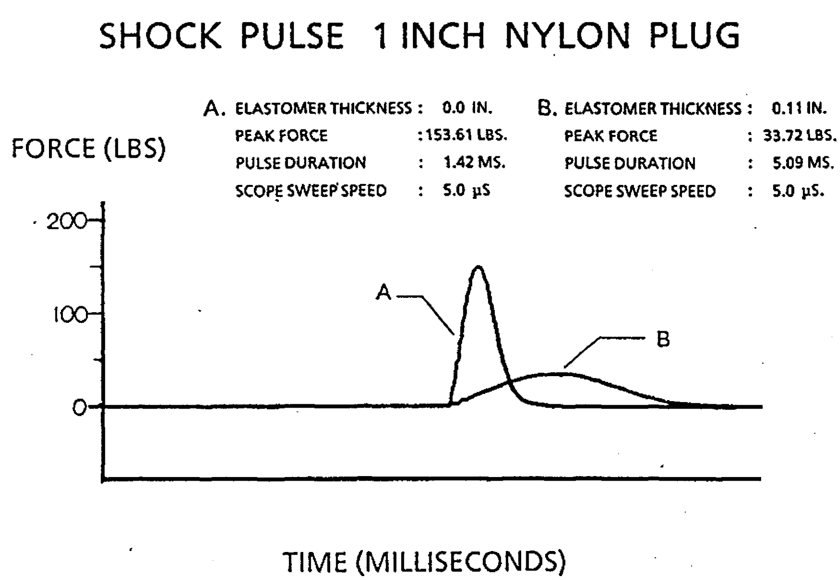

Figure 3.2 Comparison of force-time curves for a physiological impact on; A) bare nylon plug B) nylon plug with a single elastomeric layer.

controlled.

ii) <u>Results</u>

When a single elastomer disc was added on top of the nylon plugs, peak impact forces were reduced by 78 to 82% as compared to those for bare nylon. Doubling and tripling this thickness gave an additional 5 to 10%, and 1 to 2% attenuation respectively, yielding a total peak force attenuation of 89 to 91% with three elastomer discs. Similarly, shock pulse time durations increased an average of 434%, 791%, and 1009% when one, two and three layers of elastomer discs respectively, were used in comparison to bare nylon. These results are highlighted in figure 3.2 where a pulse from impact with bare nylon, and an attenuated pulse from the addition of one elastomeric disc sample are superimposed.

Summary

Although limited, the results of this preliminary work were very encouraging. The HP100 elastomer demonstrated adequate material stiffness as well as very promising fatigue resistance and shock attenuating characteristics. Recommendations from this work included more thorough and extensive testing in each of the three areas, testing of a wide variety of shapes and sizes of elastomeric samples, and movement to more simulated impact testing incorporating human bone and knee implants. These results and recommendations formed a basis for the work presented herein.

CHAPTER FOUR

DESIGN CONSIDERATIONS AND TEST SAMPLES

Introduction

With a candidate material and experimental testing indentified, along with some preliminary data, it was considered necessary to address as many design parameters relating to placement of a compliant interface into a total knee prosthesis as possible, so that testing would procede in a representative fashion. It should be made clear that the focus here was not to conceive a final design, but to manufacture suitable test samples incorporating several design criteria, which would yield useful experimental results.

4.1 Perceived Location In A Total Knee Replacement

Initial consideration had to be given as to where an elastomer cushion might be placed in a modern total knee prosthesis. Referring back to figure 1.2, it is apparent that the faces of the femoral and tibial components adjacent to bone are reserved for cemented fixation. Previous attempts to introduce silicone elastomers between the bone and prosthesis have failed, the elastomer not proving durable when placed directly against bone [50,52,53]. A layer of elastomer secured between the articulating surfaces of the joint would be subjected to simultaneous large relative motions and compressive loads, creating very difficult wear and fixation problems. The remaining location, a flat space between the metal and polyethylene tibial components, was clearly seen as the most feasible. Such a flat space would provide solid backing for an elastomer sheet up to a maximum of about 30 cm^2 in surface area. In addition, metal and polyethylene tibial components are not required to slide or move relative to each other, and experience largely compressive loads in service. This fits well with the percieved role of the elastomer cushion as being primarily a compressive force damper and load distributor.

In practice orthopaedic surgeons generally work so as to minimize the amount of bone removal necessary to implant a knee prosthesis. The amount of bone remaining is of particular significance should the implant fail and repair surgery be required to reseat new components. It was therefore deemed very important that an elastomeric cushion be designed as thin as possible so as not to significantly increase the overall thickness of a prosthesis. Currently, tibial tray thicknesses range from 1mm to 2mm, while polyethylene components can range from 4mm to 16mm in thickness. If a cushioning medium were proven effective in protecting joint components, thinner polyethylene components might be employed in future designs, allowing extra space for an elastomer cushion. For the current investigation however, it was decided that elastomer thicknesses be limited to a range of 3 to 4mm.

In choosing a flat space between the metal and polyethylene tibial components as the location for an elastomer cushion, two important size constraints for test samples were determined. Samples could occupy a flat surface area of up to 30 cm^2, and should be limited to 3 to 4 mm in thickness. From literature presented in Chapter two, compressive loads seen at the knee during normal walking can be estimated to be in the range of 2 to 4.8 times body weight, which would translate into 1373 to 3296 N loads for an 70 Kg. individual. Thus, basic size constraints and forces experienced in service were established.

4.2 Factors Determining Elastomer Stiffness

An elastomer is a natural or synthetic material capable of retaining its original shape after having experienced large strains. Silicone rubber, and rubber like materials in general conform to a few rules useful in designing any type of cushion or bumper. For these materials, the resistance to change in volume under pressure is very large, and of the same order of magnitude as that for liquids. Extreme pressures are required to produce minute changes in volume if forces are applied to all sample faces at once [40,43]. Therefore, these materials have no practical application as compression springs or dampers unless compressed along one axis only, and allowed to deform laterally along the remaining axes. When used in this configuration, the stiffness of an elastomer block will be determined by three interrelated components [43]:

i) the inherent stiffness of the material

ii) stiffness added by surface restraint

iii) stiffness added by the shape of the piece itself

The first of these can only be changed by selecting a different material. The second and third are discussed as follows.

ii) The stiffness of an elastomeric specimen is partly determined by the ease with which lateral movement (or slippage) can occur at the compression plate interface. For a given specimen, ease of lateral deformation will depend greatly on the surface conditions between the loaded sample faces and the compressing faces. Lateral movement at the compression plate face may be resisted completely via bonding of the elastomer to the plate, intermediately under dry, unadhered conditions, or may be facilitated by the addition of a lubricant.

Tests conducted on rubber have shown that restriction of movement at the loading faces greatly stiffens a sample, particularly when the size ratio of width to height is large. Stiffness of a single piece of rubber can be altered as much as sixfold between extremes of surface conditions (bonded to lubricated). Also, it has been noted that in the case where test surfaces are smooth, dry, clean and unadhered, sample stiffness is very close to that of the bonded case [43].

iii) For elastomers and rubber-like materials, specimen geometry can also affect apparent stiffness. As an infinite number of shapes and sizes of specimens are possible, there are a few rules of thumb that can be generally applied as follows:

A) *Similarity Rule* : This rule states that similarly shaped pieces of the same material require the same unit load to give an equal percentage of deflection. As seen in figure 4.1, if the dimensions of a small block of rubber are all increased by the same factor to form a similar large block of rubber, both blocks will require the same psi loading to achieve the same percentage compression strain.

B) *Shape Factor* : The shape of an elastomer piece as distinguished from its size may affect the unit compressive stiffness to a large degree. To account for this, a convenient empirical 'shape factor' is defined as the ratio of the area of one load face, to the area of those peripheral surfaces free to expand laterally. When lateral movement of a sample is restricted, this ratio has a significant and reliable influence on stiffness as shown in figure 4.1.

The shape factor ratio applies to sample pieces having parallel loading faces with sides normal to these faces. For other, more elaborate shapes, the shape factor may be estimated by breaking the piece down into similar shapes. For example, a truncated cone could be considered to have one load face area equal to the average of the two actual load faces. A dome shaped piece might be considered as a truncated cone, etc. Shape factor should only be applied to sample pieces which are within the limits of stability. Portions which tend to buckle should not be considered.

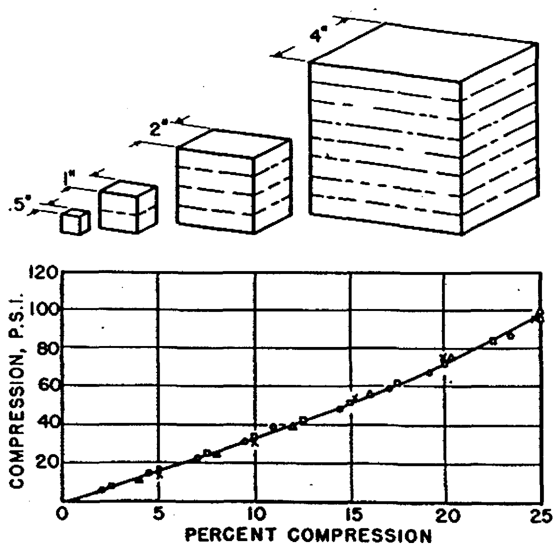

(a)

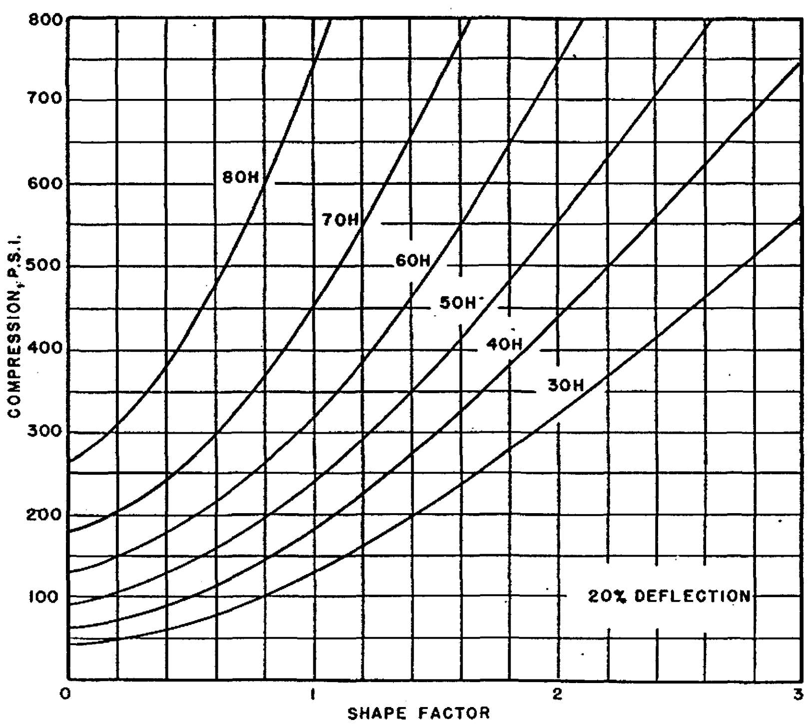

(b)

Figure 4.1 (a) Similarity rule as applied to cubes (b) Relation of shape factor to compressive force (from Kimmich 1956).

Tests with rubber samples have revealed that as sample height is increased, surface conditions become less important, and with low shape factors, this effect almost disappears. Conversely for high shape factors surface conditions become much more important. As a result, it was recommended that where large shape factors are needed, that rubber be bonded to metal surfaces to avoid accidental lubrication of surfaces and abrasion. It is generally considered good practice to keep shape factors low, however, factors below 0.25 may permit buckling [43].

These mechanical factors affecting stiffness reveal important design considerations for an elastomer cushion. To obtain a desirable degree of compliancy, elastomer samples must not be fully constrained but allowed to deform or bulge in lateral directions. Because of the influence of shape factors, it is anticipated that shape will play an important role in designing a cushion to fulfill shock and stiffness requirements. Further, it is clear that surface constraint factors must be kept in mind and stated during any design or testing stage.

The idea of bonded surface conditions was not considered at this point in the investigation. To the author's knowledge, bonding of elastomer sheets to various prosthetic components had not been done successfully, and introduces the need for a biocompatible adhesive material.

4.3 Shock Absorbtion

The ability of an elastomer cushion to absorb shock will likely depend largely on the mechanical stiffness factors described in the last section. In considering the need for lateral deformation, as well as shape factor effects, it was intuitively clear that a piece of elastomer such as a single flat sheet, 30 cm^2 in surface area, and 2 to 4 mm in thickness, would not provide necessary compliancy and shock reduction benefits. An effective elastomer cushion would more likely be comprised of load bearing supports, and regions of non support or voids, the ratio of which needs to be determined.

Excluding surface conditions, the variables determining the shock absorbing characteristics of an elastomer cushion are :

1. material properties
2. thickness
3. surface area
4. shape

The first of these pertains to material stiffness and damping characteristics, and is again a matter of materials selection. As previously discussed, both of one and two above have been essentially determined as a test material has been selected, and space constraints limit the elastomer thickness to approximately 4 mm. The third variable refers to the actual surface area of elastomer available to bear impact loading. The fourth variable incorporates both shape factor considerations as well as actual elastomer geometry. Load bearing supports might be, for example, square, cylindrical, conical or irregularly shaped. An equivalent load bearing area might also be comprised of several smaller supports having low shape factors, or a few larger supports having higher shape factors. Because variance in both thickness and material properties remained limited in this application, it was anticipated that shape and surface area would likely be the dominant variables in testing for a suitable cushion design.

4.4 Basic Considerations

In conceiving an elastomer cushion design a number of other considerations were realized. Due to the nature of the application, it is important that elastomer surfaces be as smooth and continuous as possible to avoid sharp notches which might act as stress risers and promote fatigue cracking. Secondly, it was realized that when implanted, spaces or voids in an elastomer cushion would be occupied by body fluids, and therefore provision would have to be made for fluid escape on compression of the elastomer. If fluids became entrapped between the metal and polyethylene tibial components they might significantly alter the intended mechanical properties of the elastomer cushion. Thirdly, it was decided that initial elastomer specimens be uniformly designed so as to be without directional tendencies. That is, the mechanical properties over the surface of the elastomer cushion should not change with directional variance. Thus, certain designs such as a flat elastomer sheet with parallel grooves cut in one direction over the surface, were, for example, excluded. This constraint was imposed for the sake of initial testing and material evaluation. Once more is learned of the materials behavior, more elaborate cushion designs could be considered for actual knee joint application. Lastly, it was perceived that an aspect of a preferrable design would be one in which elastomer supports are initally compliant to enhance shock reduction, but become increasingly stiffer at a high rate when further compressed, so as to limit overall deflection. Such a non-uniform spring rate might be achieved if elastomer supports were notably curved or tapered, having a larger base area and a smaller load bearing area at the top. A hemispherically shaped support with a flat base, or a truncated cone would be ideal examples of such a shape.

4.5 Manufacture

A final aspect that was considered in creating elastomer test specimens was manufacturability. Uncured silicone elastomer is a viscous material which does not soften much when heated and flows only under pressure. Fabrication of elastomer pieces requires the use of pressure techniques such as compression molding, transfer molding, calendering and extrusion. Whatever test samples were conceived, they would have to be specially fabricated and the difficulty of practically making a specific cross section considered.

On consulting with the Dow Corning Corporation, it was discovered that a simple press was used to manufacture flat uniform sheets of elastomer as well as various other prototypes. The press consisted simply of two flat, heated, parallel plates which could be brought together at a desired temperature and pressure. Once pressed into shape, the addition of heat accelerates curing of the elastomer into a uniform solid which retains its shape. With this method available, it was conceived that placement of a specially fabricated metal plate within the press might be employed to make more elaborate shapes. The plate itself would be flat with various features machined into one surface, onto which uncured elastomer would be pressed. Although previously untried, this method remained the most practical and inexpensive method of attempting to manufacture test specimens.

4.6 Elastomer Test Samples

After consideration of the various design criteria as well as shape and configuration possibilities, it was decided that samples be manufactured in the form of flat uniform sheets with individual, geometrically shaped surface features molded onto one side. Such features would protrude normally from the sheet surface to serve as load bearing supports. This type of sample was deemed to practically incorporate most of the previously discussed design considerations. The flat sheet form fits within space constraints discussed. Each individual geometric support would act as a mechanical spring fixed at one end to the base sheet and free to deform laterally when compressed. A wide variation in shapes and sizes of geometric spring supports should provide variation in mechanical properties. The design also allows space for fluid exchange between supports which, if uniformly spaced, create a sheet sample with no directional tendancies. Tapered supports could also be tested. Lastly it was believed that a series of sheet type samples would prove practical as a single geometrically shaped support could be removed from the sheet, or a large number of small supports could be handled conveniently for test purposes. The following geometric shapes were chosen for fabrication:

1) conical - 4 sizes
2) hemispherical - 4 sizes
3) cylindrical - 3 sizes

Central cross sections and dimensions for each of the shapes chosen are presented in figures 4.2 through 4.4.

4.6.1 Hemispherical and Conical Test Samples

Elastomer sheets with hemispherical and conical surface features were manufactured using the method described in the previous section. Hemispherical and conical shaped cavities were bored into the surface of a flat, smooth 25.4 x 25.4 x 0.64 cm. (10"x10"x1/4") aluminium plate to a uniform depth of 2.6mm, using ball end milling tools and specially fabricated conical cutting tools. The plate surface was divided into eight 6.7cm x 6.7cm square areas. Within each square area, cavities of one specific shape and size were uniformly spaced such that the sum of the flat surface areas occupied by the base of each individual geometric support, totaled as close to 50 % of the total square area as possible (i.e. 50% of the 6.7 x 6.7 cm square area). It was felt that equal coverage of base sheet surface areas by geometric supports might later prove useful in comparing the performance of different sheet

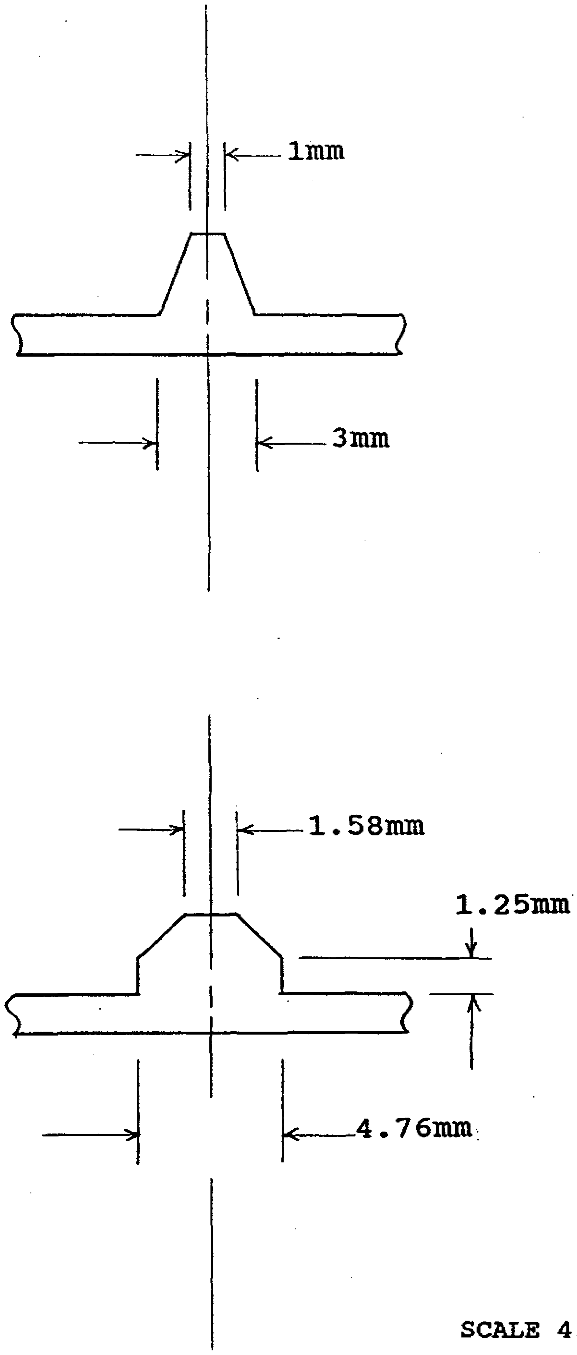

Figure 4.2 Central cross sections of truncated conical elastomer surface features molded on flat uniform sheets. For each shape; 1) overall thickness is 3.8mm 2) flat sheet thickness is 1.2mm.

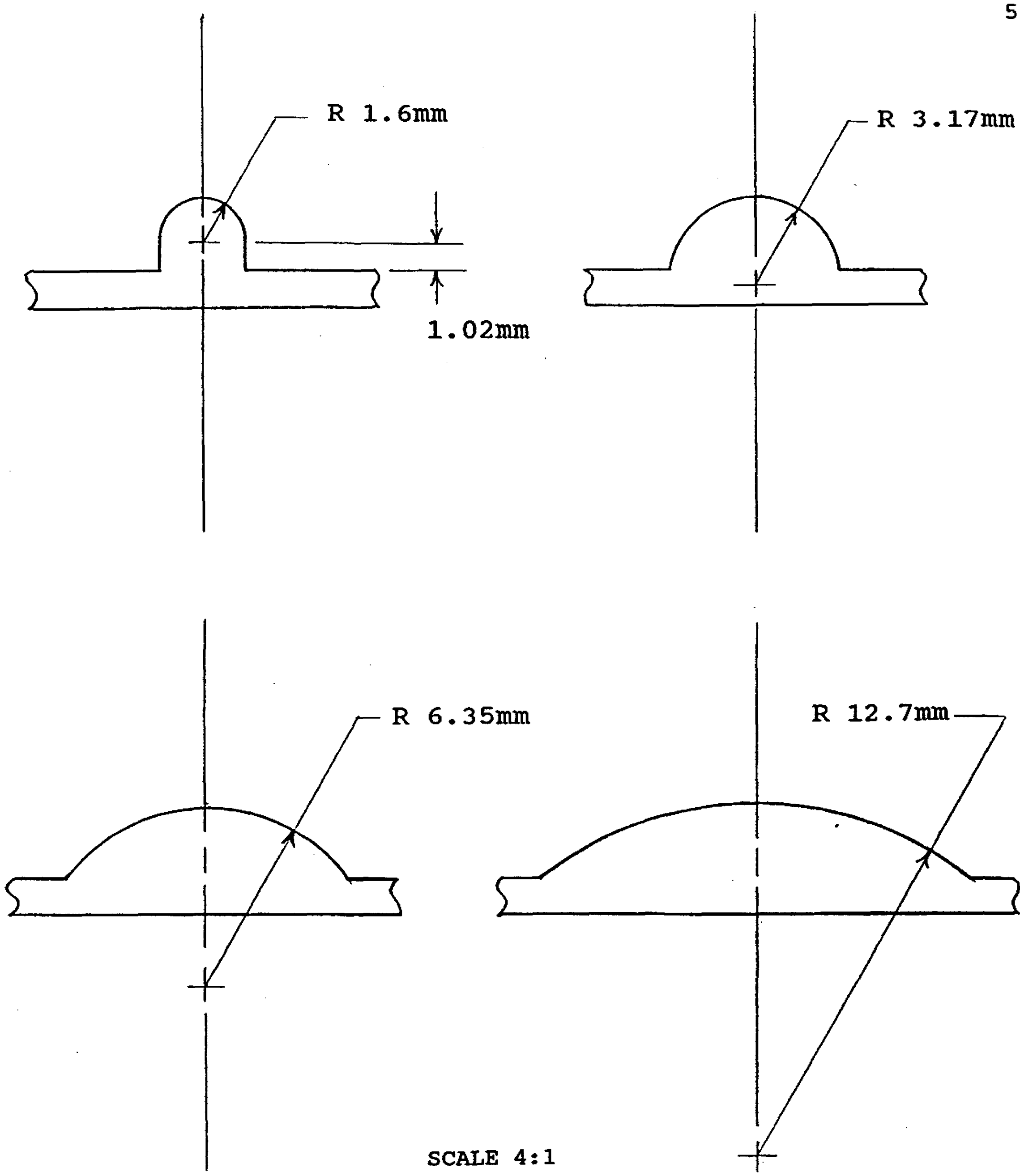

Figure 4.3 Central cross sections of hemispherical elastomer surface features molded on flat uniform sheets. For each shape; 1) overall thickness is 3.8mm 2) flat sheet thickness is 1.2mm

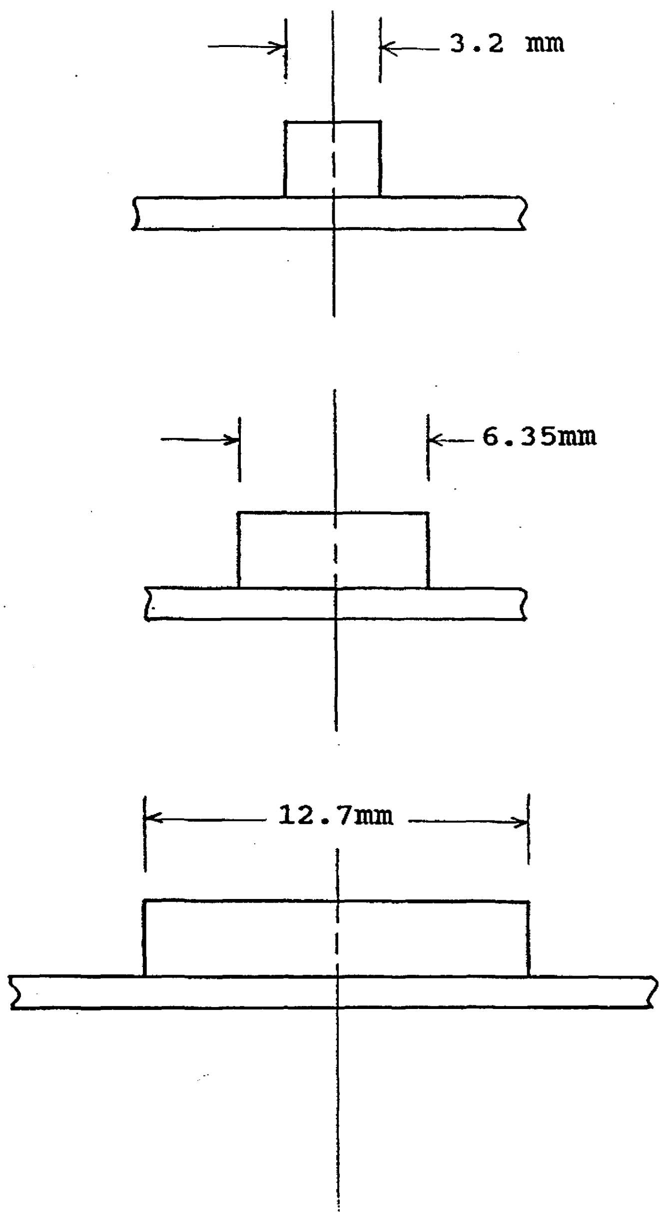

SCALE 4:1

Figure 4.4 Central cross sections of flat cylindrical elastomer discs adhered onto flat uniform sheets. For each shape; 1) overall thickness is 3.54mm 2) flat sheet thickness is 1.0mm samples. Uncured elastomer was pressed onto the face of the aluminium plate, filling machined cavities and forming a flat sheet on top of the plate. Flat base sheet thickness was approximately 1.2 mm yielding a total average sample thickness (sheet and support shapes) of 3.8 mm. Elastomer sheets were postcured at 400^{o} F for four hours. Hemispherical and conical sheet samples are pictured in figure 4.5. The aluminum molding plate is pictured in figure 4.6.

4.6.2 Cylindrical Test Samples

Sheet samples with right cylindrical features on top were made by hand. Using a leather punch, elastomer discs 3.2mm, 6.4mm, and 12.7mm (1/8", 1/4" and 1/2") in diameter were stamped from a smooth flat sheet approximately 2.54 mm in thickness. For each size, discs were evenly spaced and adhered onto a flat circular elastomer sheet, 30 cm^2 in surface area and 1 mm in thickness, so as to cover as close to 50 % of the sheet surface as possible. Discs were adhered to the flat sheets with a silicone based adhesive to simulate a single continuous sample as in the molded case. Figure 4.7 shows each of the three cylindrical sheet samples.

From hence forth, different cylindrical featured sheet samples are referred to by the diameter of the discs which occupy their surfaces. Similarly, different conical featured sheets will be identified by the base diameter of the conical shapes molded on top of the sheet. Hemispherical featured sheets are distinguished by the spherical

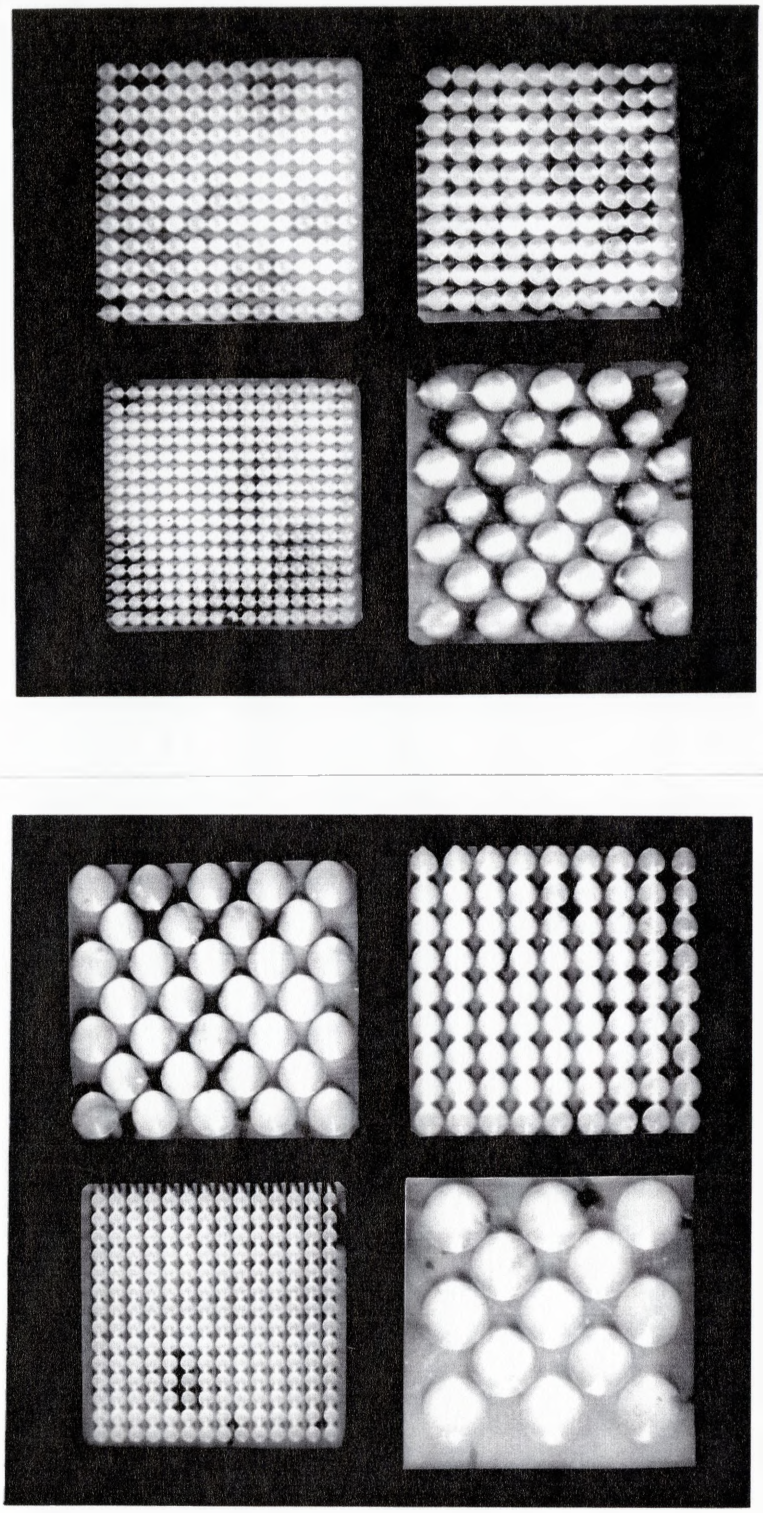

Figure 4.5 Molded conical (above) and spherical (below) featured elastomer sheet samples.

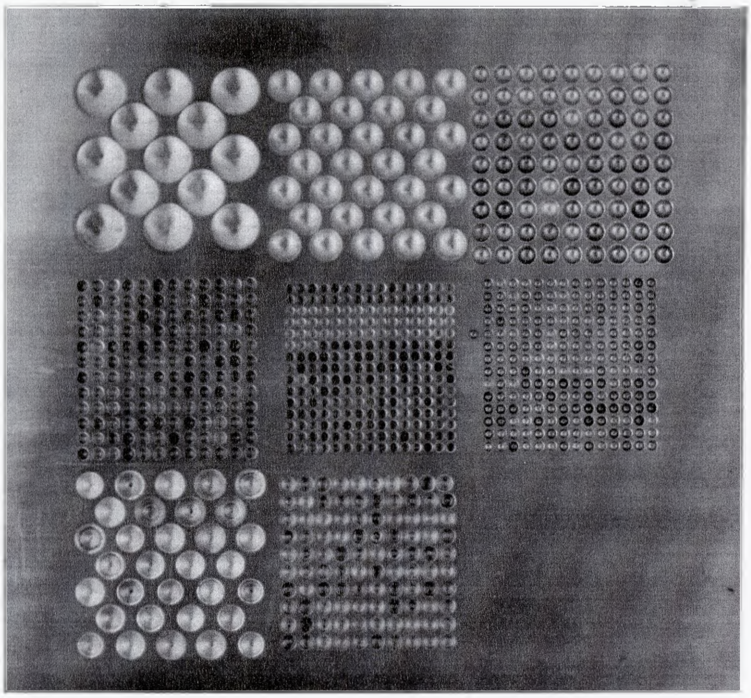

Figure 4.6 Aluminum molding plate.

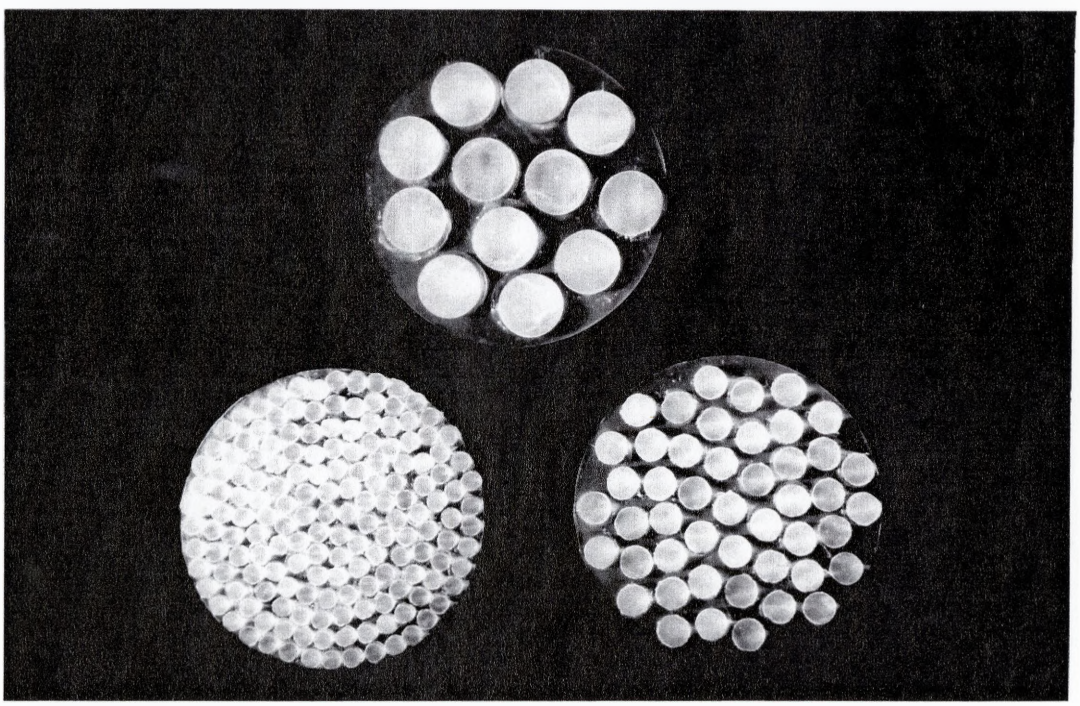

Figure 4.7 Cylindrical featured elastomer sheet samples.

diameter of hemispherical sections molded on top.

4.7 Maximum Design Strain

The amount of amplitude of the strain cycle is one of the most important factors affecting dynamic fatigue life of an elastomer cushion [47,58]. It was therefore decided that in the interest of preventing excessive strains in service, and maximizing fatigue life and durability, elastomer sample strain be limited to about 20% as a design constraint. Selection of this value was based on judgement and previous work. Similar compression strains have also been recommended for the continuous use of rubber samples having the same hardness and shape factors as elastomer samples herein [43]. The bulk of all dynamic compressive testing presented in the following chapters was therefore conducted with sample strains of 20%.

4.8 Test Sample Flaws

Although the method of press molding proved successful, samples did possess some unanticipated flaws which should be mentioned here. When sheet samples were removed from the molding plate after pressing, some very small regions of the elastomer surface were torn away and remained adhered to the mold. As a result, on subsequent pressings some of the geometric surfaces contained surface flaws in the form of small cavities and crevices. Bits of debris present between the mold and elastomer also became molded into the surface or body of samples. Geometric surfaces were not perfectly smooth but covered in very shallow, narrow and uneven cocentric rings. These were the result of fine machining scores or marks left on the molding plate after boring. In addition, due to nonuniform addition and flow of raw elastomer in the press, overall sample thicknesses varied slightly. Of the sheet samples selected for testing, average thicknesses ranged from 3.6 to 4.0 mm, the total average thickness of all samples being 3.8 mm. On any one sheet containing a specific geometric shape, variance in overall height was typically $\pm$ 0.1 mm from the average thickness, the single worst case noted as $\pm$ 0.2 mm from the average. Because of nonuniform thickness in flat sheet stock, cylindrically featured sheet samples ranged from 3.40 mm to 3.6 mm in average thickness, with height variances on any one sheet sample the same as those mentioned above.

For a basis of comparison all samples were constructed such that the geometric features occupied approximately 50% of the 30cm^2 base sheet surface area. Actual coverage over all of the test samples ranged from 43 to 58%, the majority of values lying close to the mean of 52%. This variance as well as variance in sample thickness are acknowledged to contribute to some error in this respect.

In hindsight, smoother molding surfaces, effort to minimize sticking and debris contamination during molding, as well as stopping blocks to better control press height, and hence sample thickness, should have been employed to improve sample quality.

CHAPTER FIVE

ELASTICITY TESTING

Introduction

To assess elastic behaviour of the HP100 elastomer, compressive tests were conducted on the various manufactured sample shapes. Testing was broken down into the three main following types; force-strain testing, variable strain rate testing, and recovery time testing. These three tests were chosen and designed so as to give a direct and basic understanding of the elastomers stiffness characteristics and suitability for prosthetic knee joint application.

5.1 APPARATUS

i) Force and strain generation

A material test systems (MTS) machine was used to generate compressive loads on elastomer test samples. This machine applies force by means of a vertically mounted hydraulic piston. Desired amplitude and rate of movement of the piston are input through control panels which include a function generator. The function generator allows for control of piston movement such that its position versus time profile is a common waveform shape (ex. ramp, sine, haver sine). Compressive forces exerted on elastomer samples were measured using PCB model #212A charge mode quartz force ring and a Kistler model #5004 charge amplifier. The force ring was calibrated using static weights and mounted into the MTS crosshead. The force ring was mounted between two plates with a compressive preload of 1500 lbs to ensure a rigid set up, and that measured force values were well within the working range of the ring. A schematic diagram of the force ring and compression plate set up is shown in figure 5.1. The entire test set up is pictured in figure 5.2. For all of the following compression tests movement of the MTS hydraulic piston, thus determining strain and strain rates imposed upon elastomer samples was a controlled input, while the resistance force of the samples as measured by the quartz force ring was the resulting output.

ii) Data aquisition

Stroke and force voltage signals from the MTS machine and force ring respectively were filtered at a cut off frequency of 100 hz, through a Rockland Model 432 Dual Hi/Lo Pass filter, to eliminate high frequency noise from the MTS machine hydraulic pump. Signals were converted to digital form using a Data Translation DT 2821 analoge to digital board. Data was sampled and stored using Notebook software by Labtech Corporation, on a Zenith 286 pc with 8287 math coprocessor. Analogue voltage signals were simultaneously sent to a Nicolet model 3091 digital oscilloscope for immediate observation and recording of results. Lotus spreadsheet, and Sigmapot graphical software were used to analyse and present data.

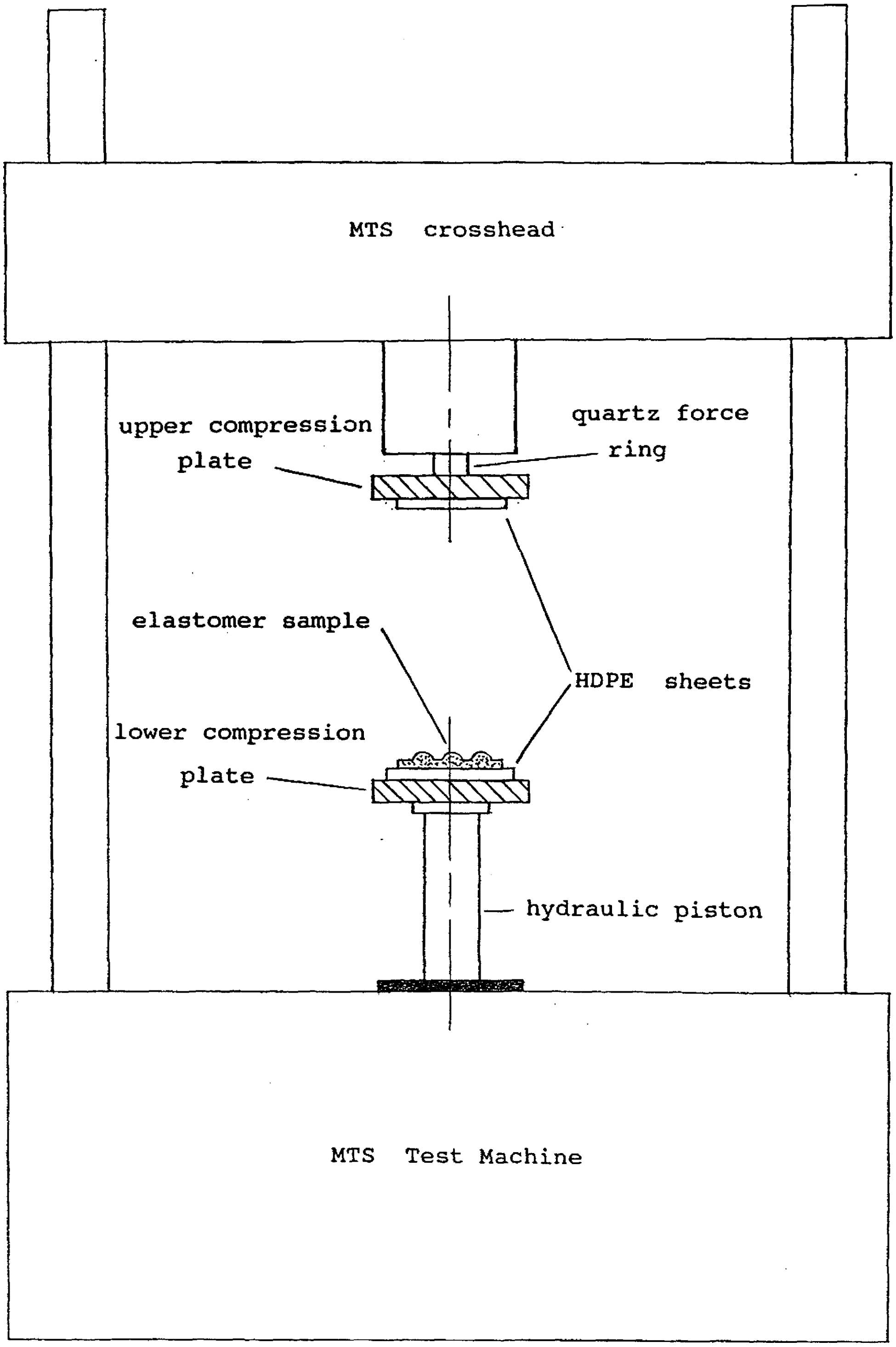

Figure 5.1 Schematic figure of sample placement and set up for compression testing in the MTS machine.

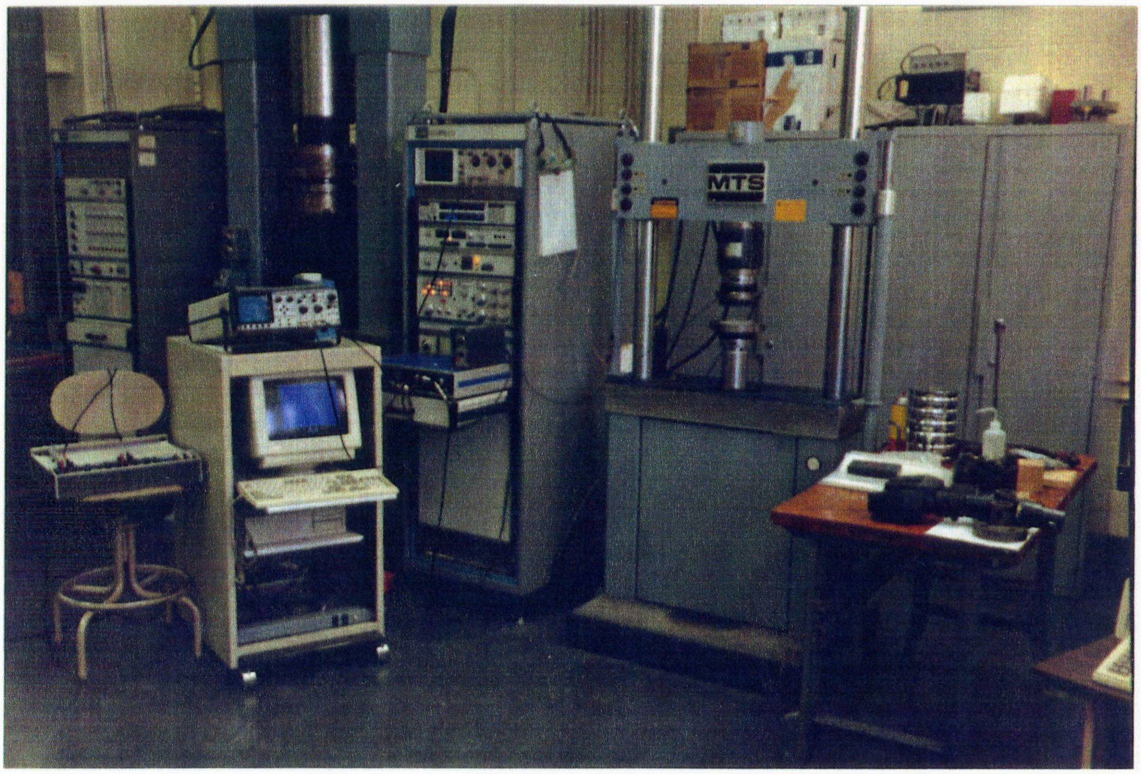

Figure 5.2 Compression test apparatus.

iii) Sample mounting

Elastomer samples were compressed between two flat smooth parallel compression plates. The lower compression plate was bolted to the MTS hydraulic piston while the upper plate was tightened directly against the quartz force ring and mounted to the MTS crosshead. To both upper and lower compression plates a single 1.6 mm thick sheet of high density polyethylene (HDPE) was secured. Elastomer samples were placed centrally on top of the polyethylene sheet on the lower compression plate which was then raised to the test starting position. For all of the following tests elastomer samples were compressed in a clean dry state against smooth polyethylene surfaces. Samples were not constrained in any other fashion and remained free to deform laterally.

Attempts to determine an initial starting point for the hydraulic piston by visual observation did not prove consistent. It was therefore decided that all 30 cm^2 elastomer sheet samples be preloaded by an amount of 22 N (5 lbs) before initiation of compressive tests. This was done to provide a uniform procedure and common starting point for the testing of all sheet samples. In addition the small preload value ensured a fuller even contact of geometric elastomer surface features with the upper compression plate prior to testing. This was significant since elastomer sample thickness was not always uniform.

5.2 Force Versus Deflection Tests

Introduction

When loaded within a normal physiological range it is important that an elastomer cushion possess the appropriate stiffness so as not to be severely deformed or crushed when loaded, yet retain a degree of compliancy so as to provide shock reduction benefits. The focus of this testing therefore was simply to assess basic stiffness values, and elastic nature of the various HP100 elastomer test samples conceived and manufactured as outlined in chapter four.

5.2.1 Method

Each of the fabricated elastomer sheet samples with geometric surface features (four conical, four spherical, and three cylindrical types), as well as smooth flat elastomer sheets layered singlely (2.3mm thick) and doublely (5.0mm thick) were tested totalling thirteen samples in all. All test samples had a base sheet surface area of 30 cm^2. Each sample in turn was mounted into the MTS machine and preloaded to 22 N as described in section 5.1. Once adjusted, each sample was loaded to a maximum engineering strain of 20% and released using a triangular waveform stroke profile and cycle frequency of 3Hz. The triangular waveform stroke profile provided constant loading and unloading rates, as well as equal loading and unloading times. The cycle frequency of 3Hz provided a total loading and unloading time of 0.33 seconds which is somewhat representative, though slightly faster than, that seen across the knee joint during the stance phase of normal gait. In addition one representative elastomer sample from each geometric family was selected and similarly compressed to 30% engineering strain. Test samples were loaded in this manner for three trials each while stroke travel, peak loading force, and total compression and release time were recorded using the digital oscilloscope. On the third trial stroke and force voltage signals were sent to the A to D board and sampled at a rate of 100 hz for computer storage, analysis and plotting.

5.2.2 Results

For the sake of brevity, one representative force versus deflection curve for each geometric family of shapes is presented. Figures 5.3 to 5.6 show compression curves for the 4.76 mm conical, 12.7 mm spherical, and 6.35 mm cylindrical featured geometric sheet samples, as well as the single layered flat sheet sample. The remainder of the compression curves for both 20% and 30% compression strain can be found in appendix A. For all samples tested average peak compression force, as well as calculated percentage energy losses due to hysteresis are presented in table 5.1.

i) General Observations

Force versus displacement curves presented are each indicative of the remaining test curves for that particular geometric shape. All of the test curves reveal a non linear behaviour with elastomer samples becoming increasingly stiff as strain is increased. Due to hysteresis effects, all of the unloading curves fall below the loading curves

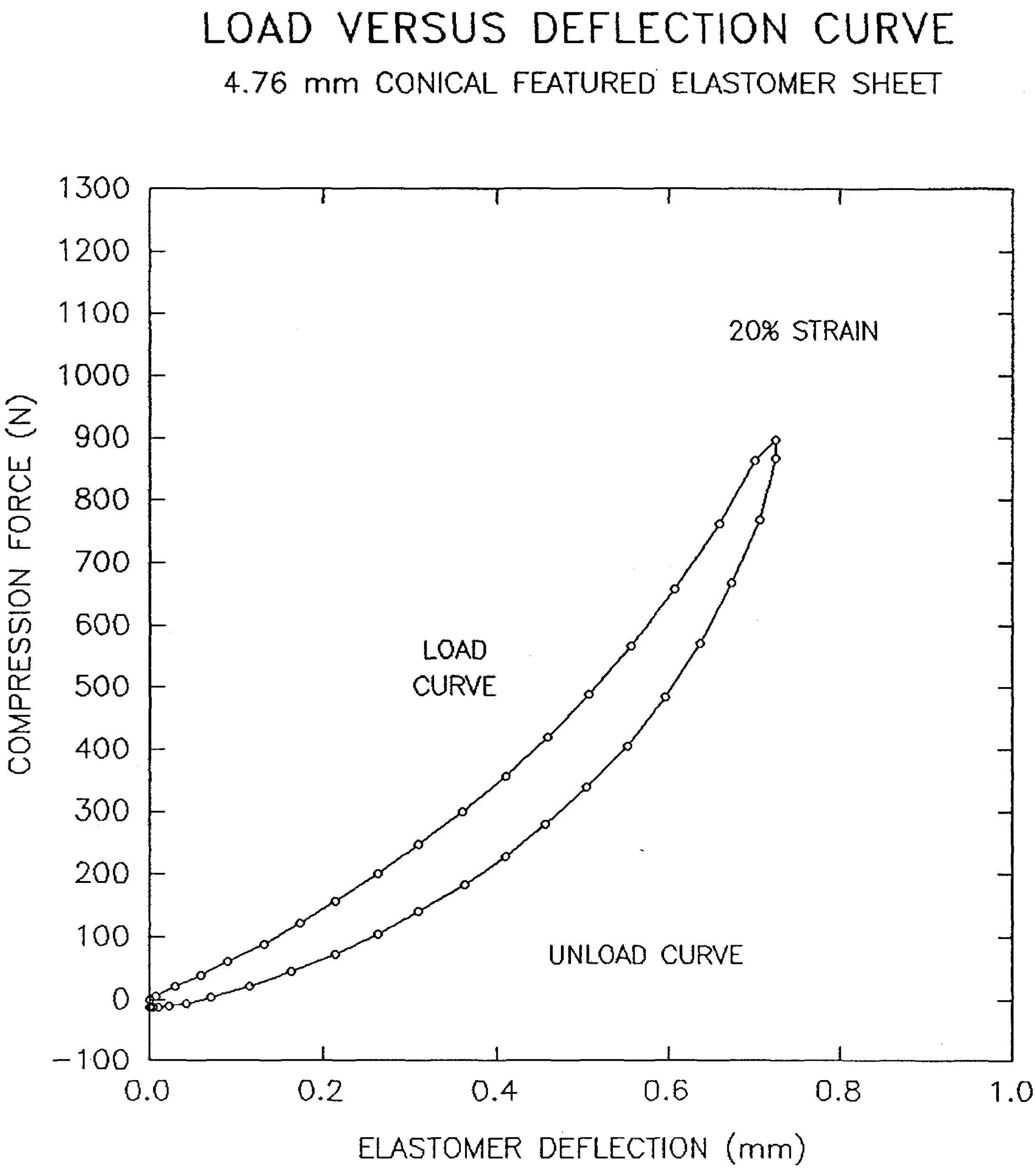

Figure 5.3 Force deflection curve for $30cm^2$ conical featured elastomer sheet loaded to 20 % strain at 3 Hz.

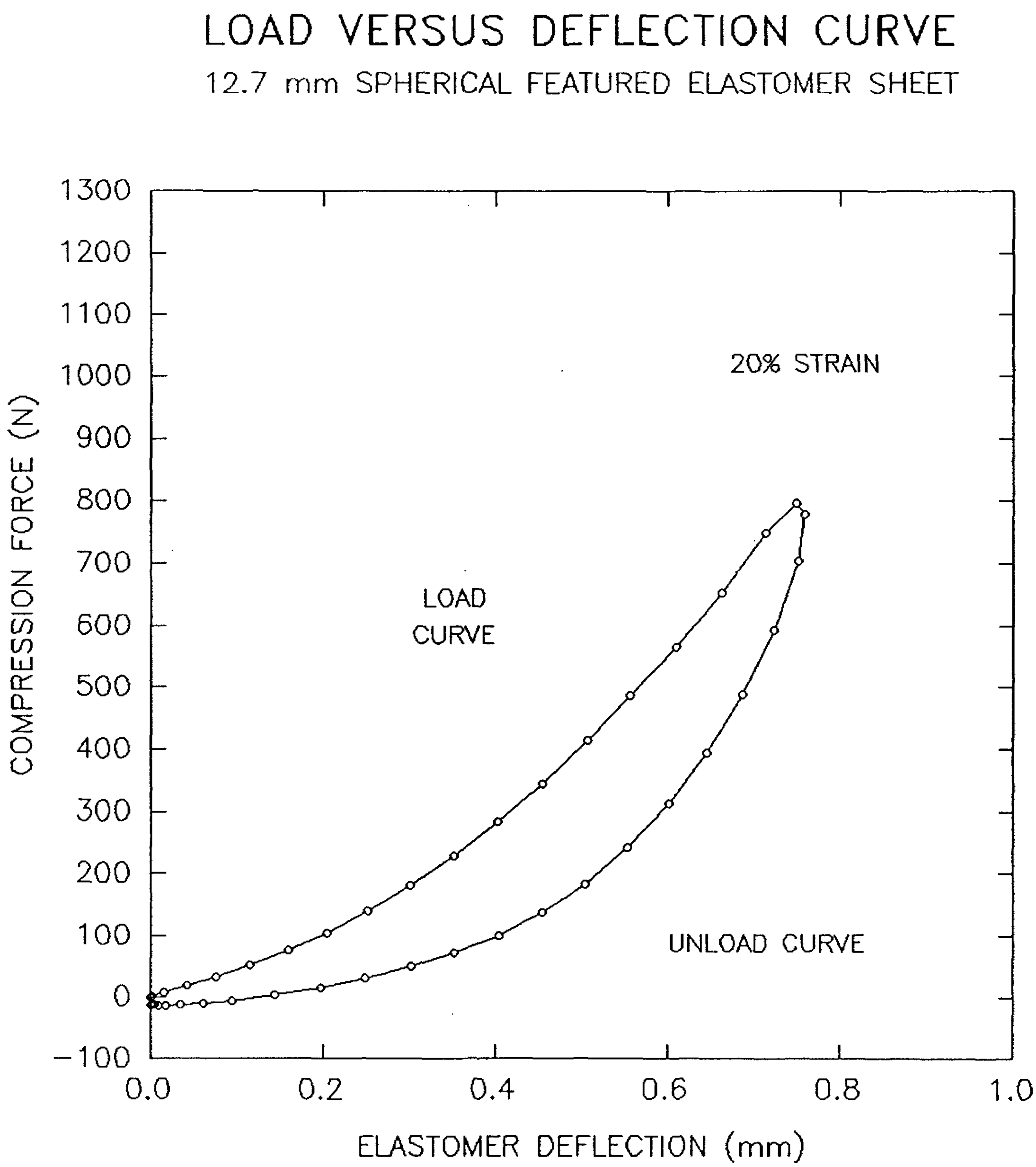

Figure 5.4 Force deflection curve for $30cm^2$ spherical featured elastomer sheet loaded to 20 % strain at 3 Hz.

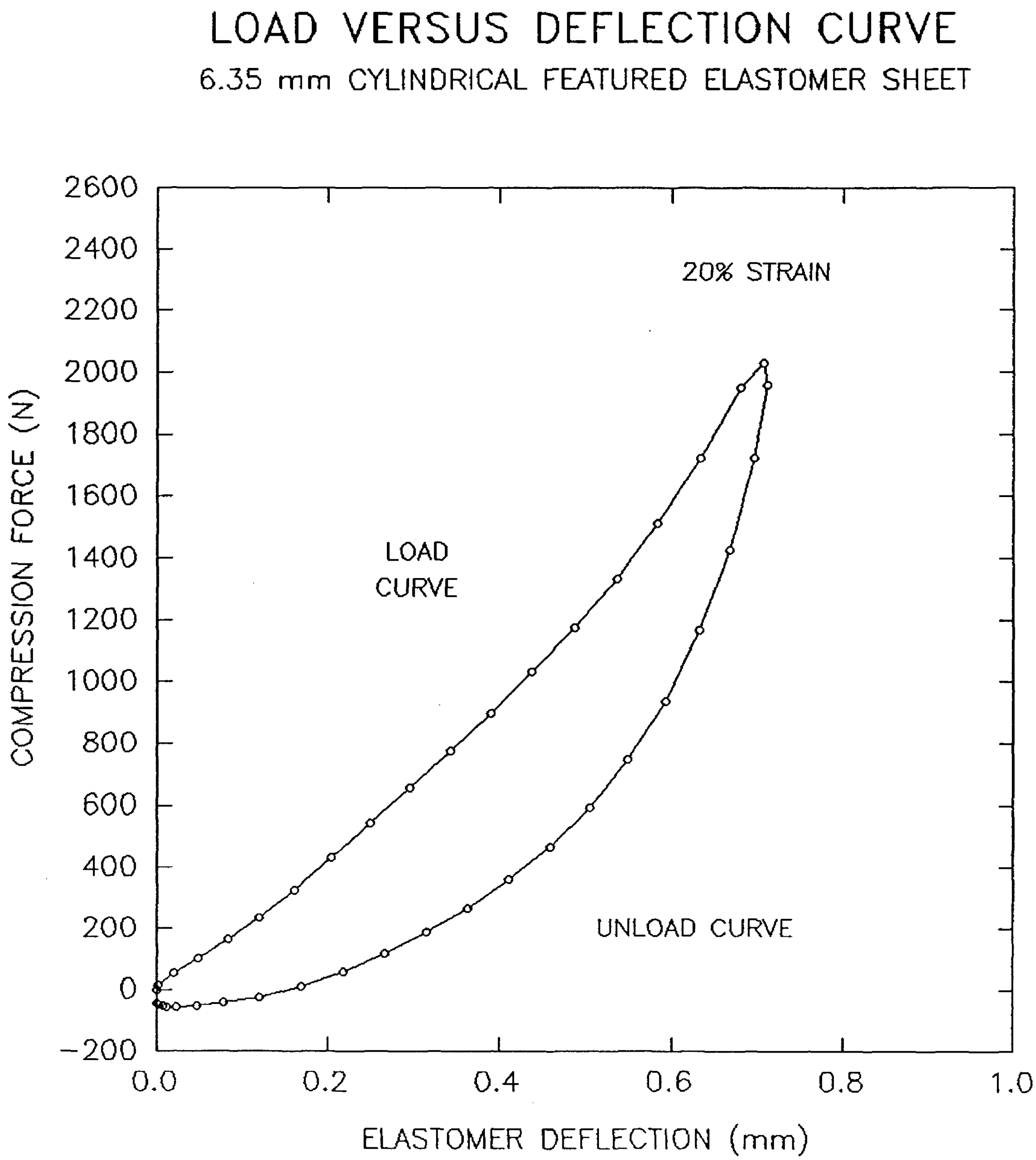

Figure 5.5 Force deflection curve for $30cm^2$ cylindrical featured elastomer sheet loaded to 20 % strain at 3 Hz.

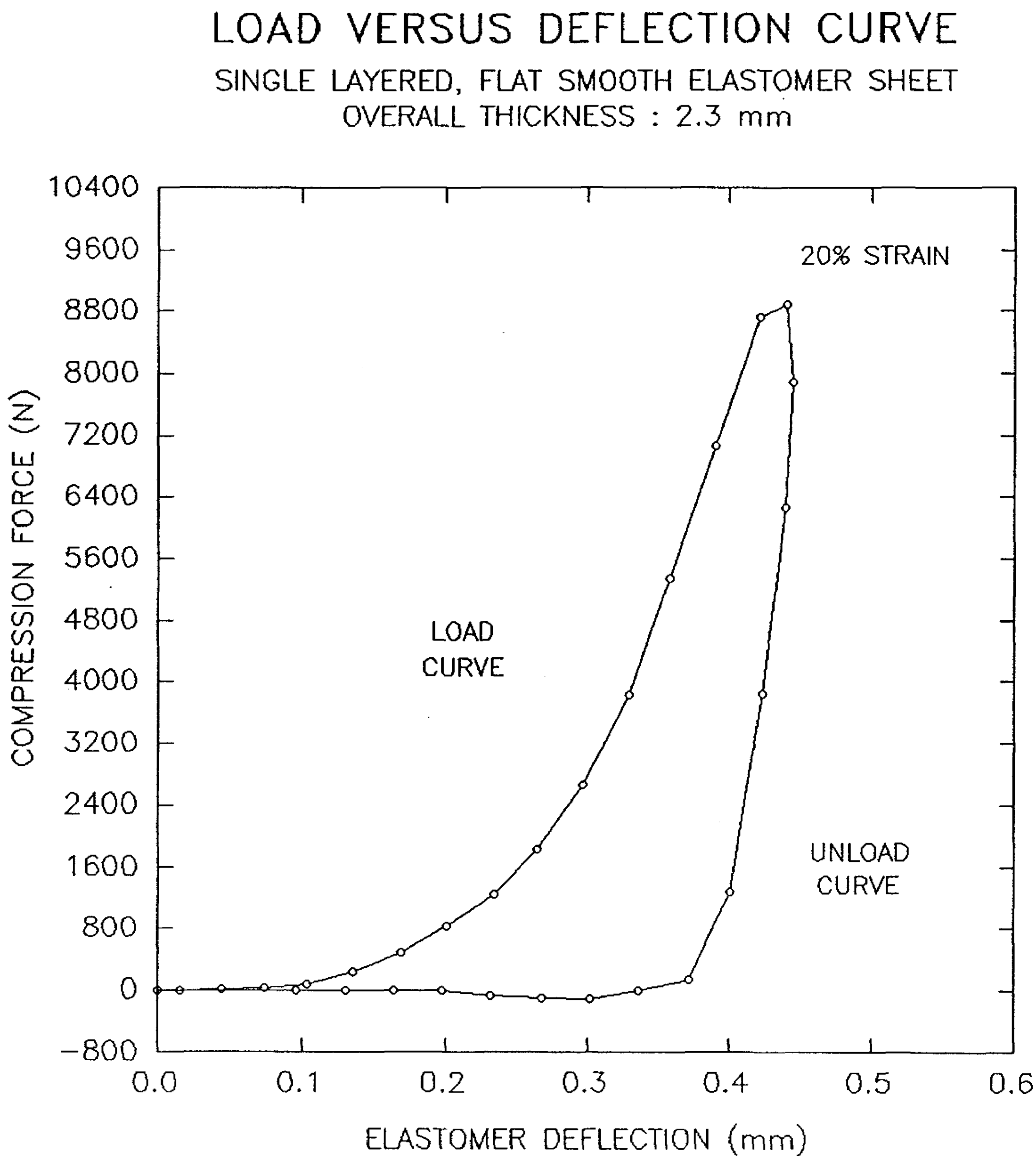

Figure 5.6 Force deflection curve for $30cm^2$ flat elastomer sheet loaded to 20 % strain at 3 Hz.

Elastomer Sample	Compression Force (N)		Hysteresis Loss (%)	
	20% Strain	30% Strain	20% Strain	30% Strain
3.2 mm Sphere	890	-	28.1	-
6.35 mm Sphere	854	-	31.4	-
12.7 mm Sphere	801	1857	46.4	58.7
25.4 mm Sphere	729	-	55.7	-
3.0 mm Cone	694	-	25.5	-
4.0 mm Cone	770	-	26.5	-
4.76 mm Cone	899	2380	29.3	33.9
9.5 mm Cone	632	-	40.5	-
3.2 mm Cylinder	1717	-	41.6	-
6.35 mm Cylinder	2055	5137	50.1	57.8
12.7 mm Cylinder	2317	-	66.9	-
2.5 mm Flat Sheet	9034	-	81.7	-
5.1 mm Flat Sheet	5914	-	92.4	-

Table 5.1 Average compression forces and percent hysteresis losses for elastomer samples loaded to 20% and 30% strains at 3 hz.

reaching a zero force value at some point before the strain itself has returned to zero. At this point the sample can be said to be no longer exerting any resistance on the compresion plates as they are separating. Any subsequent negative valued forces appearing on the curves represent a tensile force on the test sample due to the tendancy of the elastomer to stick to the smooth compression surfaces.

Generally speaking the force versus displacement curves generated for elastomer test samples resemble typical compression curves for rubber. Due to the non linearity simple Hooke's law may not be applied. With such materials it is customary to define a 'secant' modulus whereby the stress required to obtain a certain deformation is quoted. With large strains, the modulus may be more accurately defined by the slope of the tangent to the curve at identified points [43].

A further observation to be noted is that on most of the compression curves the slope of the force curve as well as the force values themselves can be observed to decrease just prior to the point of maximum strain. This decrease is the result of viscoelastic behavior. Elastomers have been described as having a complex modulus which is the resultant of two distinct out of phase components [47]. The first is an elastic component which remains in phase with the strain, and the second a viscous component which is 90° out of phase and in advance of the strain. Since the viscous resistance depends on the rate of deformation, its maximum occurs when strain is increasing most rapidly and vice versa. Although a ramp stroke profile was used on the MTS machine, the hydraulic piston cannot change directions (from loading strain to unloading strain) instantaneously and must experience some deceleration prior to reversing direction. Because of this decrease in strain rate the viscous stiffness component falls off or decreases with the net effect of an overall decrease in stiffness, even though maximum compression strain has not yet been reached.

ii) Sample stiffness

Because it was originally conceived that a maximum service strain of 20% be imposed in the interest of preserving fatigue life, overall sample stiffnesses at 20% strain were of particular interest. Table 5.1 summarizes the average peak force values generated for all test samples compressed to 20% , and those additionally compressed to 30% strain. Spherical and conical featured elastomer sheets required forces in the range of 729 to 890 N, and 632 to 899 N respectively to achieve 20% deflection. Significant increase in forces ocurred with cylindrical and again with flat sheet samples, the former ranging from 1717 to 2317 N and the latter from 3941 to 9034 N. All three samples tested to 30% strain showed large increases in compressive force demonstrating an increasing resistance to further deformation. Increasing the compressive strain to 30% required increases in force of 232% , 265% , and 250% for the 6.35 mm spherical, 4.76 mm conical, and 6.35 mm cylindrical featured shapes respectivley over the 20% strain condition.

An overall observation of the results is that as geometric cross sections more closely resemble a right cylindrical shape, ie) having less and less taper in width from top to bottom, the greater the compressive resistance they possess. This observation was not only seen between shapes, since cylindrical shapes required significantly higher force values, but within shapes as well. With spherical featured sheets as the hemispherical radius decreased, compressive resistance increased. Similarly with conical featured sheets the 3 mm, 4 mm, and 4.76 mm sizes required increasing forces of compression while the 9.5 mm shape required the least force of all having the most gradual taper from top to bottom surfaces (refer to figures 4.2 to 4.4). Because of their constant diameter, cylindrical shapes occupy a greater volume of space for a given height than tapered shapes. A larger volume of elastomer and subsequent greater number of intermolecular attractions to overcome, as well as reduced free space in which to deform resulting in predominantly radial deformations, likley combine to yield greater resistance to compression.

With spherical and conical shapes the effects of shape factor remain difficult to quantify owing to their irregular shapes and changing surface areas of contact during compression. Qualitatively it may be said that there is little difference in stiffness between these two series of shapes tested. For cylindrical shapes having 3.2 mm, 6.35 mm, and 12.7 mm diameters and shape factors of 0.22, 0.47, and 0.87, (these figures include added height from the base sheet itself) the unit compressive loads to generate 20% compressive strain were 133.8, 138, and 152.4 N/cm^2 respectively. For single and double layered flat sheets the corresponding shape factors and unit compressive loads were 6.3, 3.1, and 301, 197 N/cm^2 respectively. These results illustrate the trend of increasing compressive resistance with increasing shape factor.

iii) Hysteresis

In the case of a perfect spring the force versus deflection profile is a straight line with the triangular area enclosed underneath representing the total energy input and stored in the spring. Upon release the return curve coincides with the compression curve and all of the stored energy is returned. Elastomeric materials generally have an enormous capacity to store energy, as high as 150 times that for an equal weight of spring steel [47] however, owing to their molecular nature the return curve never coincides with the compression curve. The resulting area enclosed bounded by the loading curve, unloading curve and x-axis represents a loss of energy which is dissipated in the form of heat. Since all of the force displacement curves presented demonstrated a considerable amount of hysteresis it was decided to quantify this result in the following manner. Using the graphical data points both the loading and unloading curves were integrated to the x-axis using simple trapezoidal rule technique. The difference of these two results for each graph represents the net area enclosed by the curve. The ratios of the enclosed areas to the areas under the loading curves (total energy input) are expressed as percentage hysteresis losses in table 5.1. Values of these results should represent a good and consistent approximation of hysteresis losses.

The results of table 5.1 show high hysteresis losses ranging from 28% to 92% . These results also show a clear trend for the larger geometric supports to have the greatest energy loss. For example, with spherical shapes losses increase from those with the smallest to the largest diameter, opposite to the trend of increasing stiffness with decreasing diameter. Also, the cylindrical shape with a 6.35 mm diameter showed an almost 20% higher loss than the hemispherical support of equal diameter. These results are likely attributable to volume and shape effects as mentioned in section ii) on stiffness, which result in increased amounts of relative molecular movement and hence greater losses.

5.2.3 Discussion

From chapter two it was seen that peak knee joint contact forces have been typically reported in the range of 2 to 4 times body weight. Taking as an example a 70 kg person and peak force value of three times body weight, this translates into a compressive force of 2060 N at the knee joint. Of the samples tested only two of the cylindrical featured samples and both of the flat sheet samples could adequately support such a load without exceeding a maximum design strain of 20%. Owing to a low degree of stiffness spherical and conical samples tested would all meet or exceed 30% strain under such a load. To remain within a 20% strain limit would require more than doubling the number of spherical or conical supports on each sheet. This could not be done without significant overlap of the individual supports since all of these shapes are round and already occupy 50% of available surface area on the base sheet. In the event that knee joint loading were to exceed three times body weight, remaining within both 20% strain, and 30 cm^2 surface area limits would be impossible with these shapes. With flat sheet samples the calculated average knee joint load is easily handled. However, these specimens leave no room for design variation unless surface area is removed in some manner. In this respect the cylindrical featured samples proved best since 15 cm^2 of load bearing surface area of out of a possible 30 cm^2 was required to carry a 3 times body weight force, and still remain within a proposed 20% strain limitation. Not only does this stiffness fall well within the desired range, but the ability to add or delete extra cylindrical supports leaves considerable room to control stiffness, maximum strain and overall design versatility. Thus in terms of compressive resistance to physiological knee joint loads, the cylindrical shaped samples tested appear to be the best suited and offer the most design versatility.

The results of percentage hysteresis losses listed in table 5.1 indicate tremendous potential for an elastomer cushion to dissipate energy from peak knee joint loads, as presented by Morrison [9] for example, for normal gait. Resulting elastomer heat build up, which for some rubbers can have serious effects on mechanical properties, is not anticipated to be a problem in this application owing to the relatively low frequency of cycling and excellent heat resistance of silicone based elastomers. It should be cautioned however that these results represent one compression cycle frequency only. With rubber for example, hysteresis and internal damping coefficient vary with frequency of application so that slower loading rates do not necessarily indicate what would happen at higher frequencies [48].

5.3 Variable Strain Rate Tests

Introduction

The molecular movements involved in deforming elastomers cannot occur instantaneously since intermolecular attractions must first be overcome. At higher strain rates the molecules may not have time to re-arrange with the result that a compliant material behaves more like a rigid solid. Tests with rubber have shown that impact loading usually causes an apparent increase in stiffness [43,47]. In the human knee joint a wide range of loading rates might be imposed on an elastomer cushion, particularly if activities other than walking were considered. For these reasons it was decided to select a few elastomer samples and investigate the dependancy of elastomer stiffness on compression strain rate.

5.3.1 Methods

One representative sheet sample was chosen from each geometric family for testing, namely the 12.7mm spherical, 4.76mm conical and 6.35mm cylindrical featured sheets all 30 cm^2 in surface area. Samples were mounted into the MTS machine as outlined previously in section 5.1. Tests were conducted using a haver sine stroke profile to approximate knee joint loading conditions. It was noted that at high speeds of compression the piston movement deviated from a true half sine becoming skewed on the return stroke. For this reason only the time taken for the piston to travel from rest (0 % strain) to full compression of the sample (20 % strain) was considered. Each sample was loaded beginning from slowest to fastest over a range of different frequencies which resulted in the following range of compression times: 4.5 s, 2.3 s, 500 ms, 110 ms, 52 ms, 40 ms, 33 ms, 27 ms, and 19 ms. Once the hydraulic piston stroke and frequency were adjusted to the appropriate values, each sample was compressed to 20 % strain for at least three trials while piston travel, time to maximum strain, and peak compression force were recorded.

5.3.2 Results

Test results for compression of the three elastomer sheet samples are presented graphically in figures 5.7 to 5.9. Referring to these figures, it is seen that all three test samples exhibited a significant sensitivity to strain rate becoming increasingly stiff as time of compression decreased. The stiffness increase appears gradual within the 5.0 to 0.5 second range rising more rapidly as time approaches zero value. Conical, spherical, and cylindrical samples exhibited overall

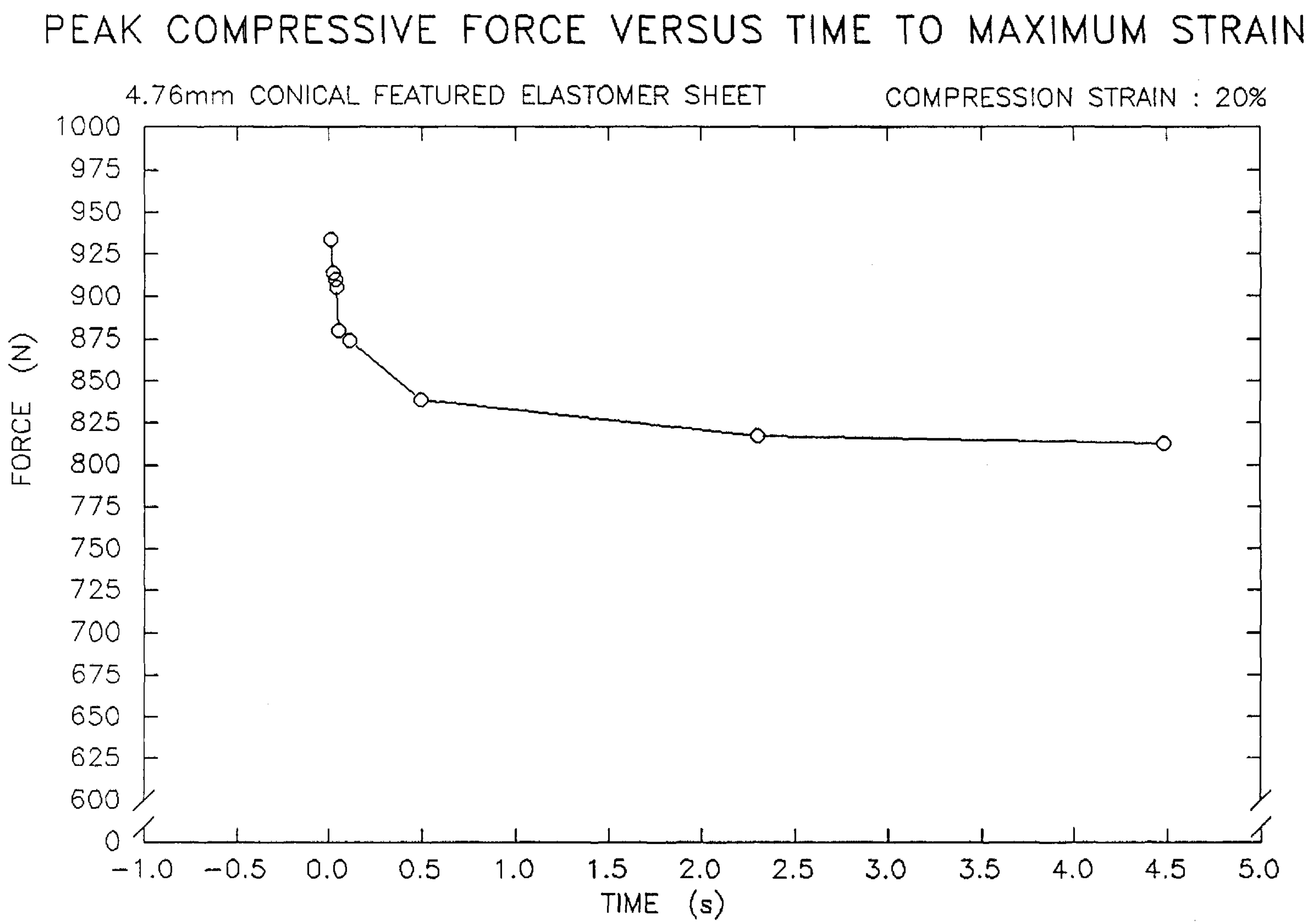

Figure 5.7 Peak compressive loads required to strain conical featured elastomer sheet at various speeds of compression.

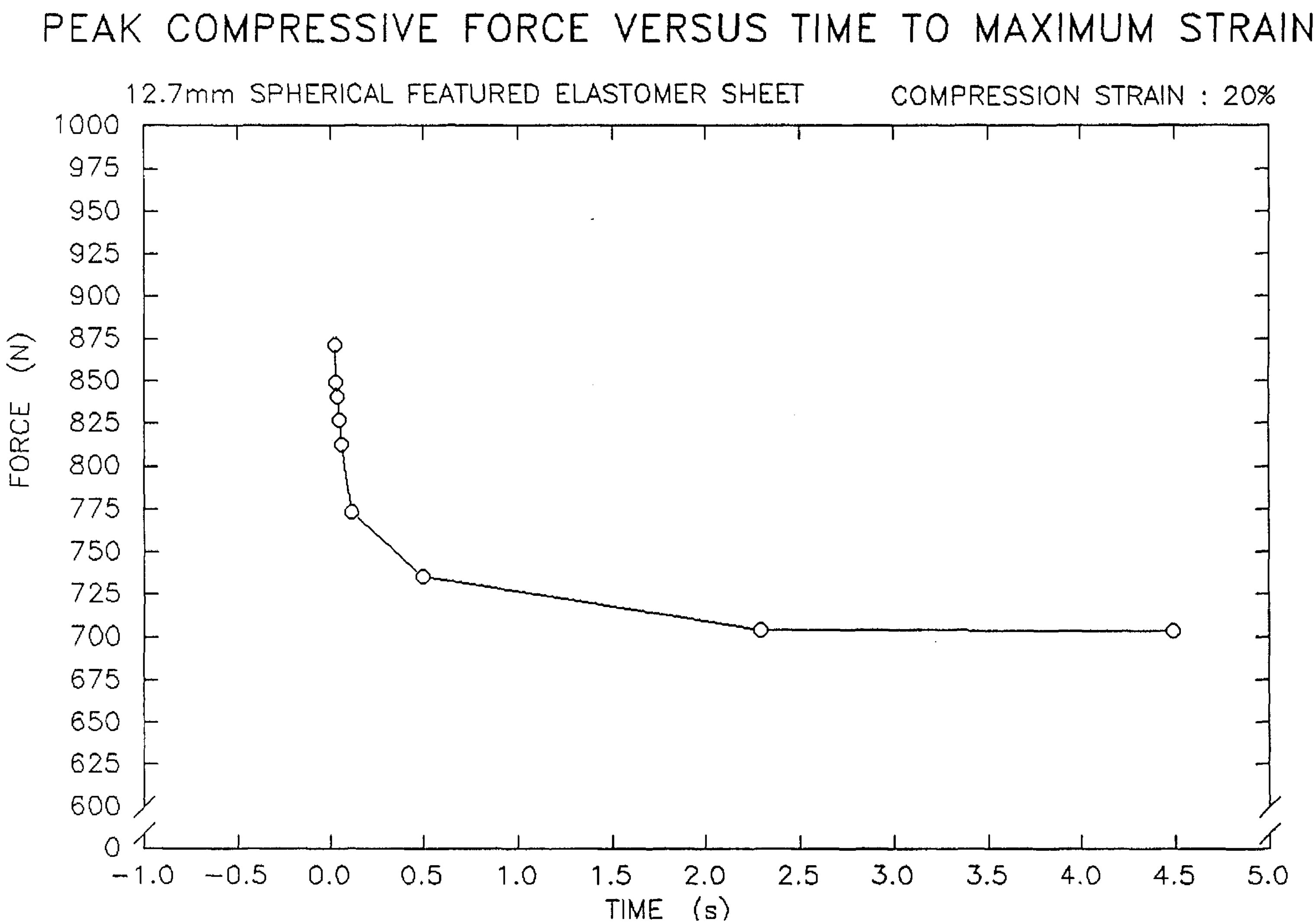

Figure 5.8 Peak compressive loads required to strain spherical featured elastomer sheet at various speeds of compression.

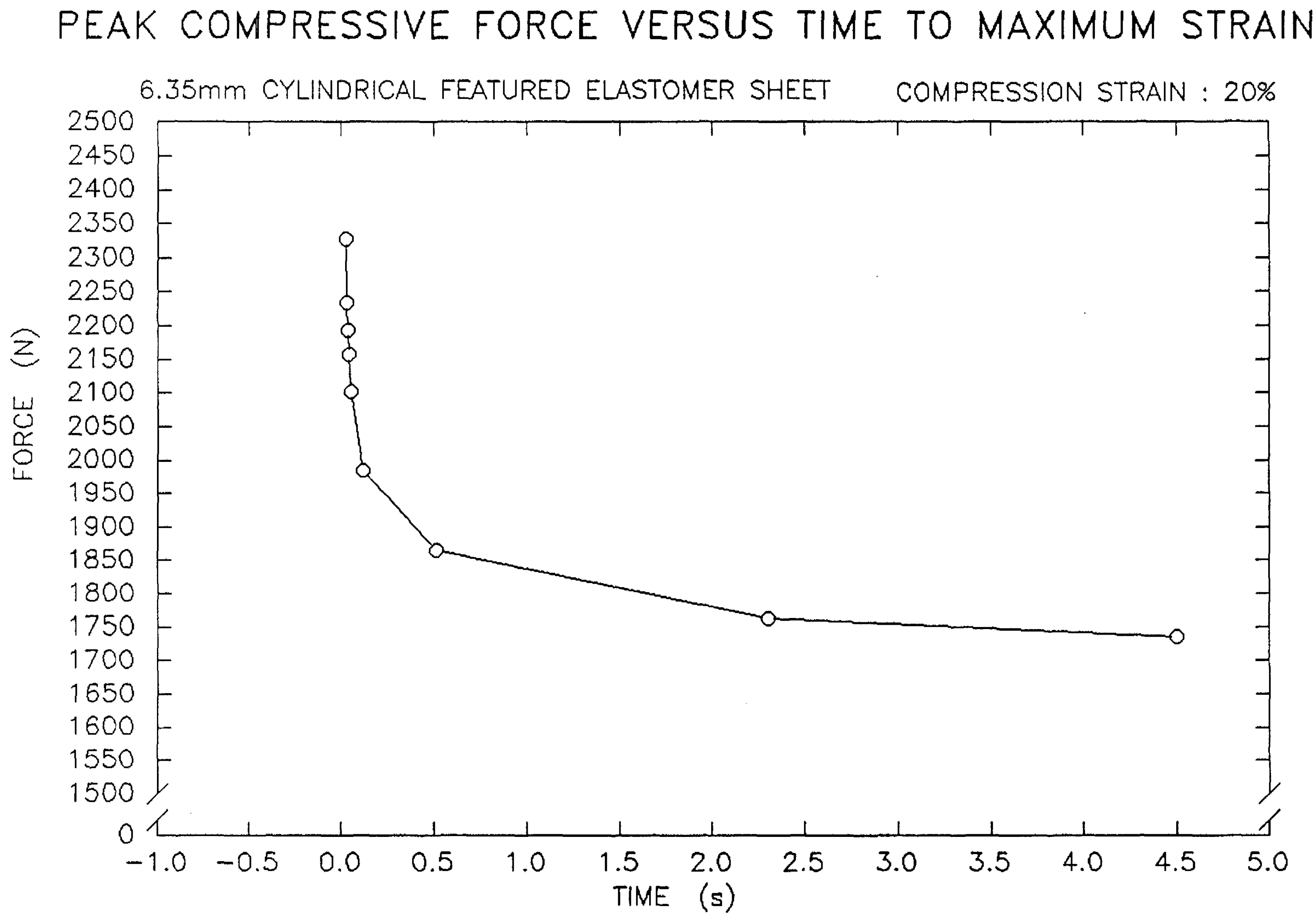

Figure 5.9 Peak compressive loads required to strain cylindrical featured elastomer sheet at various speeds of compression.

increases in compression force of 15% , 24% , and 34% respectively over the range of times tested. The somewhat large differences in percentage force increase can be made sense of if the percentage hysteresis losses for the same three samples of 29.3%, 46.4%, and 50.1% for conical, spherical, and cylindrical shapes respectively, are taken into account. As mentioned previously, due to variations in shape and volume some samples exhibit a greater degree of viscous behavior. Subsequently these samples stiffen to a greater degree when strained rapidly. Strain rate sensitivity then appears dependant upon sample size and shape which determine the degree of viscous behavior.

5.3.3 Discussion

Although limited, these results show that with this material an increase in stiffness can be expected with increased loading rates. This property is desirable serving to keep sample strain at or below a minimum design level when strained more rapidly. Further, the results indicate that a compliant cushion should be designed using stiffness values from slower loading times in the interest of preventing excessive strains during service. That samples could not be compressed faster than 19 ms (due to mechanical limits of the MTS machine) leaves a significant question as to sample behavior at higher strain rates. That is, does the force increase only marginally or asymptotically as compression time is further decreased towards zero?

5.4 Recovery Testing

Introduction

Because walking is such a common daily activity, the vast majority of loads seen by an elastomer cushion in an artificial knee joint would be of a repetitive nature as described at the beginning of chapter two. Since the main intended purpose of such a cushion is to lessen the severity of impulsive loads by deforming under impact, it is essential that the material recover sufficiently to its undeformed state in time to attenuate subsequent loads during walking. Elastomer samples were therefore subjected to repetitive compression loading to assess the materials response and ability to recover.

5.4.1 Methods

The 4.76 mm conical, 12.7 mm spherical, and 6.35 mm cylindrical featured elastomer sheets were chosen for testing. Samples were mounted in the MTS machine as in previous tests. Each of these three samples was subjected to repetitive compressions from 0 to 20% strain to a total of 5000 cycles. A sinusoidal stroke profile at 3 hz frequency was used to simulate rapid knee joint loading. In addition to these tests, it was decided to try a more severe or worst case test condition. Subsequently the cylindrically featured sample, having the greatest hysteresis loss and stiffness values, was further cycled to 30% strain at 3 hz, and to 20% strain at 5 hz, both for a total of 1000 cycles.

For each test conducted a sampling of stroke and force voltage signals was captured on the digital oscilloscope as the test was initiated. Several parameters were measured including peak and minimum stroke and force values, times at which they occurred, time at which force falls to zero, and any amount of decay in peak force values over time. Once the desired number of cycles was reached, a sampling of stroke and force voltage signals was again stored and the various parameters remeasured. Stoke and force voltage signals were also sent to the A to D board and sampled at 100hz for computer storage and plotting.

It was reasoned that if the recovery times of the HP100 elastomer samples were slower than the MTS machine cycling frequency the elastomer samples would not maintain constant contact with both compression plates, particularly on the piston return stroke from maximum to zero compression strain. Slowness in recovery or tendancy of the elastomer to separate from the upper compression plate would be readily apparent by a sudden decrease in measured force by the quartz ring mounted directly above the upper compression plate. In this way elastomer response to the MTS cycling speed, and hence ability to return to its undeformed state could be evaluated.

5.4.2 Results

Results of repetitive cycling tests are presented graphically in figures 5.10 to 5.14 where compression forces are plotted against time for each test condition. Referring to these figures it is seen that

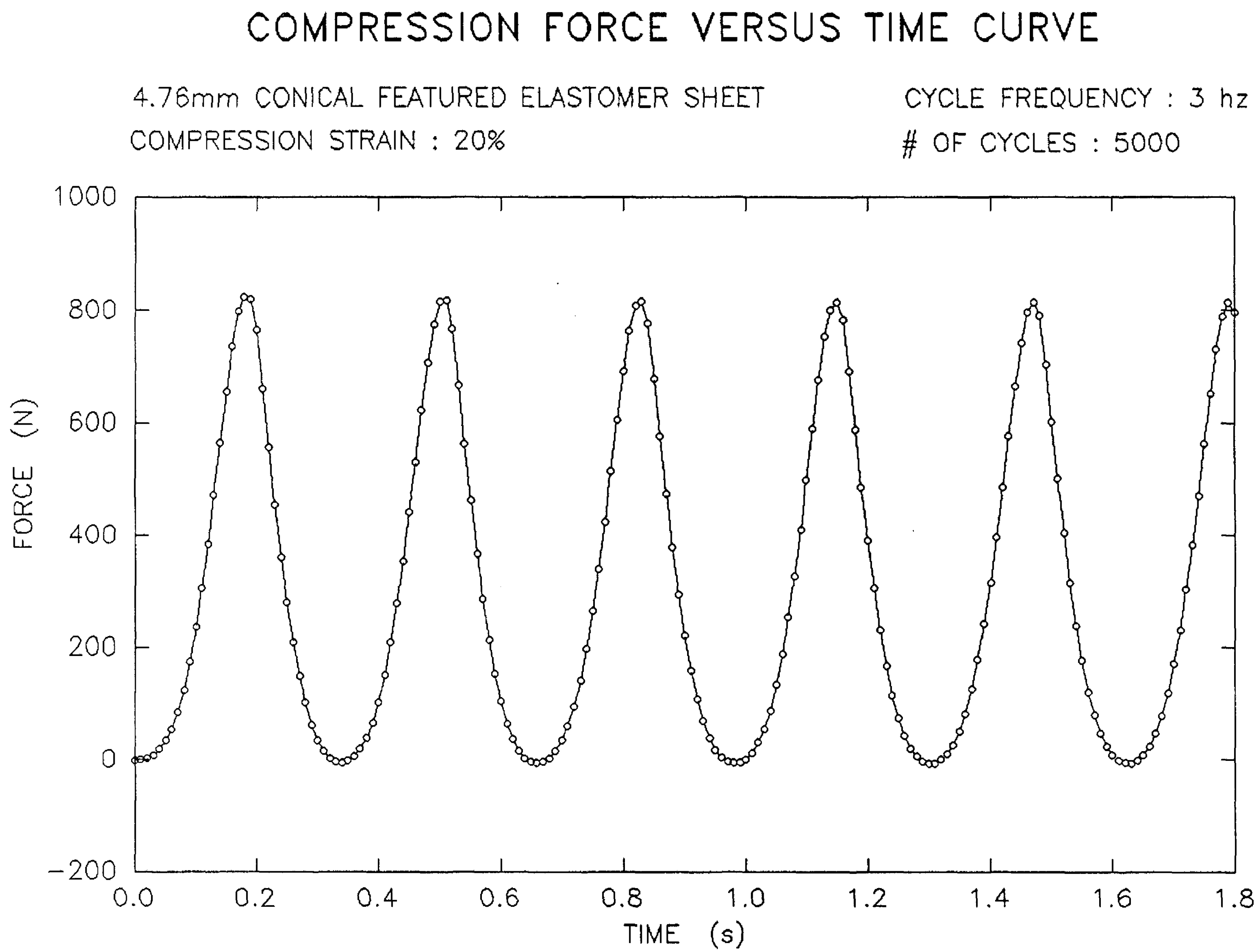

Figure 5.10 Force response profile of a conical featured elastomer sheet to repetitive sinusoidal strain cycles.

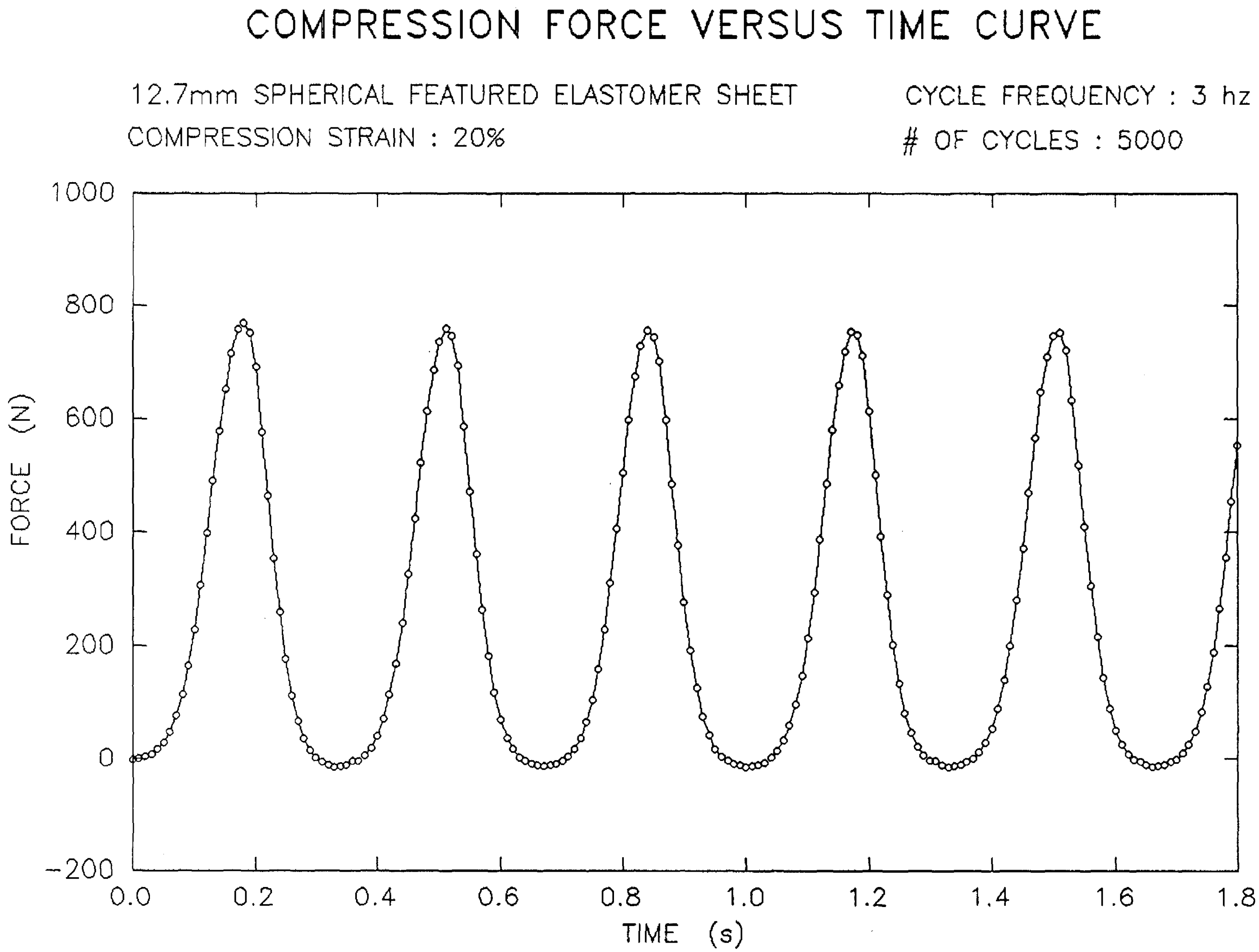

Figure 5.11 **Force response profile of a spherical featured elastomer sheet to repetitive sinusoidal strain cycles.**

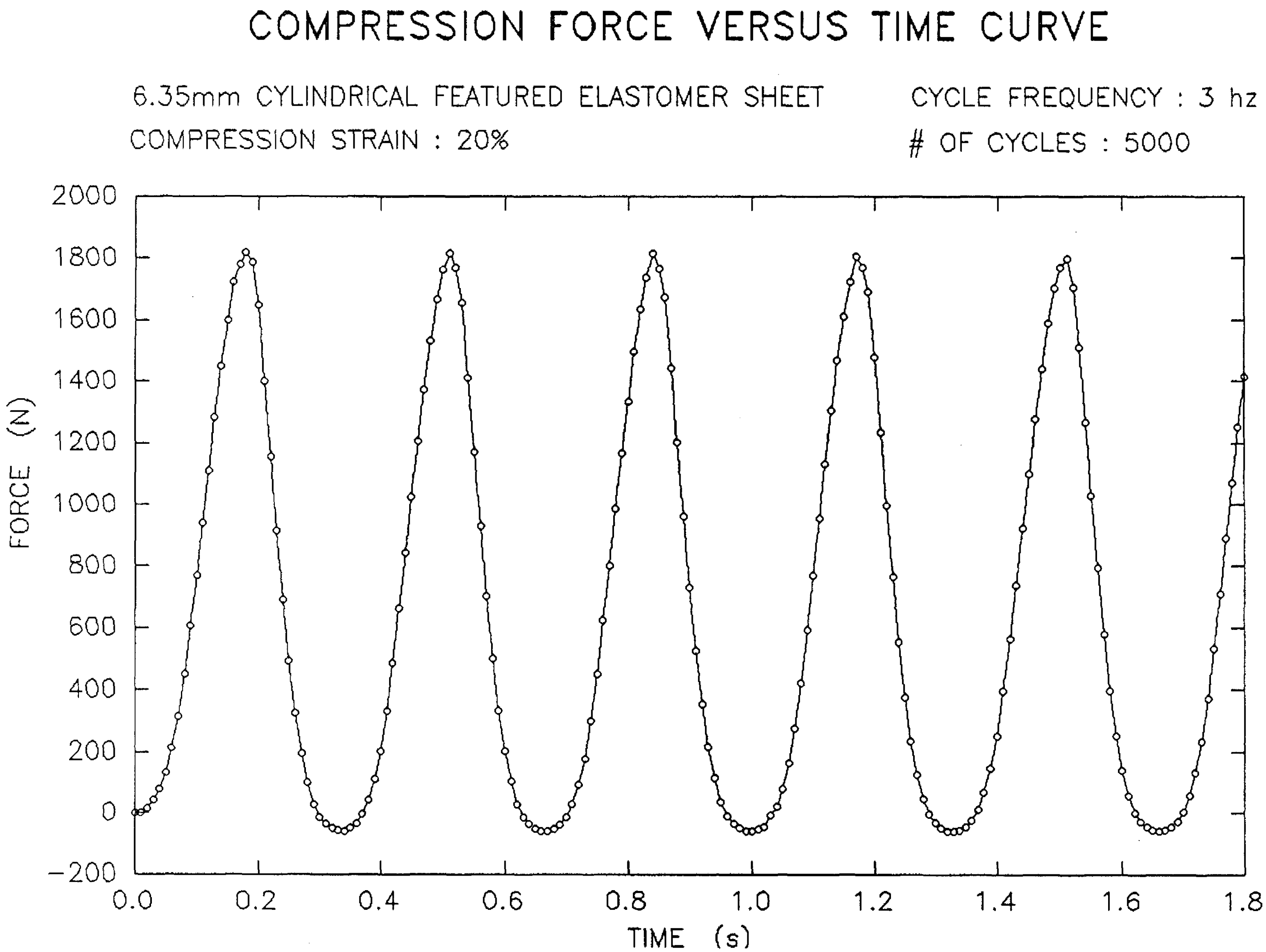

Figure 5.12 Force response profile of a cylindrical featured elastomer sheet to repetitive sinusoidal strain cycles.

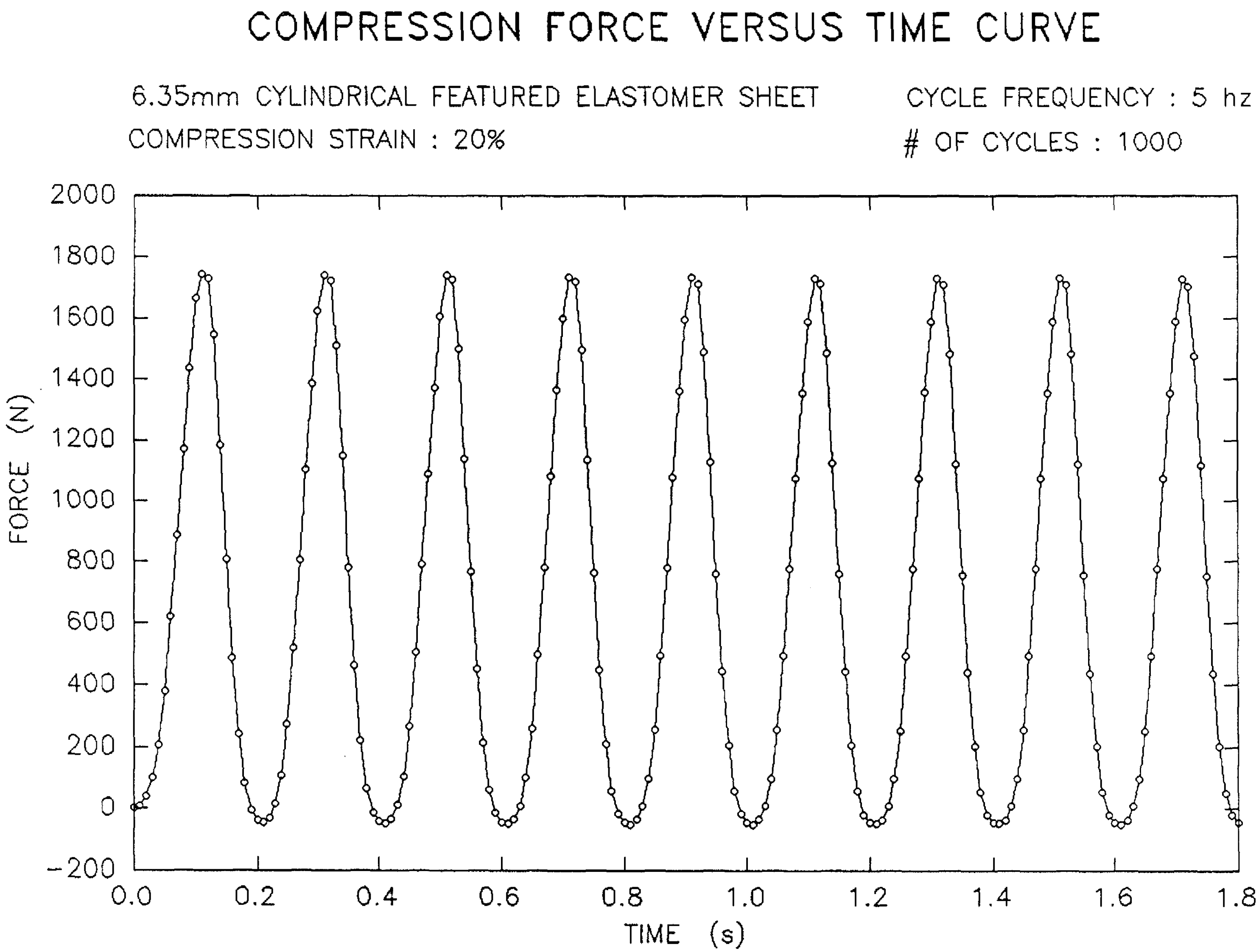

Figure 5.13 Force response profile of a cylindrical featured elastomer sheet to repetitive sinusoidal strain cycles.

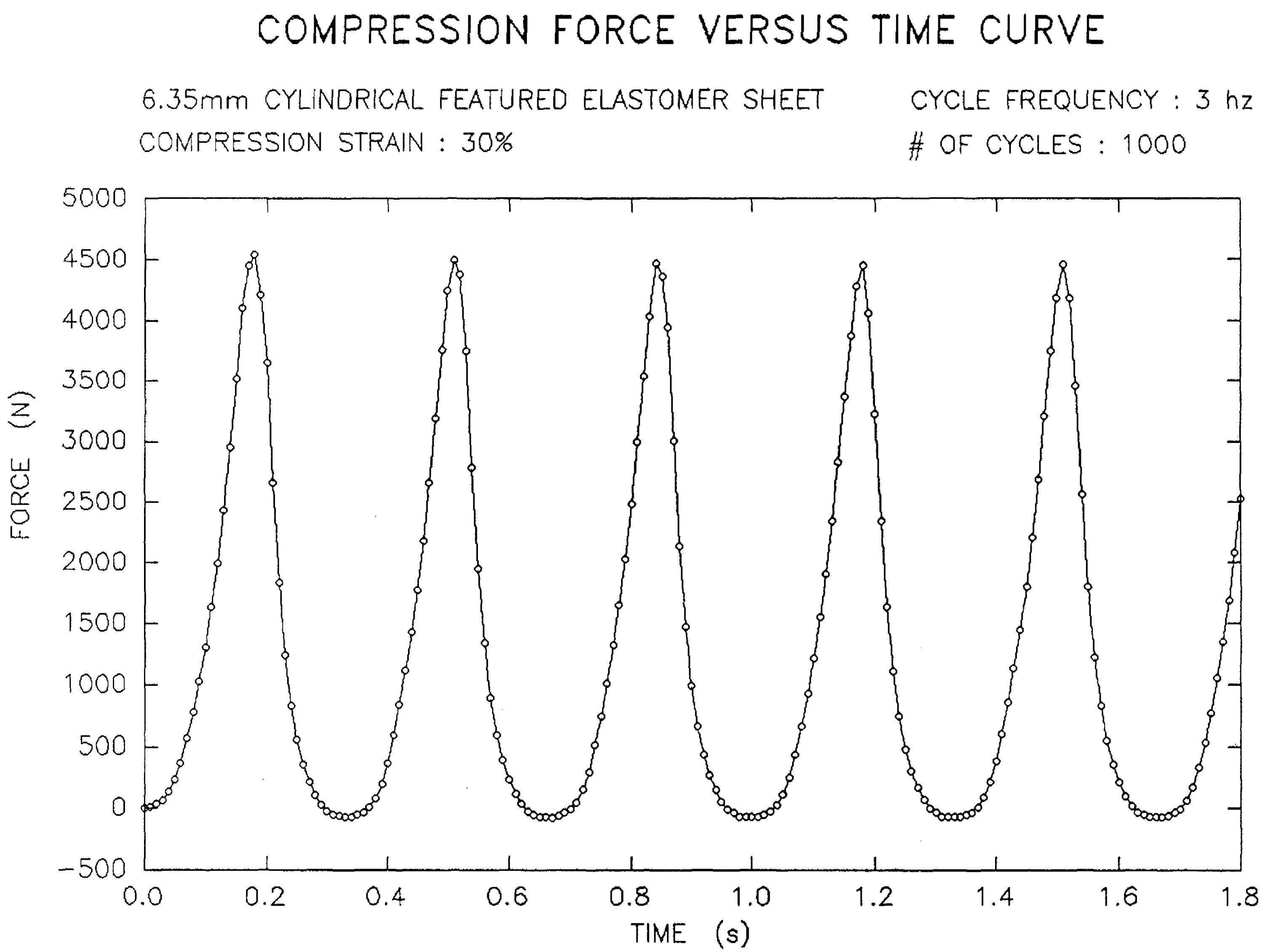

Figure 5.14 Force response profile of a cylindrical featured elastomer sheet to repetitive sinusoidal strain cycles.

the force versus time curves generated all show a smooth continuous force response to cycled strain. All of the curves exhibit a period of time over which the compressive resistance force of the elastomer sample becomes zero. As with the force versus deflection curves positive force values represent compressive resistance while negative values indicate a slight tensile force on samples due to their tendancy to 'stick' to the smooth compressing surfaces. Periods of zero or negative force all occurred as the strain cycle neared and passed through its minimum. The general absence of discontinuities or sudden vertical drops to zero in the force profiles indicate that the elastomer samples remained in contact with the compression plates, and responded continuously with repeated strain.

The effects of a viscous component of modulus which is strain rate sensitive were again noted as in section 5.2.3. Owing to deceleration and acceleration of the hydraulic piston during the sinusoidal cycle, compressive resistance of the elastomer fell to zero prior to the point of minimum strain and remained until some time after the zero strain point had passed. Anaylsis of the data recorded showed that for the 20% strain and 3 hz test condition, conical, spherical, and cylindrical featured samples spent 10.7, 20.9, and 23% respectively of the total force cycle time exerting zero compressive resistance. Again these figures appear to roughly correlate with the percentage hysteresis losses for the same samples of 29.3, 46.4, and 50.1% respectively as presented in table 5.1. As would be expected samples exhibiting a greater degree of hysteresis are less able to maintain an elastic response under cyclic loading. For the cylindrical featured sheet cycled at 3 hz and 30% strain, and at 5 hz and 20% strain, the percentage times of no compressive resistance were 20% and 22.2% respectively. These percentages overall are surprisingly low given the high degree of hysteresis exhibited by the same samples under single cycle loads.

With repeated compressions elastomer samples exhibited significant reductions in peak force over the single cycle case. For the 3 hz and 20% strain condition conical, spherical, and cylindrical samples showed peak force reductions relative to the very first compression stroke of 8, 5, and 11% respectively. For the cylindrical sheet sample at 3 hz and 30% strain, and 5 hz and 20% strain test conditions the force reductions were 15% and 16% respectively. The vast majority of these reductions in compressive force occurred in the first five cycles. Thereafter any decrease was very small and gradual with no further decrease at the 1000 or 5000 cycle marks. Other parameters defining the force profiles such as period, time of peak force, time at which force falls to zero and duration of zero force all remained extremely consistent and repeatable, indicating no other changes in the force profiles over the number of cycles tested.

5.4.3 Discussion

Overall these results bode well for the repetitive use of elastomer shapes tested. Samples showed various degrees of viscous behavior but were able to keep up with the repeated strain exhibiting no loss of contact with the compressing plates. During normal walking actual stance phase or loading cycle time would be closer to 0.6 seconds. In addition stance phase is followed by swing phase lasting about 0.4 seconds during most of which the knee joint is lightly loaded. Both of these factors would mean that during actual walking the elastomer would have more time to recover than in the current test, and would not have to recover completely to zero strain after each loading cycle. Thus while elastomer samples may not have returned to their exact undeformed state, and actual percent recovery was not quantified, the samples tested appear dynamically responsive enough to handle repeated loads at normal gait speeds and faster. Lastly these results indicate that an allowance for a 10 %to 15% reduction in overall stiffness with repetitive use should be factored into an elastomer cushion design.

CHAPTER SIX

IMPACT TESTING

Introduction: Compliancy And Shock Reduction

In many shock absorbing applications a degree of damping is employed depending on the required response, with the desirable effect that some of the input energy is dissipated in the form of heat. However, the goal in achieving maximum attenuation need not be to maximize damping. A compliant material may provide significant shock reduction benefits simply through deformation and elastic storage of energy, as highlighted by the following example. A perfectly rigid sphere of fixed mass is allowed to fall to impact upon two different flat surfaces. The first flat surface is rigid, and the second an equally rigid surface covered with a compliant elastic sheet of material analagous to rubber. The results of these two impacts are described as follows:

Case i) Rigid flat surface: In this case because the impacting surfaces do not yield or deform the falling sphere is stopped abruptly to zero velocity, and quickly rebounds. Stopping the sphere in a short amount of time requires a high deceleration value and subsequently a large force must be provided by (and is exerted on) the flat surface. An appropriate force versus time profile for the total impact and rebound is illustrated in figure 6.1 a).

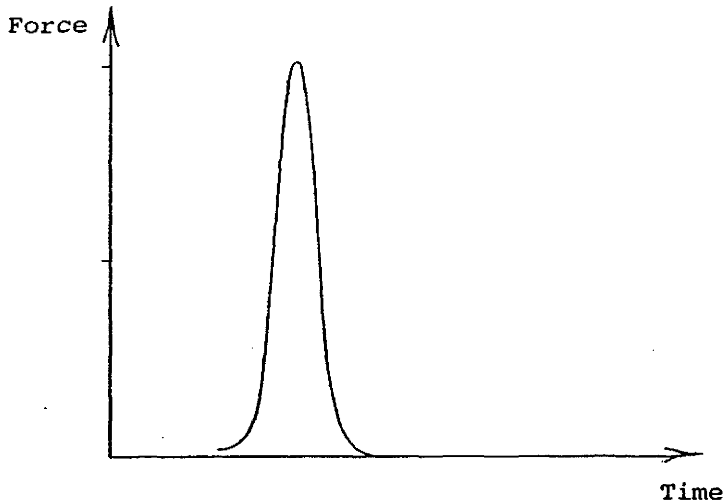

(a) rigid surface

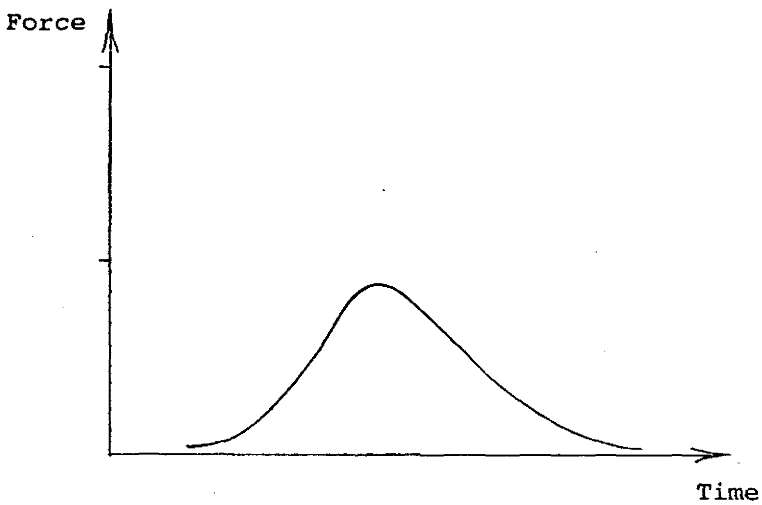

(b) compliant layered surface

Figure 6.1 Force versus time profiles illustrating the effects of adding a compliant interface to a solid impact.

Case ii) Compliant layered surface: In this case because the compliant surface is able to yield as the sphere strikes, the sphere is slowed to a stop more gradually, over a longer time period against increasing resistance of the compliant layer as it deforms. As a result the sphere experiences a lower deceleration value requiring less force to be provided by (and exerted on) the underlying flat rigid surface. The resulting force versus time profile for this case is illustrated in figure 6.1 b).

Since the same sphere and drop heights were used in both cases the momentum involved in bringing the falling sphere instantaneously to rest is the same in both cases. Recalling that impulse and momentum are related by;

$$F \times \Delta t = M \times \Delta v$$

where; F = applied force

Δt = time period of applied force

M = mass of object (sphere)

Δv = velocity change of object (sphere)

and assuming no energy losses, the areas under the two force versus time curves in figure 6.1 are the same. The compliant layer therefore served to change the overall shape of the force versus time profile resulting in two important benefits; firstly a reduction in peak transmitted force, and secondly a reduction in the rate at which the force is applied thereby reducing the strain rate experienced by the impacting surfaces.

6.1 Experimental Focus

The hypothesis of the current work as stated at the outset relies on the ability of a layer of cushioning material to provide significant shock reduction benefits. The numerous potential benefits , both mechanically and physiologically, resulting from peak force and strain rate reductions were discussed in chapter two. The main problem in assessing the ability of HP100 elastomer to cushion physiological impacts was that a reference condition had to be established where the effects of adding (or removing) elastomer samples could be quantitatively evaluated in a meaningful way. It therefore became necessary to simulate not only physiological impact loading, but the prosthetically replaced knee joint itself. Ideally such a simulation requires the use of cadaver knee joint specimens fitted with prosthetic replacements, and it was decided to pursue this approach. The focus of the work presented in this chapter therefore was to first create a prosthetic knee joint test jig incorporating human bone and prosthetic materials. Then, by applying physiological impacts to the test jig, evaluate the potential of the HP100 elastomer samples to attenuate these loads in vitro.

6.2 Drop Test Apparatus

The apparatus available for testing was a Lansmount Corporation Model # 23 Shock Test System pictured in figure 6.2. This system basically

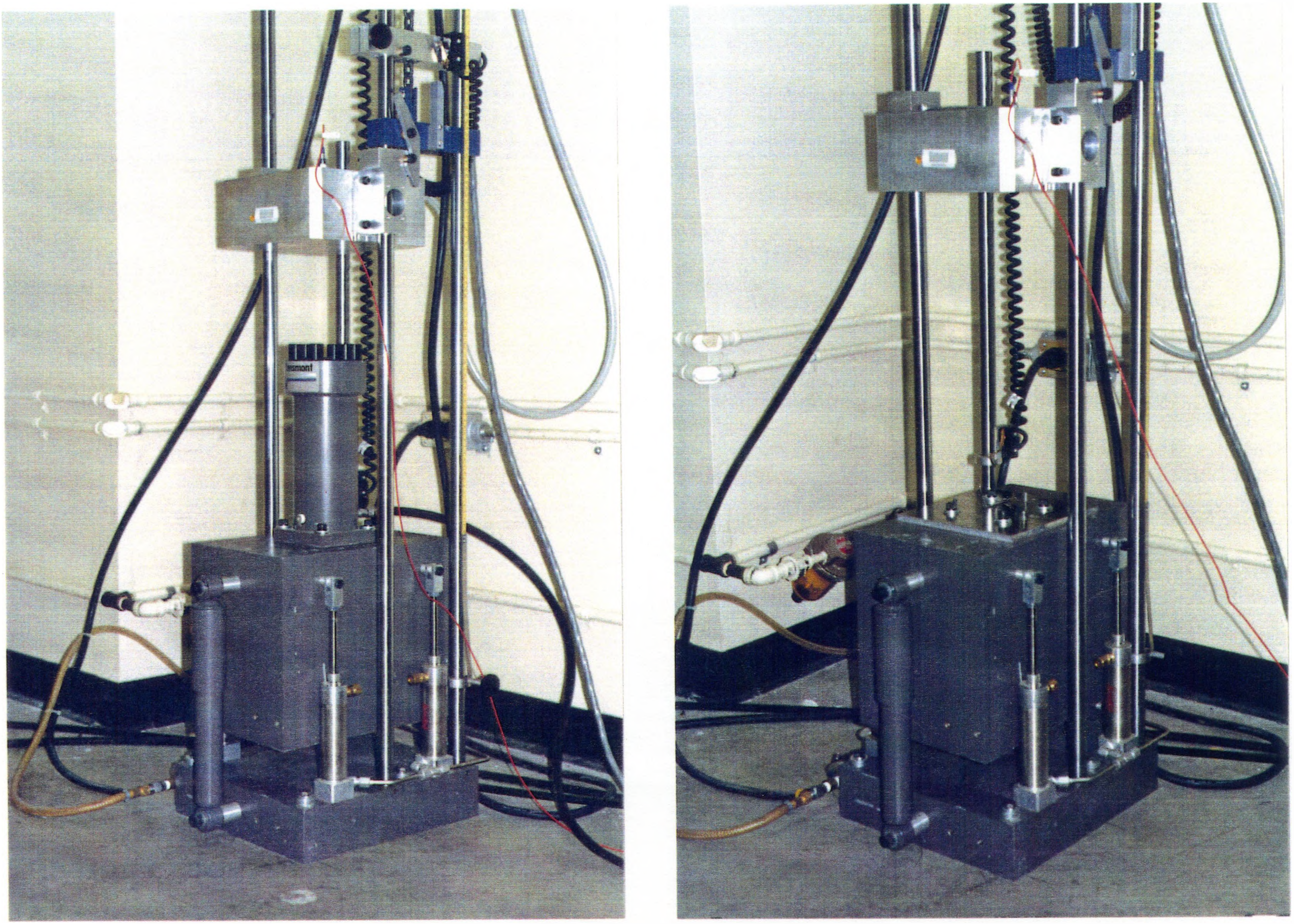

Figure 6.2 Drop test table. Left; with programmer in place. Right; as used for tests herein, with programmer removed and aluminum plate bolted in place.

consists of a 23cm $\times$ 23cm metal drop table 18kgs in mass which is guided on vertical bearings. The bearings in turn are supported by a heavy rectangular floor mounted base. The table can be suspended to any desired working height (up to about 1.5 m), and released to free fall by means of internal air brakes which clamp onto the bearing rod surfaces. A cylindrical unit (seen in figure 6.2) mounted to the rectangular base called a 'programmer', can also be used to determine the type of shock loading, ie) sine or square wave type, through the use of special contact pegs and variable nitrogen pressure within the cylinder. It is possible to use the drop test table apparatus in two different configurations. In the first, the object to be tested is bolted to the table top and the table released to impact with the programmer. An accelerometer mounted to the object records the impact experienced by the object. In the second configuration the programmer is completely removed leaving an exposed flat surface on top of the base unit that is parallel with the underside of the table. A test object is then mounted to the top of the base unit and the table released to fall onto the object. In this case an accelerometer mounted on the table records the shock experienced by the table and hence that imparted to the object. The latter of these two methods is often used to evaluate different cushioning materials, of varying thicknesses and surface areas.

Additional equipment used in conjunction with the drop test table and control panel included an endevco model # 2225 accelerometer, and

Kistler Model # 5004 charge amplifier. Shock pulses were recorded and analysed on an AT computer using Lansmount Corporations Test Partner shock software version 1.21.

6.3 Test Specimens

6.3.1 Embalmed Bone

Although fresh unembalmed bone is always preferrable for experiments, specimens can be very difficult and time consuming to obtain particularly if several are required. For the current study bone specimens from embalmed cadavers were readily available. However, concern existed as to what extent embalming might alter the properties of retrieved bone samples and thereby affect experimental results. In a review of the effects of embalming on the mechanical properites of bone by Evans [45], various and sometimes contradictory results are presented. In one of the studies reviewed (conducted by Calabrisi and Smith), human cortical bone plugs showed a 17% increase in ultimate compressive strength due to embalming, while in another study (by McElhaney et al), tests conducted on cortical beef bone revealed little change in various properties except for a 12% decrease in ultimate compressive strength and a 6% decrease in compressive modulus of elasticity. Tests conducted on wet cortical bone from adult human tibias by Evans, revealed mean increases of 16% and 10% in modulus of elasticity and ultimate tensile strength values respectively with embalmed specimens. A separate study Greenburg et al [46] reported that the flexural spring rate for centrally loaded tibia-fibula complexes of adult dogs was stiffened by an average of 8% as a result of embalming. While all of these studies typically show some change in one or more mechanical properties due to embalming, these changes are generally not large. Both Evans and Greenburg reported greater changes in mechanical properties of bone as a result of drying. In a review of the effects of drying Evans [45] notes that all investigators have found significant increases in tensile and compressive strengths, elastic moduli and hardness values, as well as decreases in energy absorbing capacity of the order of 28% with drying. It was therefore decided that for the current investigation acceptance of embalmed test specimens would not offset experimental results to a large degree so as to be invalid. Moreover the importance of keeping bone specimens moist was realized.

6.2.3 Test Configuration

Design of the knee joint test configuration evolved to its final form out of both experimental and practical limitations. Because testing involved cushioning assessment of a material the second of the two apparatus configurations described in section 6.2 had to be used. This required that the knee joint test configuration bolt directly to the base of the shock test machine and be subjected on top to vertical impacts from the falling table. Bone and prosthetic specimens therefore had to be rigidly secured in an upright position. Remembering the basic goal of elastomer evaluation and considering the potentially large experimental scope, it was decided that testing be limited to uniform flat faced impacts only. Special conditions such as eccentric or uneven loading were not considered. In keeping with the perceived elastomer placement discussed in chapter four, elastomer samples would be located between polyethylene and metal tibial components. Also, since several identical knee joint prostheses were not available for testing all prosthestic components had to be simulated using the appropriate materials.

In light of these factors it was decided that incorporating the femoral prosthetic component into the experiment added unecessary complexity. Factors such as joint conformity, alignment, and angle of flexion would all have to be addressed. Since flat faced impacts were required, impact loads could be transmitted directly to the polyethylene tibial component from the drop test table. As a result femoral prosthetic components and bone specimens were omitted entirely. The final form of the test configuration was therefore comprised of proximal tibial cadaver bone specimens vertically mounted, and fitted with simulated tibial prosthetic components made of the appropriate materials. Elastomer sheet samples were to be placed freely between metal and polyethylene tibial components. Both of these components also had to be aligned parallel with the underside of the drop test table in order to absorb flat faced impacts.

6.3.3 Tibial Specimen Mounting And Preparation

Five embalmed proximal tibial specimens were retrieved and cleaned of soft tissue. From each specimen the tibial plateaux were excised with a minimal amount of bone removal so as to just leave a flat exposed surface of cancellous bone roughly perpendicular to the long axis of the bone. Overall final specimen lengths averaged 11.5 cm. All of the specimens were approximately fifty to sixty years of age.

To hold the tibial specimens five metal rings were fabricated each 4.5 cm in height with an outer diameter of 9 cm, and 0.5 cm wall thickness. Into the side of each ring three holes were equally spaced through which three locating screws could be threaded. Each ring could also be mounted to a 20 x 20 x 0.95 cm aluminum base plate by means of three 'L' shaped brackets. These brackets were first bolted to the ring sides leaving a small gap between the bottom of each bracket and base plate. The brackets were then bolted directly to the base plate drawing the plate and ring tightly together. To secure the tibial specimens each ring in turn was bolted to the base plate and a specimen held upright in the center using the locating screws. By direct measurement the flat proximal tibial surfaces were aligned as parallel as possible with the aluminum base plate. Liquid cerrobend (a low melting point alloy used for fixturing) was then poured into each ring and allowed to cool until solid thus securing each specimen within its ring which could then be removed from the base plate.

Once fixtured in their rings each tibial specimen was fitted with a simulated prosthetic tibial component. Stainless steel plates 1.25 mm in thickness were cut for each specimen so as to cover the entire proximal surface and just overlap the cortical shell on all sides. Stainless tibial components were adhered to the bone using polymethylmethacrylate cement and lightly pressed into place using a metallurgical sample press. Use of this hand operated press helped ensure penetration of the cement into the cancellous bone, as well as parallel alignment of the flat stainless component with the aluminum base plate. To simulate the polyethylene component a single flat rectangular block 10 mm in thickness and 35 cm^2 in surface area was machined from ultra high molecular weight polyethylene sheet stock. This block rested flatly on top of the tibial specimens being held against the stainless steel component by two small tension springs pulling downward from either side of the block to the base plate. The underside of the polyethylene block which rested against elastomer samples was left unmachined having a very clean smooth factory finish.

6.4 Test Method

With the shock programmer removed the aluminum base plate was bolted to the shock test machine base unit. Each of the five potted tibial specimens were in turn mounted tightly to the base plate and tested. Figure 6.3 shows a tibial specimen mounted with an elastomer sample in place. During the course of testing bone samples were kept wrapped in wet cloth and moistened frequently. Drop height between the polyethylene component and drop table was controlled using a variable height threaded stopping block and vernier calipers. To set the table

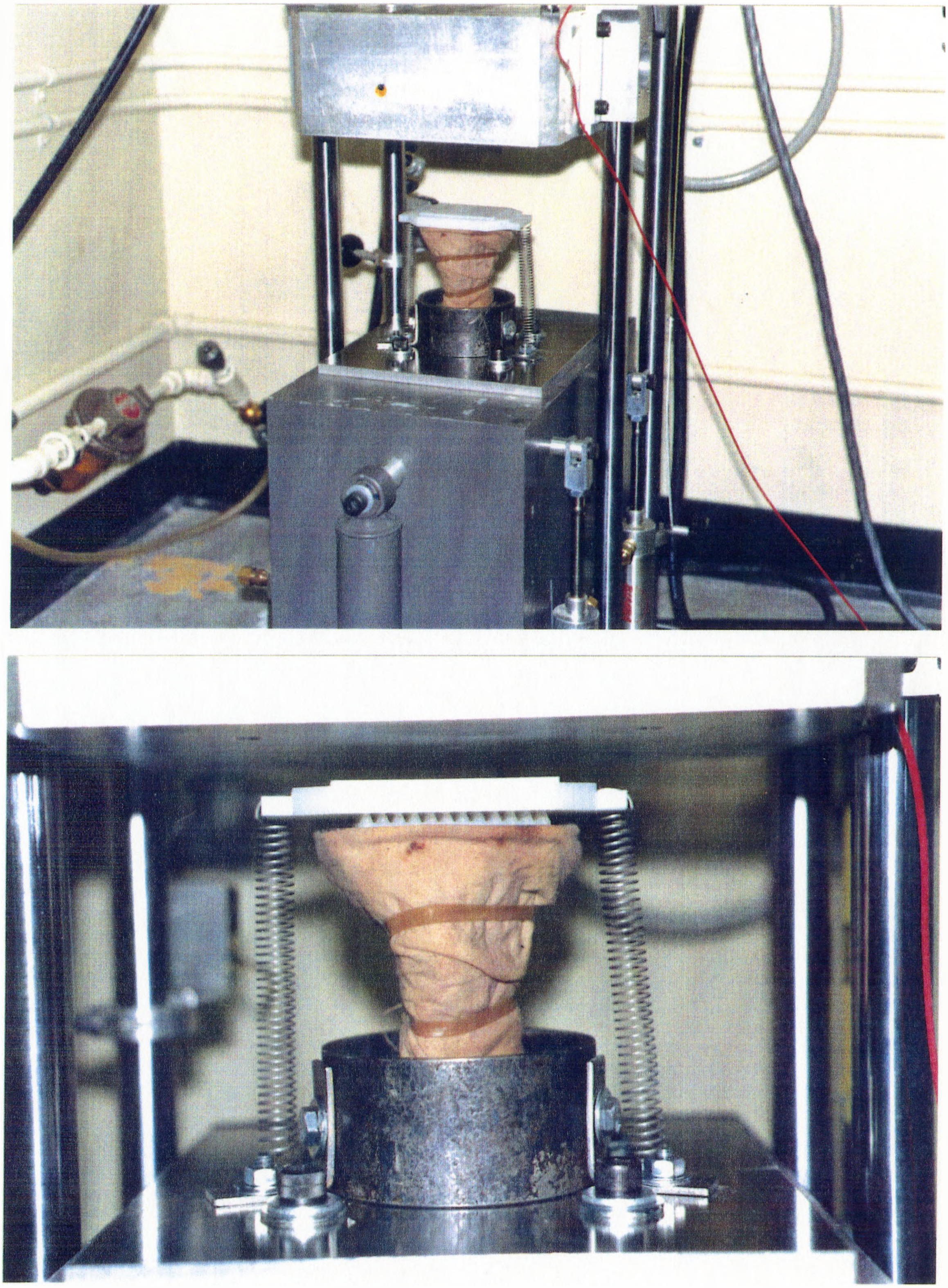

Figure 6.3 Above: tibial specimen bolted to the drop table base with polyethylene block in place. Below: The same specimen with elastomer sample added and drop table positioned above for testing.

height the metal block was adjusted to the desired height and placed under the table. The table was then brought to rest directly on top of the block and locked into position with the air brakes. With the block removed the table was released to fall onto specimens and the resulting impact recorded by a table mounted accelerometer. The above method of height control had to be devised since extremely low drop heights for which the table is not normally used were required to produce impact forces in the physiological range. Drop heights of 2.5, 5, and 10 mm generated average peak contact forces on tibial specimens (with no elastomer present) of 2830, 4850, and 7935 N respectively. The lowest of these forces is representative of peak knee joint contact forces during normal walking of approximately four times body weight as determined by Morrison [9]. The lowest two force values are also in good agreement with peak impact forces observed in implanted knees of 1940 to 3820 N by Hoshino and Wallace [26] in their impact study of cadaver knee joints. These authors determined their force values from a pilot study of a person descending one step onto a force plate. The highest loading value is perhaps outside the range of normal daily activities such as walking, but may well be representative of more rigorous or occasional activities such as ascending and descending stairs quickly, jogging, running or playing sports. This height was therefore kept as an extreme loading range. Overall, high mass and low 'g' type of impacts such as those generated by the drop test table at low heights, are thought to most accurately simulate physiological loading because of the low velocity of impact. Owing to concerns of repeatability and increase in potential errors drop heights lower than 2.5 mm were not used.

Tibial specimens were each impacted with and without elastomer samples for each of the three aforementioned drop heights. Elastomer samples were placed centrally on top of each specimen between the stainless steel and polyethylene tibial components. In all thirteen different elastomer samples were tested which included all eleven geometrically featured sheet samples as well as smooth flat sheet samples layered singlely (2.5 mm thick) and doublely (5.1 mm thick). As was discussed previously in section 4.3 both elastomer sample shape and surface area of support were perceived to be the dominant variables affecting elastomer cushioning performance. To assess the effects of varying surface area, geometric sheet samples were cut and sectioned at the base so that base sheet surface areas of 18, 24, and 30 cm^2 could be tested. Flat sheet samples were not cut and hence tested at 30 cm^2 surface area only.

For each test configuration at least three trials were performed for which peak acceleration, shock pulse duration and area underneath the pulse (representing velocity change) were recorded. Shock pulse duration was determined by first locating the points equaling ten percent of the peak acceleration value at the beginning and end of each pulse, and then computing the time interval between these points. This was done to offset potentially large errors resulting from distortion of the pulse at the very ends as shock pulses are not always smooth and symmetrical. All of the shock pulses were filtered at a cut off frequency of five times the full sine wave frequency of the pulse itself.

6.5 Results

i) Repeatability of Results

For all tibial specimens and elastomer samples test results over a series of identical trials were very repeatable, the vast majority of results having a deviation of less than ± 5 % from the mean result of all of the trials. The single worst deviations from the mean result of a series of repeated trials noted were 13% in peak acceleration, and 14% in shock pulse duration. Comparison of test results for each of the five tibial specimens impacted with no elastomer present showed the largest standard deviation in results to be 12% of the mean peak g value at the 2.5mm drop height. Further, for each drop height values of peak acceleration and pulse duration from the five specimens all fell within normal distributions to the $p=0.05$ confidence level indicating that none of the test specimens were significantly different and therefore comparable.

6.5.1 Surface Area

A total of seven different geometrically featured sheets which included samples from each of the three different shape groups were impact tested with different surface areas. All of the test trials using surface areas of 18, 24, and 30 cm^2 showed no significant change in peak force attenuation over the no elastomer condition as a result of varying surface area. Percentage attenuation values for different surface areas fell within the normal variance of attenuation results for testing at a given single surface area. Results for increase in shock pulse duration over the no elastomer condition were similar showing little change with varying surface areas. A few larger deviations in pulse duration results as high as 13 % were noted but were inconsistent and no trend could be established. A sampling of test data illustrating these results is shown in table 6.1, where peak acceleration and shock pulse duration values are presented for the 4.76 mm conical featured sheet sample tested over three different surface areas and drop heights. Because no indications were evident after these trials of any significant or repeatable changes in results, further investigation of surface area was abandoned and not carried out in full for all of the remaining elastomer samples.

6.5.2 Attenuation

Figure 6.4 presents sample shock pulses for both the with and without elastomer test conditions illustrating visually the cushioning effects of the elastomer sheet. Figures 6.5 to 6.7 present average peak force reductions resulting from addition of the various elastomer samples to each of the five tibial specimens. Values in these figures are expressed as percentage reductions of values recorded from the no elastomer test condition. All of the results presented are for sheet

Surface Area (cm^2)		2.5 mm Drop	5.0 mm Drop	10.0 mm Drop
18	Peak 'g'	6.2	11.4	19.4
	Time (ms)	11.3	8.5	7.6
24	Peak 'g'	6.2	10.8	19.4
	Time (ms)	11.1	8.6	6.9
30	Peak 'g'	6.1	10.6	19.1
	Time (ms)	11.0	8.5	6.7

Table 6.1 Peak acceleration and pulse duration values recorded for the 4.76 mm conical featured sheet, tested over three different drop heights and surface areas.

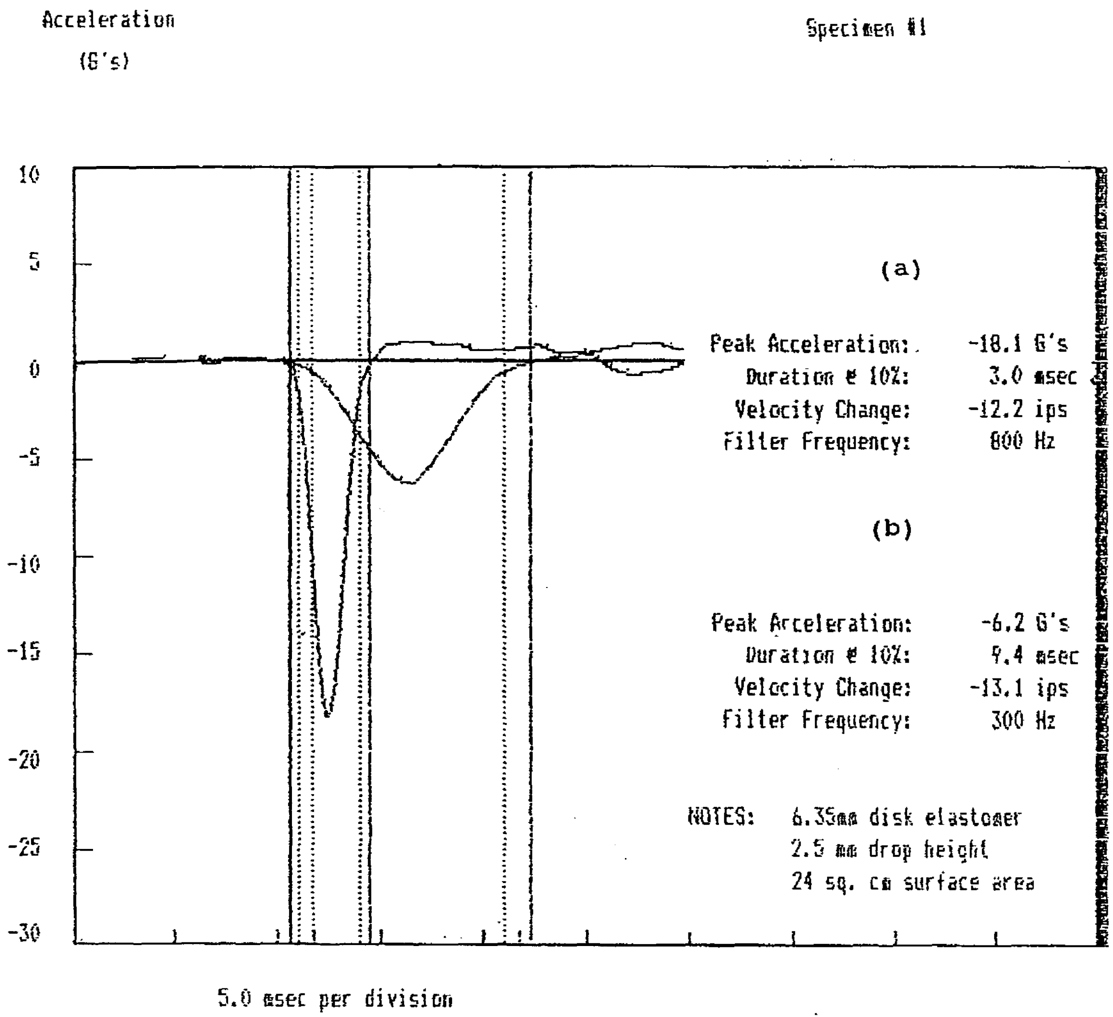

Figure 6.4 Sample shock pulses applied to a prosthetically fitted tibial specimen at the 2.5 mm drop height. Two conditions are superimposed for comparison; (a) with no elastomer and (b) with the 6.35 mm cylindrical featured elastomer sheet added.

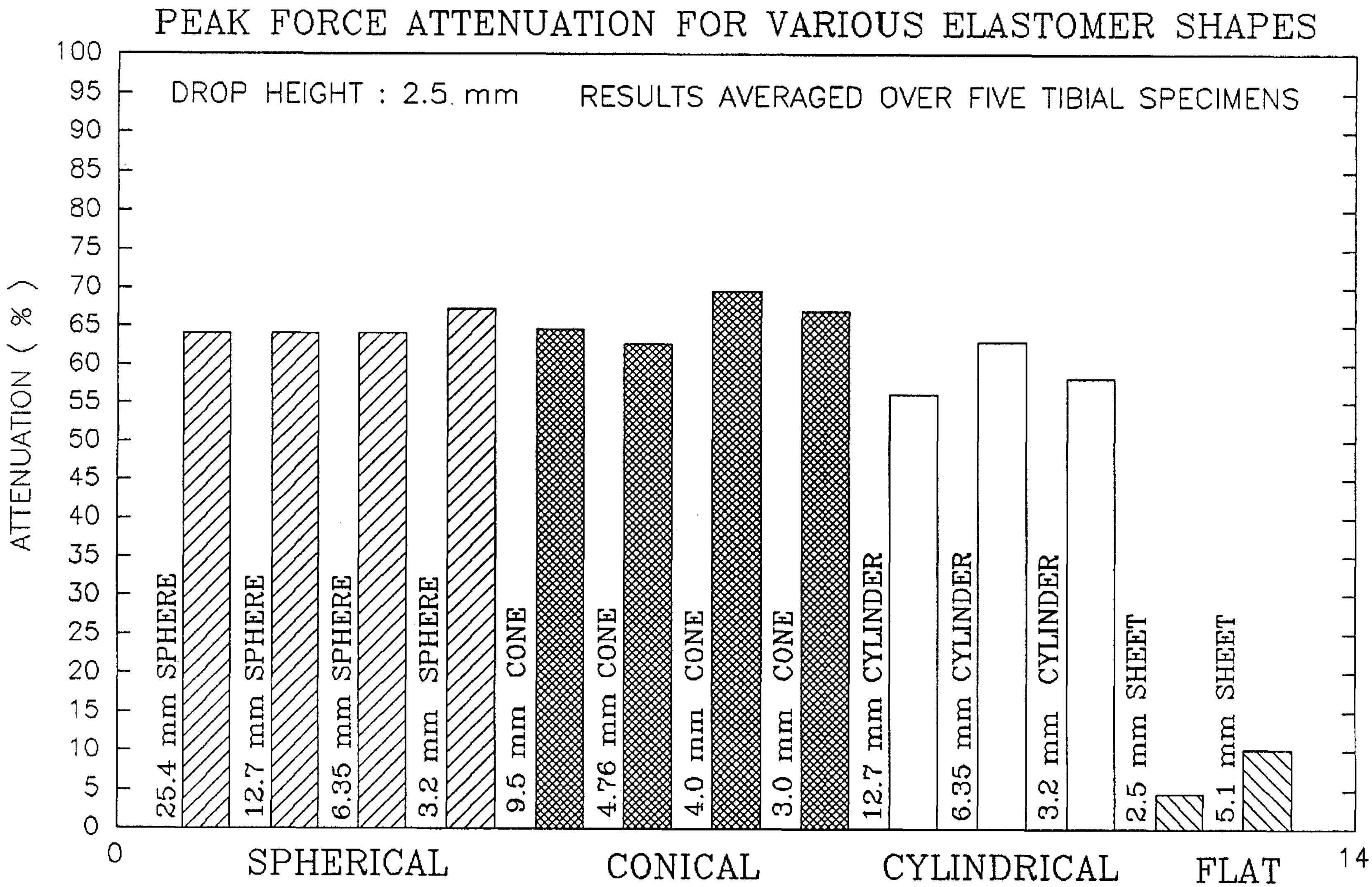

Figure 6.5 Percent reductions in peak transmitted force for various elastomer shapes tested at the 2.5 mm drop height.

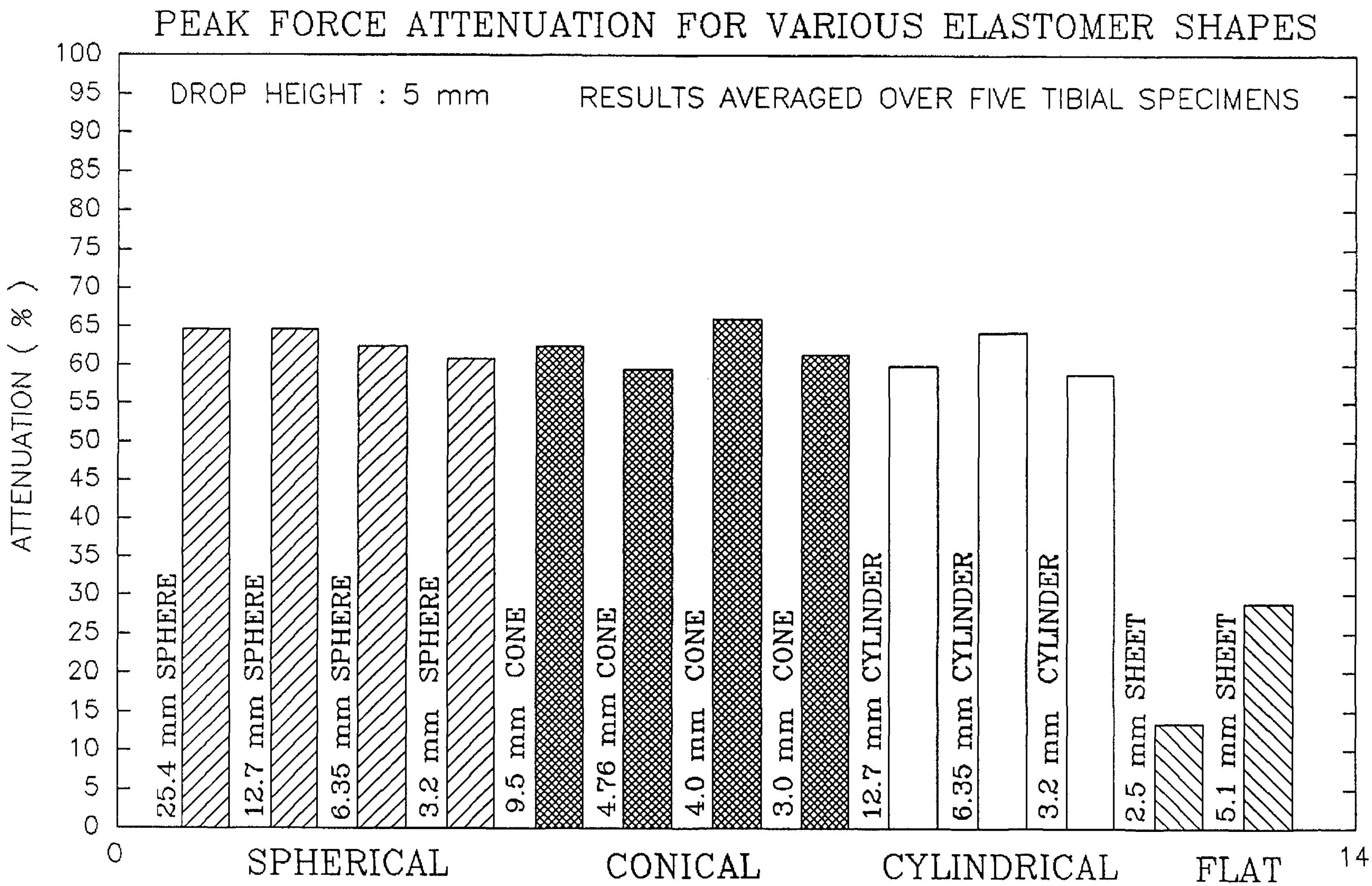

Figure 6.6 Percent reductions in peak transmitted force for various elastomer shapes tested at the 5.0 mm drop height.

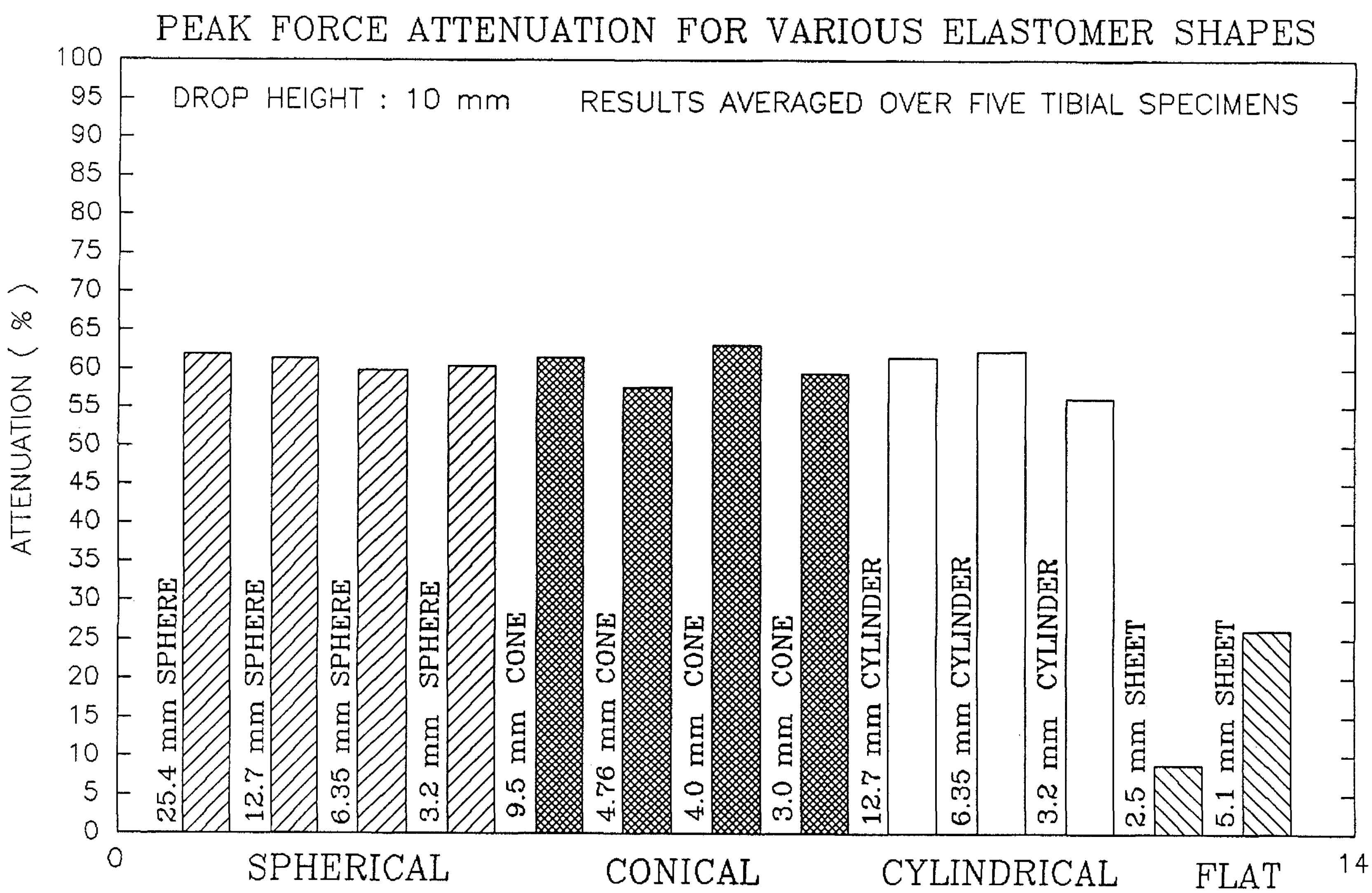

Figure 6.7 Percent reductions in peak transmitted force for various elastomer shapes tested at the 10.0 mm drop height.

samples 24 cm^2 in surface area with the exception of flat smooth sheet samples which were 30 cm^2 in surface area.

Results of figures 6.5 to 6.7 show substantially large peak force attentuation results for most of the elastomer samples tested. Within the various geometrically shaped groups differences in percentage attenuation are too marginal and inconsistent to draw any statement as to whether force reduction depends on sample stiffness, shape, hysteresis losses, or an interrelation of variables. The largest difference in average attenuation between samples within a specifically shaped group was only 7%. Somewhat more significant differences occured between the two flat sheet samples tested. The double layered sample showed consistently higher attenuation results (by as much as 17%) than the single layered sample, the difference between the two increasing as drop height increased.

Between different geometrically shaped sample groups attenuational results were also very similar. Table 6.2 summarizes average results for each shape group over the three drop heights tested. As seen from this table the percentage attenuation values for each of the spherical, conical and cylindrical shape groups are surprisingly consistent over all three drop heights. Between all eleven different geometric shapes tested over three different drop heights, the maximum range of percentage attenuation after averaging over the five tibial specimens was 56 to 70 %. From table 6.2 flat sheet samples show the largest

Drop Height (mm)	2.5	5.0	10.0
Basic Sample Shape	Average Percent Attenuation		
spherical	64.9	63.2	60.9
conical	66.0	62.3	60.4
cylindrical	59.1	60.9	60.0
flat sheet	7.4	21.1	17.4

Table 6.2 Average percentage attenuation values of different elastomer shape groups for different drop heights.

differences with respect to percent attenuation and changes in drop height.

6.5.3 Pulse Duration Increase

Figures 6.8 to 6.10 present average resulting increases in shock pulse duration with addition of elastomer test samples to the five tibial specimens. All values in these figures are expressed as percentage increases of values recorded from the no elastomer test condition. All of the results presesnted are for sheet samples 24 cm^2 in surface with the exception of flat smooth sheet samples which were 30 cm^2 in surface area.

Results of percentage increase in pulse duration, shown in figures 6.8 to 6.10, show a wide range of increases from minimal to factors of four times the original pulse length. Within differently shaped geometric

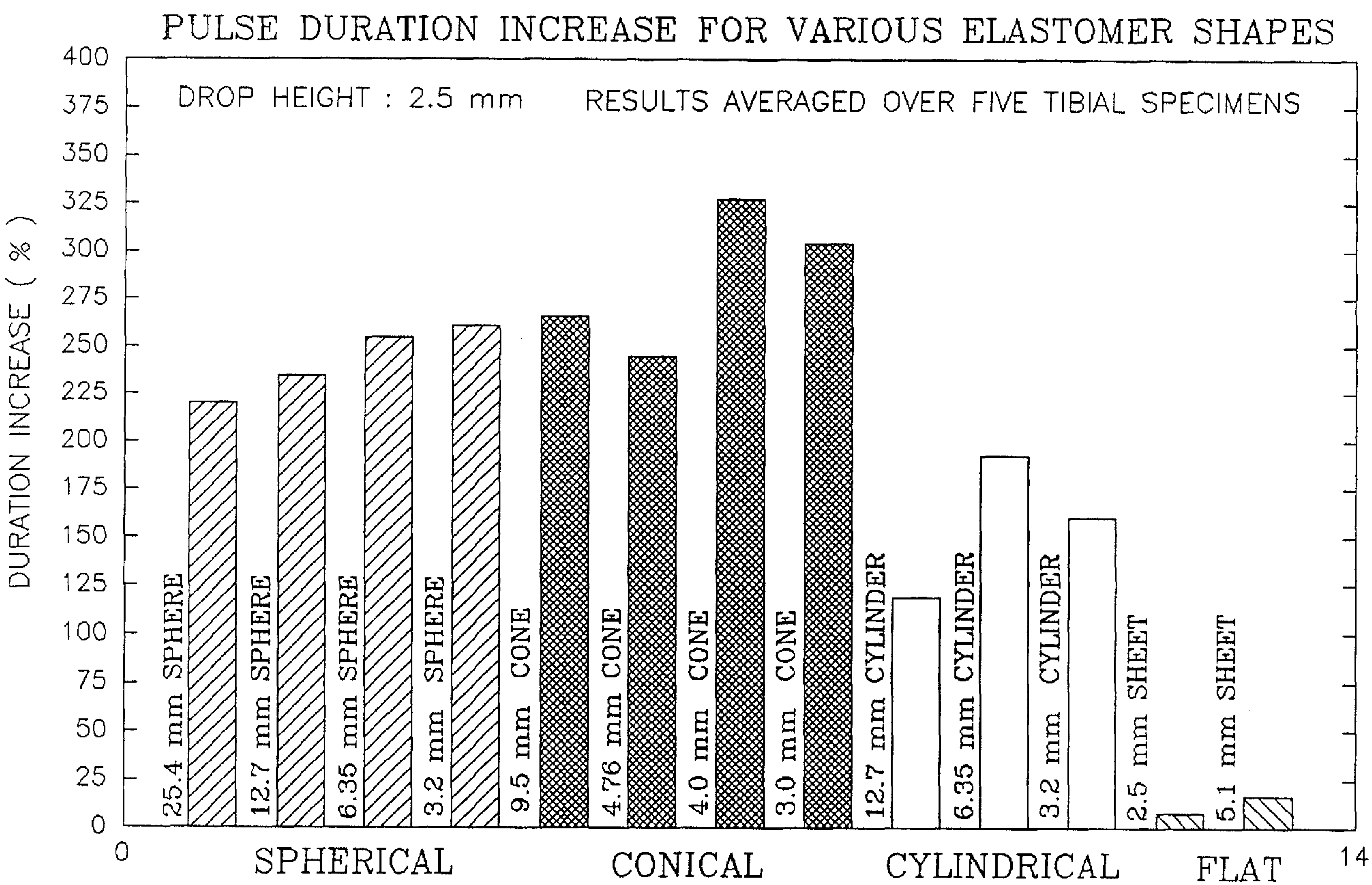

Figure 6.8 Percent increases in shock pulse duration for various elastomer shapes tested at the 2.5 mm drop height.

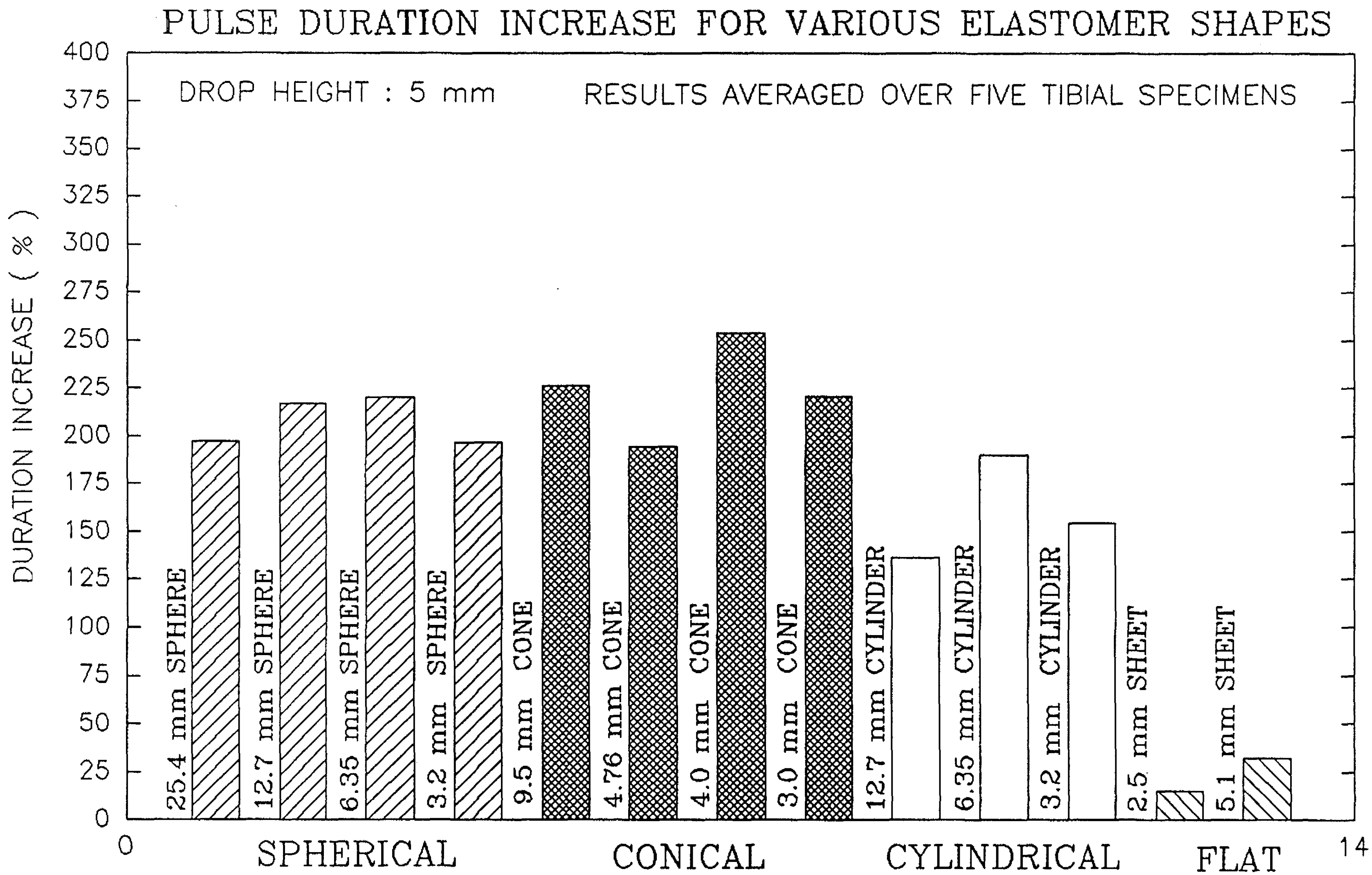

Figure 6.9 Percent increases in shock pulse duration for various elastomer shapes tested at the 5.0 mm drop height.

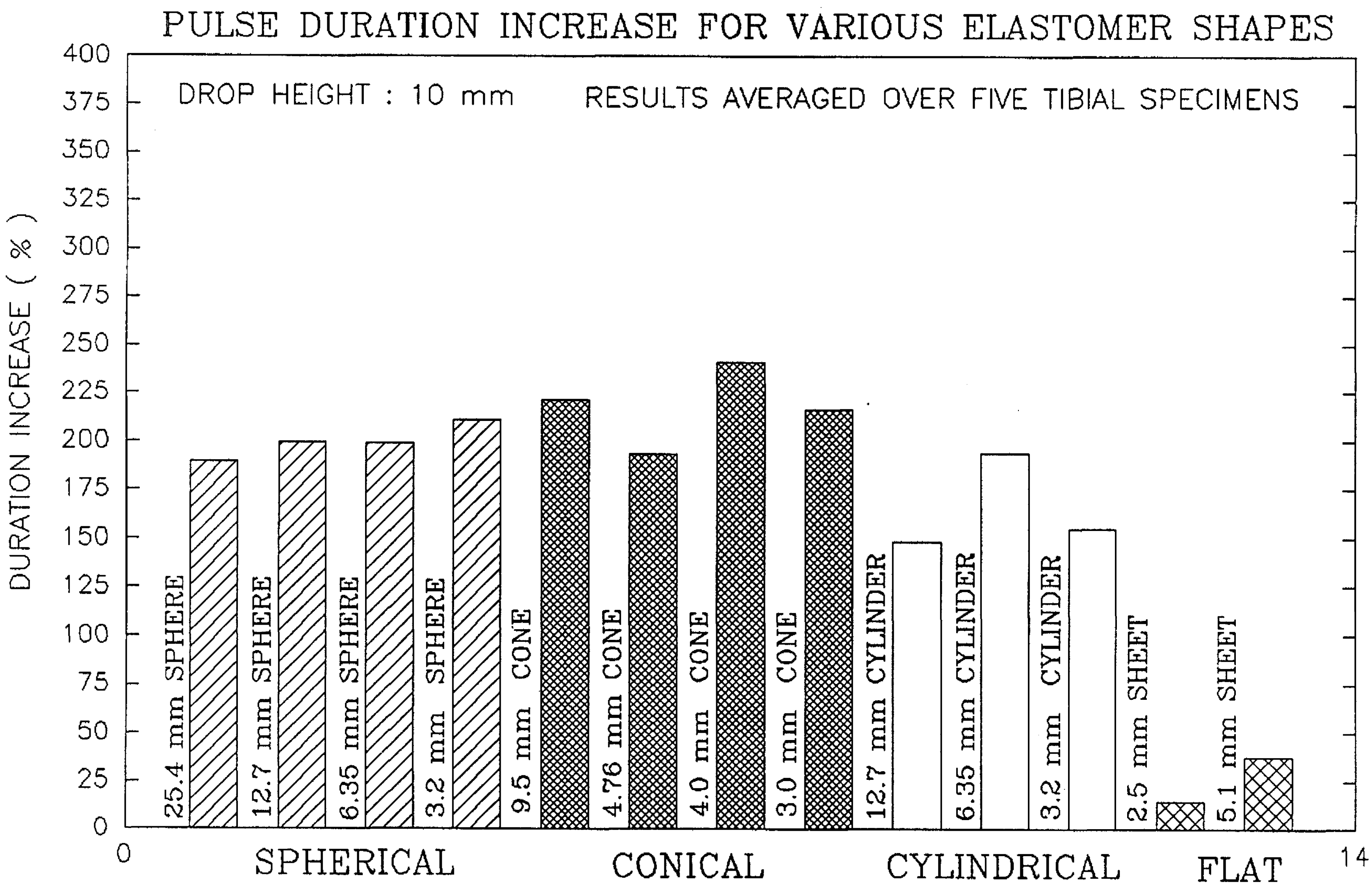

Figure 6.10 Percent increases in shock pulse duration for various elastomer shapes tested at the 10.0 mm drop height.

groups differences in pulse duration increase as high as 82% were noted as well as the appearance of trends as to which specific shapes provide the highest increases. These trends however, do not consistently correlate to individual sample stiffness or hysteresis losses as presented in chapter five. For example, the 4.76 mm conical shape was the stiffest of the conical featured samples and consistently provided the lowest percentage increase in duration of all conical shapes tested. However, the 4.0 mm size which is stiffer than both the 9.5 and 3.0 mm sizes consistently provided the highest percentage increase for shock pulse duration. Individual sample performance is therefore more likely a result of an interrelation of variables. Observation of the results tends to indicate that for all geometric groups, samples with a balance of relatively low hysteresis and relatively high stiffness seem to perform best within that family of shapes.

Referring to table 6.3 which summarizes average percent duration increases for the various shape groups over the three drop heights, it is seen that spherical and conical featured sheets provided the greatest duration increases, which tended to become highest with decreasing drop heights. Cylindrical shapes and flat sheet samples demonstrated progressively lower duration increases, with a small but opposite trend of higher pulse durations with increasing height. Between different sample groups tested table 6.3 also indicates a general trend for stiffer sample groups to provide smaller increases in pulse duration. Referring back to table 5.1 average sample stiffness

Drop Height (mm)	2.5	5.0	10.0
Basic Sample Shape	Average Percent Duration Increase		
spherical	243	208	200
conical	286	224	218
cylindrical	157	160	166
flat sheet	12	24	26

Table 6.3 Average percentage increase in shock pulse duration for various elastomer shape groups over different drop heights.

of conical, spherical, cylindrical and flat sheet samples as tested to 20% strain were 747, 818, 2028, and 7473 N respectively. However, the lack of any significant consistent changes in pulse duration with variation of surface area suggests again that stiffness alone is not a sole defining parameter since an increase in surface area would also increase overall sample stiffness.

6.5.4 Impact Strain

During all drop tests elastomer samples were allowed to deform freely. Impact strain values were neither controlled nor measured. However, in light of the question raised in section 5.3.4 as to further stiffening of the elastomer at compression times faster than 19 milliseconds, it was decided to assess some idea of strain values imposed on elastomer samples during impact. Assuming that maximum strain values occur at the point of maximum acceleration (and hence force), then double integration of an acceleration time curve (as presented in figure 6.4), from zero up to the peak acceleration value, should reveal the distance traveled by the drop table as it compressed the elastomer sample on impact. Sample strain is then simply distance travelled by the drop table divided by original sample thickness. Three elastomer samples, the 3.0 mm conical, 12.7 mm spherical, and 12.7 mm cylindrical featured sheets were selected to cover the extreme ranges of sample stiffness. Shock pulse printouts for these samples at the 2.5 and 5.0 mm drop heights were photo expanded by a factor of eight, appropriately scaled, and then digitized from zero to peak acceleration such that each pulse provided 18 to 35 data points depending on its length. For each data set, points were fitted with a cubic spline and then doubly integrated using fortran 77 library subroutines. Data points were also integrated by simple trapezoidal rule technique as a check. Results of the cubic spline integrations are summarized in table 6.4 .

The third column in table 6.4 shows maximum elastomer sample strain as determined from integration of the fitted splines. The fourth column shows peak impact forces (mass of the drop table times the peak g value) experienced by each sample. Stiffness results from table 5.1 for the same samples at the 20% strain and 3 Hz loading condition are also presented for comparison in column five. These results show that in comparison to slower loading conditions the same samples under impact reach maximum strains much less than 20 % for equal or greater

Drop Height (mm)	Elastomer Sample Shape	Impact Strain (%)	Impact Force (N)	Stiffness At 20% Strain And 3 hz (N)
2.5	3.0 mm Conical	13.0	979	694
2.5	12.7 mm Spherical	10.5	1050	801
2.5	12.7 mm Cylindrical	5.2	1263	2317
5.0	3.0 mm Conical	12.3	1779	694
5.0	12.7 mm Spherical	10.0	1708	801
5.0	12.7 mm Cylindrical	6.6	1975	2317

Table 6.4 Impact strain values from digital integration of acceleration profiles.

force loads. The impact case therefore appears significantly different, with samples indicating a stiffening behavior as would be expected from a viscoelastic viewpoint. Aside from the obvious errors associated with expanding, digitizing and fitting data points, there may be some error associated with the assumption that peak strain and peak acceleration values occur simultaneously. As was seen in chapter five, force may peak slightly ahead of maximum strain owing to viscous strain rate sensitivity. The results of table 6.4 therefore should be taken as an approximation with the true strain results possibly larger.

6.5.5 Velocity Change

The value of velocity change as seen in figure 6.4 represents the total change in velocity of the drop table from its maximum downward velocity at the instant impact begins, to its maximum upwards or rebound velocity at the instant the table just loses contact with the elastomer sample. For equivalent drop heights the value of impact velocity will ideally be the same, while rebound velocity will depend on the elastic return of energy from the material being tested. Any variation in velocity change is therefore an indication of the degree of damping or energy loss on the part of the test material. For all of the drop tests conducted values of velocity change were recorded. Results of these values can be summarized as follows:

i) spherical and conical shapes behaved very similarly averaging overall increases in velocity change of 21.7, 7.3, and 3.5 % for the 2.5, 5, and 10 mm drop heights respectively over the no elastomer condition.

ii) cylindrical shapes showed an average decrease in velocity change of 0.3 and 3.1 % for the 5 and 10 mm drop heights respectively, and an increase of 8 % for the 2.5 mm drop height over the no elastomer condition.

iii) flat sheet samples provided an average decrease of 5.8 and 4.7 % in velocity change for the 5 and 10 mm heights respectively and an average increase of 1.4 % for the 2.5 mm drop height over the no elastomer condition.

For the same acceleration profiles integrated in the previous section, table 6.5 presents both total velocity change (1st integral of the

Drop Height (mm)	Elastomer Sample Shape	Total Velocity Change (cm/s)	Velocity Change Zero To Peak 'g' (cm/s)
2.5	3.0 mm Conical	36.8	20.0
2.5	12.7 mm Spherical	34.0	18.7
2.5	12.7 mm Cylindrical	30.0	14.8
5.0	3.0 mm Conical	48.5	25.4
5.0	12.7 mm Spherical	45.5	22.9
5.0	12.7 mm Cylindrical	43.2	20.8

Table 6.5 Values of velocity change for i) entire shock pulse, and ii) section of pulse from zero to peak g value.

entire pulse) as provided by the shock test software, and velocity change from zero to peak acceleration computed from the methods of the previous section. Comparison of these results shows that values of velocity change up to the peak acceleration, range from 48 to 55% of the total velocity change value.

The above results indicate that the elastomer samples do not appear to absorb or dampen energy to any large degree relative to the bone prosthesis configuration alone. Addition of spherical or conical featured shapes appears to have created a combined overall more elastic system while cylindrical and flat sheet samples tended to provide for the most part marginal damping. The roughly equal and symmetric areas to either side of the peak g value underneath the acceleration profiles indicates that rebound velocities tended to be close to impact velocities. All of these results serve to indicate that behavior of the elastomer is largely elastic with little damping at high impact rates.

6.6 Discussion

The absence of any significant changes in test results with variance of surface area appeared surprising and difficult to rationalize. This behavior is not unusual amongst common cushioning materials where, at low drop heights, a wide range of material thicknesses and surface areas can result in only marginal differences in attenuation. Greater drop heights are therefore required to produce more and more pronounced differences. Observation of tables 6.2 and 6.3 however, show that the greatest differences in attenuation results for elastomer samples occurred at the lowest drop height, while at higher heights values tended to converge to a uniform result. Therefore the main factor which contributed to the overall similarity of results was the speed of impact. That is, higher rates of loading did not give the elastomer molecules time to rearrange thus minimizing damping effects. This is supported by the analysis of velocity change data which indicated sample response to be almost entirely elastic. Subsequently, at higher loading rates a more uniform and predominantly elastic behavior resulted which was not sensitive to the range of shapes, surface areas or impact loads tested. This is in contrast to the slower loading conditions of chapter five where large differences in stiffness and damping characteristics were noted between all samples.

Evidence from these tests again indicate that elastomer sample behavior is strongly dependent on loading rate, a characteristic of viscous materials. Under slower loading conditions significant damping effects are present, with sample shape having a significant influence on stiffness and hysteresis values. With higher loading rates, hysteresis effects tend to disappear and behavior is predominantly elastic in nature. Shock reduction is achieved through elastic storage of energy as was outlined in the chapter introduction. Results of the integration of shock pulses also indicated a significant stiffening of the material under more rapid loading. Under these conditions it appears as though elastic behavior of the material itself plays a large role in determining impact response. The ranges of geometric sample shapes and surface areas tested (excluding flat sheet samples) showed only marginal influences on test results. Thus with high rates of loading only samples with vastly different shapes and shape factors, such as flat sheet samples, will produce significant differences in attenuational results.

Overall, results of impact testing showed that elastomer samples provided consistent and significant shock reduction benefits. In terms of knee joint application these results demonstrate some important points. While the test configuration used was straight forward, it did provide for a good basis of comparison. That is, relative to prosthetic materials and a significant amount of bone, the elastomer shapes were able to attenuate incoming shock loads. The elastomer therefore created a much more compliant system when incorporated into the prosthesis. Secondly, elastomer shapes were able to moderate shock loads which were the most severe, in terms of magnitude and rate of application, that would physiologically occur at the knee joint. This shows that although viscoelastic in nature, the elastomer is able to respond to extremely rapid loads without stiffening to the point where it is no longer useful as a shock absorber. More over, under high loads the material does tend to exhibit a favourable stiffening response which prevents samples from being over strained beyond a 20% limit. These results bode well for the ability of the elastomer to respond favourably to the range of physiological loads seen at the knee joint.

CHAPTER SEVEN

FATIGUE TESTING

Introduction

Fatigue of an elastomeric material has been shown to be a progressive crack growth process intitiated from small flaws in the material which act as stress risers. Gradual changes in bulk mechanical properties may also occur as a result of prolonged fluctuating stresses, the most notable being a reduction in elastic modulus [47]. The number of fluctuating stress cycles required to cause ultimate failure of a specimen is termed the fatigue life. While the composition of Silastic HP100 has been optimized to provide minimal crack propagation, tests to evaluate crack growth are performed by flexing specially shaped specimens creating alternate tensile and compressive flexural stresses. It is believed that a high resistance to flexural fatigue will translate into high resistance to compressive fatigue. However, a purely compressive fatigue life has yet to be established. In addition, although tear and fatigue are highly dependant on material composition itself, shape of a specimen can influence fatigue via local strain energy density in the region of the crack. The focus of the work in this chapter was therefore to try to evaluate the fatigue life of the various shaped elastomer samples in compression.

7.1 Fatigue Test Apparatus

For the current study a special fatigue test machine was designed and built. This machine consisted of a continuous use AC electric motor and gear box speed reducer. Speed at the gear box output shaft was a constant 180 rpm. To the face of the gear box a special cam assembly was fastened which included two stainless steel compression plates approximately 10cm by 5cm by 1.5cm in size. The lower compression plate was held flatly on top of three threaded vertical supports by two bolts, all of which threaded directly into the assembly base plate. The threaded supports allowed for height adjustment of the lower plate. The upper compression plate was mounted flatly and guided on two vertical bearing rods. By means of compression springs this plate was held against a cam mounted to the gear box shaft. Eccentricity of the cam was adjustable allowing for variable vertical stroke travel of the upper plate as the cam rotated. This was accomplished by first mounting a small circular disc directly over the gear box shaft. The inside hole of the disc to accomodate the shaft was bored 1/32 of an inch off center. A second larger circular disc was then similarly mounted over the first, also having the inside hole offset by 1/32 of an inch and secured to the first by clamping screws. By rotating the larger disc over the smaller and locking its position, an eccentricity was created allowing vertical displacements in the range of zero to 1/16 of an inch. To minimize friction and heat build up, a space above the upper compression plate was enclosed so that the contact area between the plate and cam could be kept submerged in an oil bath.

Because of the time consuming nature of this testing as noted in the preliminary work, the current machine was designed so as to have space and rigidity to accomodate several elastomer samples at once. With this apparatus, samples could be mounted between the two compression plates and compressed to a desired strain at a loading cycle frequency of 3 hz. The fatigue test machine is pictured in figure 7.1.

7.2 Test Methods

Results of the preliminary work in section 3.4 showed that disc shaped samples had experienced significant abrasive wear. It was thought that this was largely due to a coarse machined finish of the compressing surfaces. As a result compression plate surfaces in the current apparatus were smoothly ground. Initial tests with the current apparatus in which sets of five 12.7mm diameter circular discs 2.5mm in thickness (with no base sheet) were compression loaded to two million cycles, revealed that the wear problem still existed. Samples exhibited excessive wear and shredding at the loaded faces. A second test in which 12.7mm discs were more tightly constrained peripherally so as to minimize relative movement and wandering of samples between the plate faces did not alleviate this problem. It was therefore decided that a more elaborate and perhaps simulated type of test was needed. In the hope of producing a better wear couple, flat thin polyethylene sheets were introduced covering both the upper and lower compression plate surfaces so that elastomer samples would be loaded by polyethylene surfaces rather than stainless steel. It was also decided

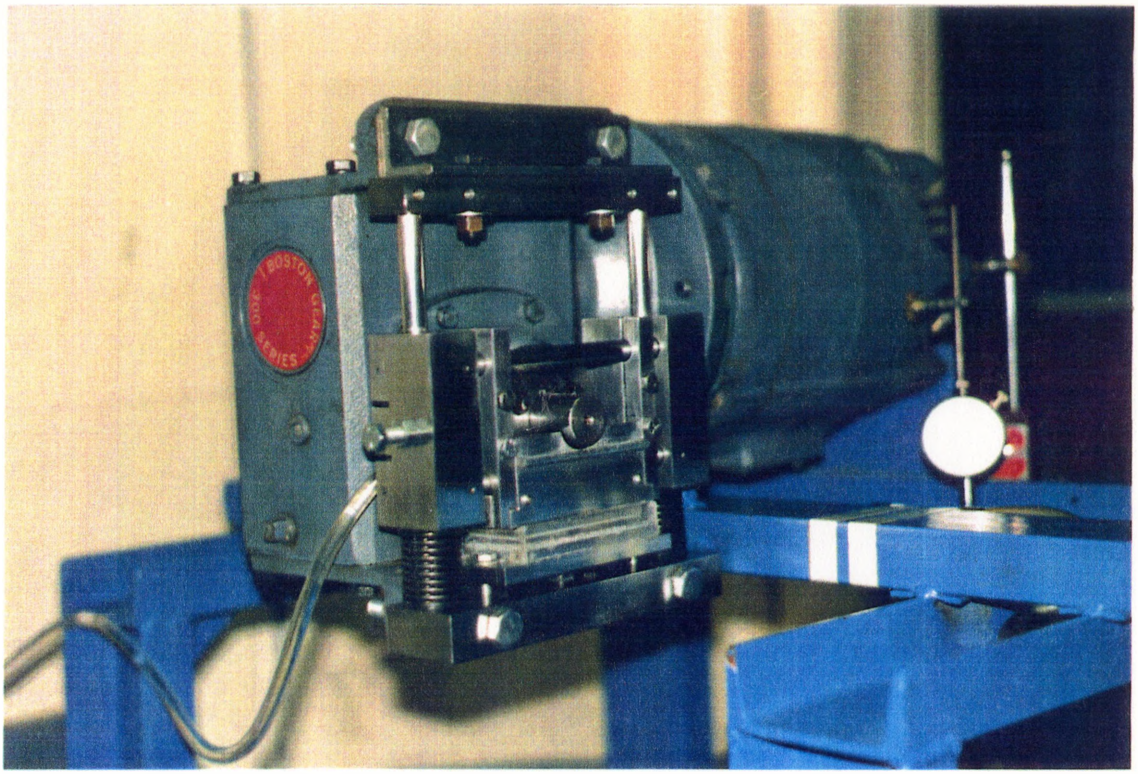

Figure 7.1 Fatigue test machine.

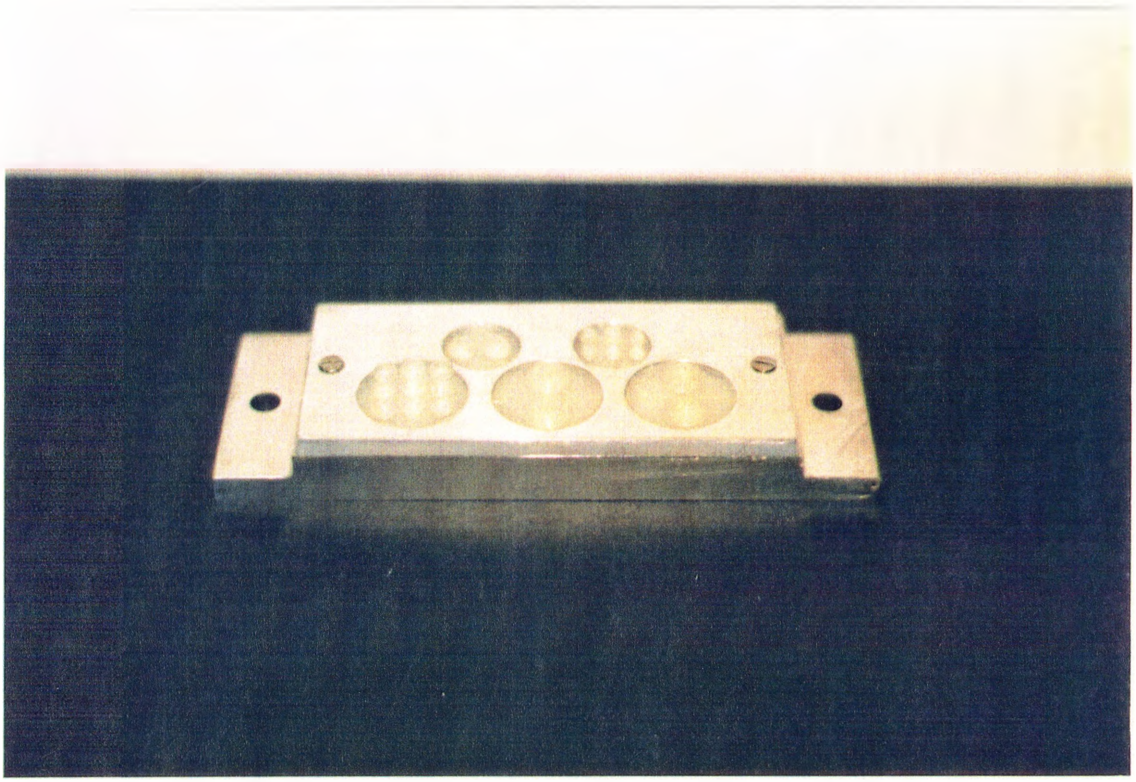

Figure 7.2 Elastomer test samples, and lower compression plate fitted with a polyethylene sheet and aluminum constraining plate.

that a lubricant be introduced. In the knee joint a natural lubricating fluid called synovial fluid is produced having remarkable lubricating qualities. However, synovial fluid is impossible to harvest to any significant amount. Previous wear studies with prosthetic joints have typically used either an artificially produced synovial fluid substitute called bovine serum, or distilled water which is an essential ingredient of natural lubricants [55]. It was decided to deliberately test samples under the most adverse possible condition, and since distilled water was readily available, it was chosen as the lubricant.

Final form of the test configuration is shown schematically in figure 7.3. Flat smooth polyethylene sheets from 1.6 to 3.2mm in thickness and approximately 6 to 15 μ inches in surface roughness were used. Both high density (HDP) and ultra high molecular weight polyethylene (UHMWP) were used in various tests. Polyethylene sheets were replaced each time new elastomer samples were tested. A 1.6mm thick aluminum constraining plate was also added with several holes into which elastomer samples rested. This was necessary to contain and prevent samples from wandering laterally between the compression plates. Small pieces of clear plexiglass were cemented around the lower compression plate to contain the distilled water bath. Distilled water from an elevated reservoir, and regulated by a needle valve, was continuously dripped into the bath at a rate so as to prevent the bath from drying due to evaporation. Lastly small jets of air were blown onto the

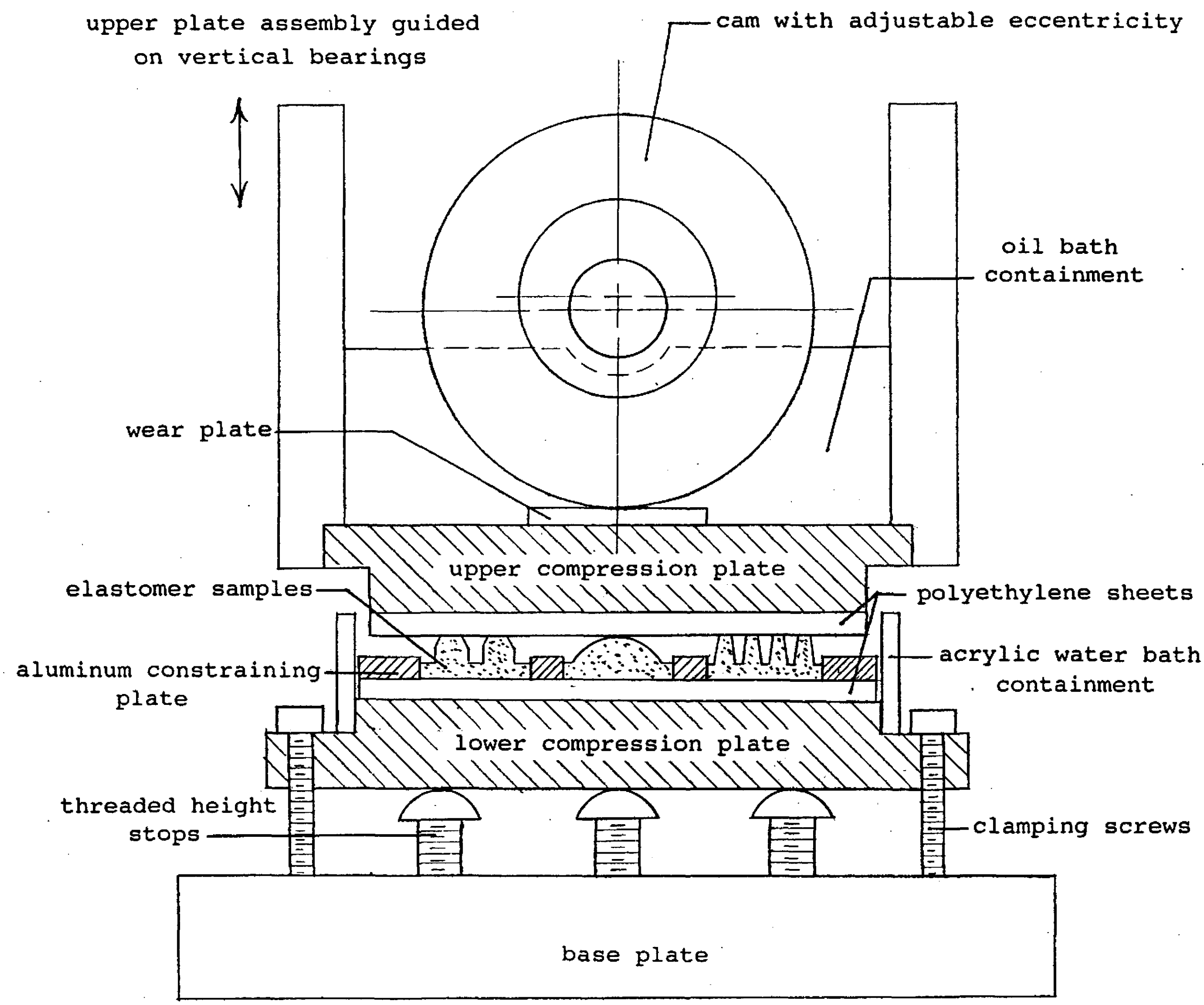

Figure 7.3 Schematic diagram illustrating fatigue test apparatus and elastomer sample placement.

outside of the oil bath chamber as the apparatus ran. This was done to cool and maintain the oil bath temperature at approximately 100 ^{o}F which created test conditions near normal body temperature, and reduced evaporation and formation of bubbles in the distilled water.

ii) Test Samples

Cylindrical or disc shaped samples were punched from flat elastomer sheet stock 2.5mm in thickness, and tested as individual discs without any base sheet added. Disc diameters of 12.7, 6.35, and 3.2mm were tested being contained in holes of 14.3, 7.9, and 4.8mm diameter respectively in the aluminum constraining plate. These hole sizes contained the samples as much as possible without interfering with peripheral bulging of samples as they were compressed. Spherical and conical shaped test samples were made by punching circular 2.2cm and 1.6cm diameter sections directly out of the larger geometric featured sheets. As far as possible the number of full supports or features on each sample were maximized, while any partial supports cut or fractioned by the punch were removed from the sample. The resulting featured disc samples rested flatly in the test machine on polyethylene sheet, located in 2.2cm, and 1.6cm diameter holes in an aluminum constraining plate. Figure 7.2 pictures several test samples punched from featured sheets, as well as the lower compression plate with polyethylene sheet, and appropriate constraining plate. For all spherical and conical molded shapes, the best possible samples having the least number of flaws were selected for fatigue testing.

iii) Test Procedure

Compression stroke travel was measured and adjusted to the required value using a vernier dial guage. Elastomer samples were then mounted into the test machine using the described set up and cyclically loaded to 20% compression strain at a frequency of 3 hz. At intervals of two million cycles (which translated into 8.4 days of continuous running) samples were retrieved and carefully examined visually for any signs of deterioration, in particular formation and growth of cracks, using light microscopy. Two microscopes were used providing observation and photography of samples at magnifictions of up to 1000 times. As testing progressed each of the various elastomer samples were tried in random order. Testing was to be discontinued for a particular sample once signs of extensive fatigue cracking or wear developed.

Elastomer samples were very prone to picking up dust and dirt due to static charging and a general 'sticky' feel. All contaminating materials such as dust or even mineral deposits from tap water and soap (in the event that samples were washed) were clearly visible under the microscope, and might facilitate surface abrasion during testing. It was therefore deemed important that samples be cleaned prior to testing. By trial and error of various methods without chemicals, including the use of a sonic bath, it was found that the only simple way to clean samples was manual washing with a very soft brush and thoroughly dissolved soap solution, followed by rinsing with hot tap water and then distilled water. This method was used to clean samples prior to each test run. The importance of such cleaning regimes in quantifying wear will be addressed later in the chapter.

7.3 Test Results

Table 7.1 summarizes all of the individual elastomer samples tested, as well as the number of loading cycles to which each was subjected. As noted in the second column at least two separate test samples were tried for every elastomer shape. The third column indicates the number of full geometric shapes or supports on each of the 2.2cm and 1.6cm diameter disc samples.

7.3.1 Summary of Observations

On the basis of microscopic evaluation the following statements summarize qualitative results and observations:

1. No fatigue cracking or fatigue failure of samples was observed.

2. All samples were prone to wear resulting in erosion of and eventual removal of regions of elastomer surfaces.

3. Wear observed ranged from mild abrasion and surface scoring to significant material removal with the following trends:
   i) the degree of wear was generally greater for samples with higher shape factors and therefore higher compressive stiffness.

Elastomer Shape	Sample #	Number of Shapes per Sample	Compression Surface (Material)	Total # of Compression Cycles
3mm Cone	1	25	HDP	6×10^6
	2	25	HDP	4×10^6
4mm Cone	1	12	HDP	4×10^6
	2	12	HDP	4×10^6
	3	12	HDP	4×10^6
	4	6	UHMWP	4×10^6
4.76mm Cone	1	12	HDP	6×10^6
	2	12	HDP	4×10^6
	3	9	UHMWP	4×10^6
9.35mm Cone	1	2	HDP	6×10^6
	2	2	UHMWP	4×10^6
3.2mm Sphere	1	22	HDP	6×10^6
	2	22	HDP	4×10^6
6.35mm Sphere	1	5	HDP	6×10^6
	2	5	HDP	6×10^6
	3	2	UHMWP	4×10^6

Table 7.1 Summary of elastomer shapes and total number of compression cycles to which each was fatigue tested.

Table 7.1 continued.

Elastomer Shape	Sample #	Number of Shapes per Sample	Compression Surface (Material)	Total # of Compression Cycles
12.7mm Sphere	1	2	HDP	2×10^6
	2	2	UHMWP	4×10^6
25.4mm Sphere	1	1	HDP	2×10^6
	2	1	HDP	2×10^6
12.7mm Disc	1	1	HDP	2×10^6
	2	1	HDP	2×10^6
	3	1	HDP	2×10^6
6.35mm Disc	1	1	HDP	2×10^6
	2	1	HDP	2×10^6
3.2mm Disc	1	1	HDP	2×10^6
	2	1	HDP	2×10^6

ii) the degree of wear was also greater for larger shaped samples having the greatest surface areas of contact.

iii) overall wear of elastomer surfaces was more severe on the continuous flat undersides of geometric featured sheet samples than on top of the various shapes themselves

4. Substantial amounts of elastomer debris removed from the wear process were observed under the microscope both loosely and tightly recompacted to elastomer sample surfaces.

5. Wear observed on polyethylene surfaces was very minimal, typically only faint scoring or dulling of the surfaces in some regions of contact.

6. No significant differences in the extent of wear or fatigue were noted on elastomer samples between the high density polyethylene and ultra high molecular weight polyethylene compression surfaces used.

7.3.2 Quantitative Assessment

Elastomer samples which were loaded to the 6 million cycle mark were also compression tested in the MTS machine afterwards according to the methods of section 5.2, to ascertain any change in material stiffness with repetitive loads. The resulting stiffness values of these samples all deviated less than 4% from the results of section 5.2 for the same shaped samples, indicating that no significant change in modulus had occured up to the 6 million cycle mark.

Because of the wear observed as testing progressed some quantitative evaluation of wear rate was attempted. This was not initially perceived as part of the fatigue test protocol and therefore not listed in the methods section. Results of these attempts were inconclusive and the methodology is outlined in the following section on wear.

7.4 Elastomer Wear: Mechanisms And Observations

As the various elastomer samples were tested in turn it became apparent that wear of the elastomer surfaces remained a problem. Owing to the degree of wear encountered as well as observation of distinct wear patterns under the microscope, some discussion and analysis of wear is merited here.

7.4.1 Mechanisms of Elastomer Wear

For elastomeric materials two body wear is the result of a stretching and tearing process rather than removal of material by ploughing as in the case of metals. For an elastomer in contact with a flat rigid surface, frictional resistance to relative sliding is the result of both material hysteresis and adhesion. Adhesion is believed to be the result of interaction between surface molecules. Additional resistance due to hysteresis arises from the delay in recovery of such materials when stretched, and is a bulk rather than surface effect [57]. For the case of an elastomer sliding over a rigid surface three distinct mechanisms of wear have been identified as follows [56,57]:

1. *Abrasive Wear*: If the rigid surface is rough with sharp projections, these asperities run across the elastomer surface causing high local deformations which result in tears of the surface perpendicular to the direction of sliding. Once a tear is produced it propogates until with successive passes particles detach. Wear then, is caused by tensile failure of the elastomer at the surface and subsequent detachment from the bulk. As illustrated in figure 7.4 if the direction of sliding is uniform, sets of parallel ridges are formed on the elastomer surface oriented perpendicular to the direction of sliding called an abrasion pattern. The pattern results in a saw tooth cross section profile and is self perpetuating in nature. Also, the coarser the abrading surface the greater the pattern spacing.

2. *Fatigue Wear*: In cases where the rigid surface is rough but with blunt or rounded asperities, the abrasion which occurs when the elastomer slides over the projections is attributed to fatigue of surface layers as a result of repeated cyclic compressive, tensile and reversed shearing stresses. Because the asperities are not sharp enough to cause tearing initially, the material must fatigue before tearing and detachment can occur. This type of wear is relatively mild and classified more as a bulk than surface effect.

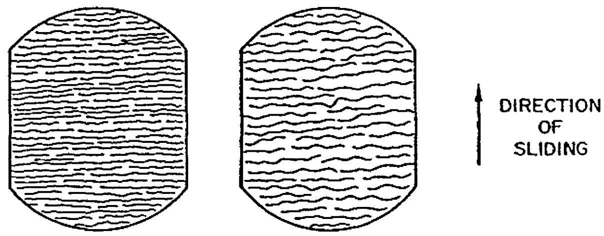

(a) Fine abradant (b) Coarse abradant

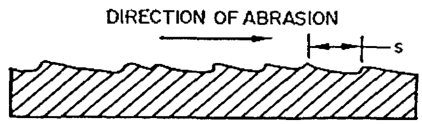

FIG. 11.5 Profile of a typical abrasion pattern

(c)

Figure 7.4 (a) and (b) Illustrations of abrasion patterns on filled natural rubber, (c) sawtooth profile of a typical abrasion pattern (from The Friction and Lubrication of Elastomers 1972).

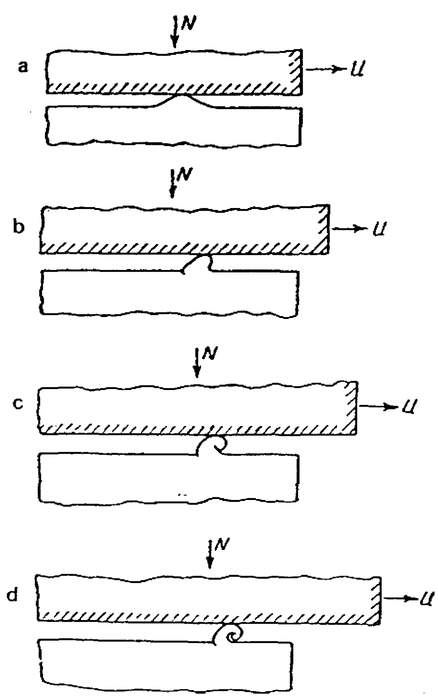

Figure 7.5 Gradual stages (a,b,c,d) in the formation of a 'roll' in the friction of rubber against a smooth abradant (from Friction and Wear 1980).

3. *Roll Formation*: This most recently recognized mechanism occurs under conditions of smooth surfaces, a high coefficient of friction, and is more specific to highly elastic materials with low tear strength. This mechanism initiates with severe local deformation of the elastomer surface because of the high resistance to slippage. This condition causes the elastomer to yield or fail internally and a cut or crack may appear in a transverse direction to the direction of attempted sliding. As illustrated successively in figure 7.5 a gradual tearing occurs until the torn section winds into a roll making relative movement possible without complete slippage. Subsequent motion occurs under conditions of rolling friction and continues to tear the elastomer in the form of a roll until the shred eventually elongates and detaches. Like abrasion, roll formation is considered a much more severe form of wear and the pattern occurring on the elastomer surface due to the smooth abradant is very similar to that for abrasion.

For most elastomer and rigid surface combinations it is likely that all three of the above wear conditions exist, and it is difficult to isolate the relative contributions of each. In general as the elastomer becomes harder, surface phenomena such as abrasive wear predominate with fatigue becoming more insignificant.

7.4.2 Qualitative Wear Assessment of Test Samples

Because of peripheral bulging when compressed elastomer samples experienced a degree of slippage or relative movement at the compression plate interfaces causing wear. The top photo of figure 7.6 shows general sample surface condition prior to testing. As mentioned in chapter four sample surfaces were not perfectly smooth and the apparent series of lines in this photo are ring marks resulting from machining of the mold itself. Initial observation of samples after testing at low magnifications showed that sample surfaces generally had a dulled appearance. At magnifications of about 200 times the appearance of small patterned lines were evident which resembled fine surface cracks. These lines are pictured below in figure 7.6. However, higher magnification still, of the order of 800 to 1000 times revealed these lines to be abrasion patterns as described in the previous section. The elastomer surface had become a very small series of parallel ridges oriented transverse to the direction of peripheral bulging. Examples of this pattern are shown in figure 7.7. The pattern appeared more well defined in areas of greater relative motion as in the photo below. It was noted that when elastomer samples were pressed flatly onto polyethylene surfaces they exhibited a very high degree of sticking and resistance to slippage, almost as if bonded. Given the smooth surfaces, a high degree of friction, and generally low tear strength of silicone vulcanates it is likely that the predominant mechanism was wear by roll formation. The abrasion patterns existed in a range of coarseness but were generally very fine requiring high magnifications to observe.

As would be expected elastomer samples received the most wear in

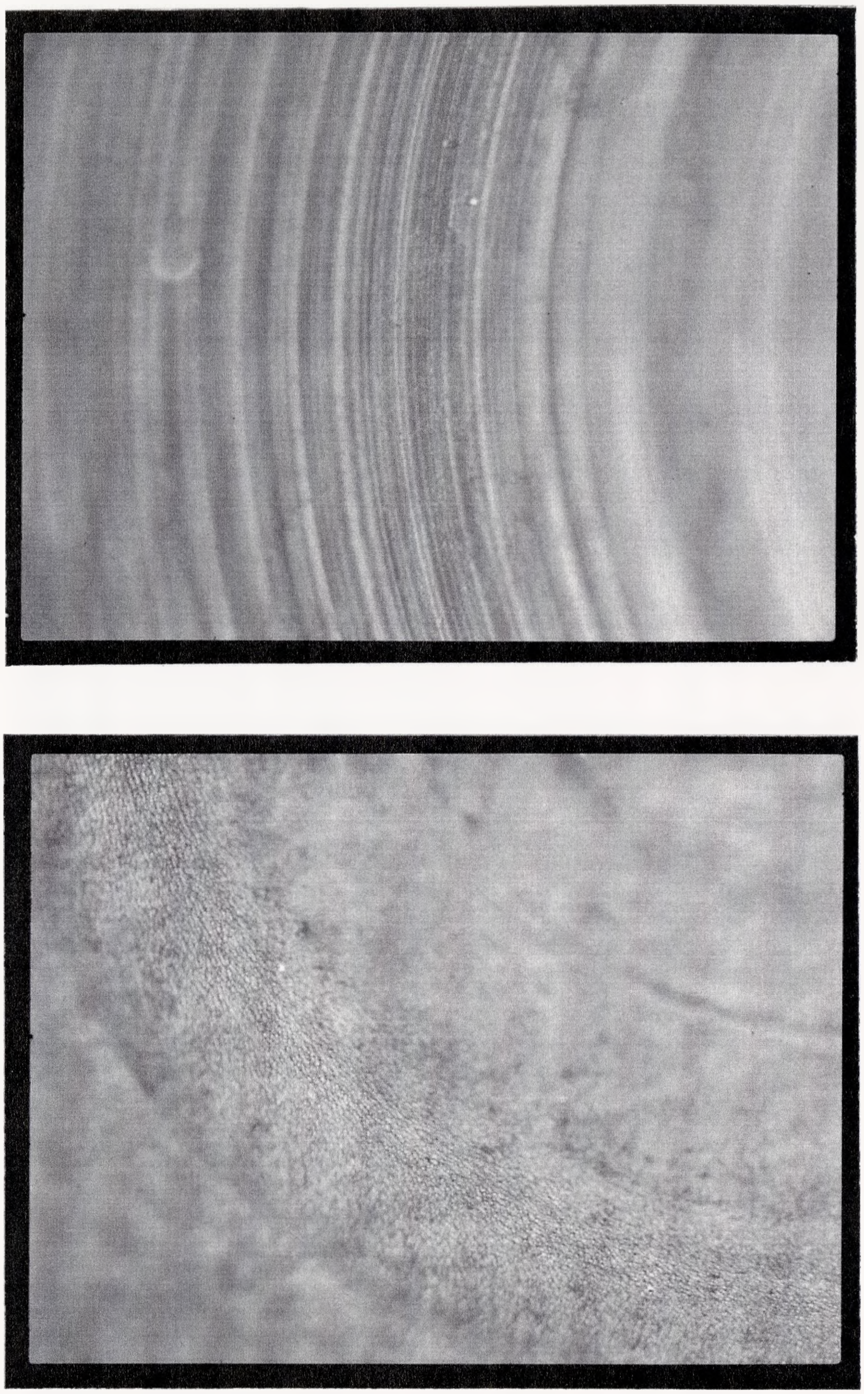

Figure 7.6 Above; photo of a 6.35mm hemispherical shape taken near the top at 200X magnification illustrating elastomer sample surface condition prior to testing. Below; photo of the surface of a 6.35mm hemisphere taken at 192X magnification after two million compression cycles.

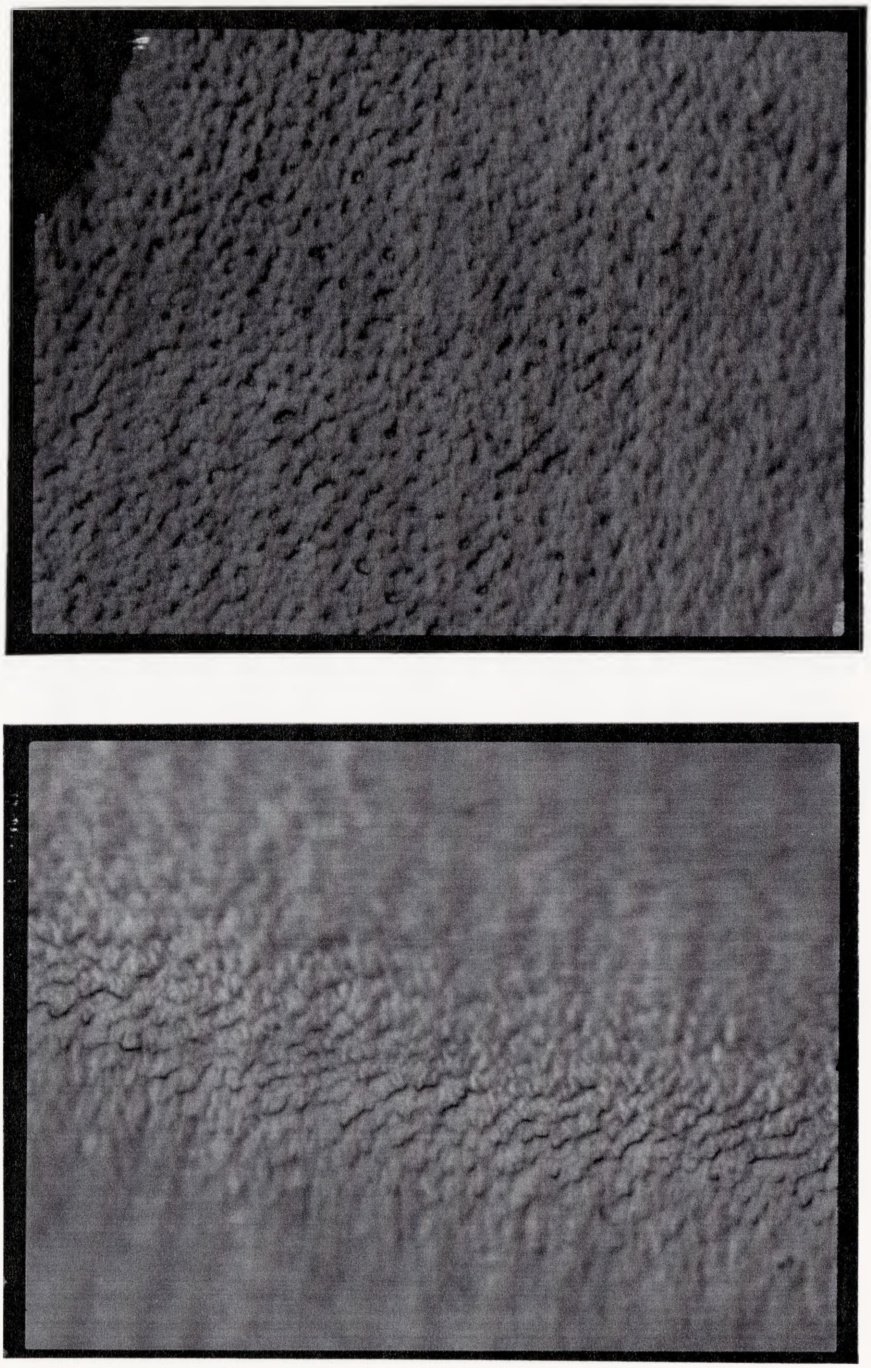

Figure 7.7 Abrasion patterns oriented transversely to the direction of sliding. Above; photo taken at 1000X magnification of the top center of a 6.35mm hemispherical sample after 4 million cycles. Below; photo from same sample taken further out from the center at 1000X magnification.

regions of highest relative motion. Very central regions of a given support for example, would receive very little wear while mid to extreme peripherial areas would experience the most wear, particularly on the flat sheet undersides and flat disc faces. Samples with a higher degree of compressive stiffness were more prone to wear likely because of a higher coefficient of friction with higher normal load. Elastomer debris was also observed on samples both loosely and in a tightly compacted form after testing. On samples with the greatest wear such as the 12.7mm disc and 25.4mm sphere, a large smooth irregular shaped mound of elastomer located centrally on flat sample faces could be observed after testing to the naked eye. Further observation revealed that these 'mounds' could be scraped away to expose the original flat elastomer surface. The explanation therefore is that small pieces removed from the surface by the wear process migrated inwardly and outwardly radially as a result of relative movement between the test sample and polyethylene surfaces. Elastomer debris moving inward to the center of the sample, where there is little or no relative slippage, thus became entrapped and remained being tightly compacted to the surface by compressive forces.

Aside from the abrasion patterns, samples showed other forms of surface degradation such as fine scoring and the existance of broader smooth scores or cavities worn into the surface. Observation of sample surfaces clearly indicated that this form of wear was the result of loose bodies of elastomer which had become entrapped and worked into the sample surface, or due to relative movements causing a ploughing action, created very smooth trenching or scoring of the elastomer surfaces. Elastomer debris was also observed to collect together resulting in surface scoring to various sizes and degrees. This three body form of wear degraded elastomer surfaces more severely than the abrasion patterns alone, and ranged from very shallow fine scores to complete erosion and removal of a surface region.

The top of figure 7.8 illustrates fine radially oriented scoring on the flat sheet underside of a conical shaped support. The central region directly under the cone (seen at the left of the photo) is the least worn. The bottom of figure 7.8 shows what could be considered an intermediate state of wear on a hemispherical sample, where the surface has begun to erode beyond the abrasion pattern. The top photo of figure 7.9 was taken from the flat sheet underside of a 25.4mm hemispherically shaped sample, and illustrates the most severe type of erosion of an elastomer surface observed. At the top of this picture is the very central region underneath the hemisphere, from which a layer of compacted debris was removed exposing an almost unworn original surface. Moving radially away from the center, the profile drops off, the original surface having been completely eroded away. Note the smoothly worn surfaces, radially aligned scoring marks, and small bits of compacted debris still adhered to the surface at the bottom left. In contrast the bottom photo of figure 7.9 shows very small eroded regions located at a constant radius on the top face of a

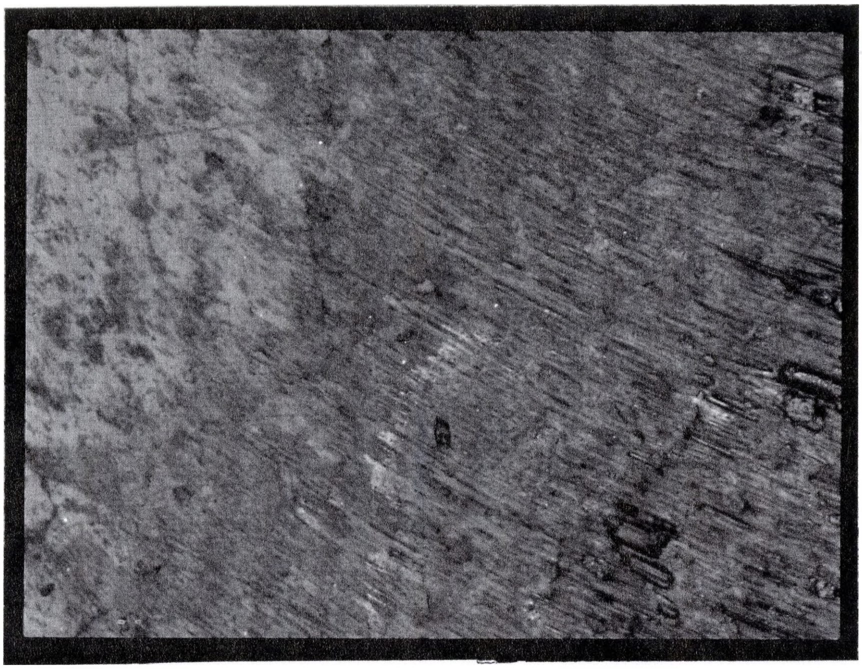

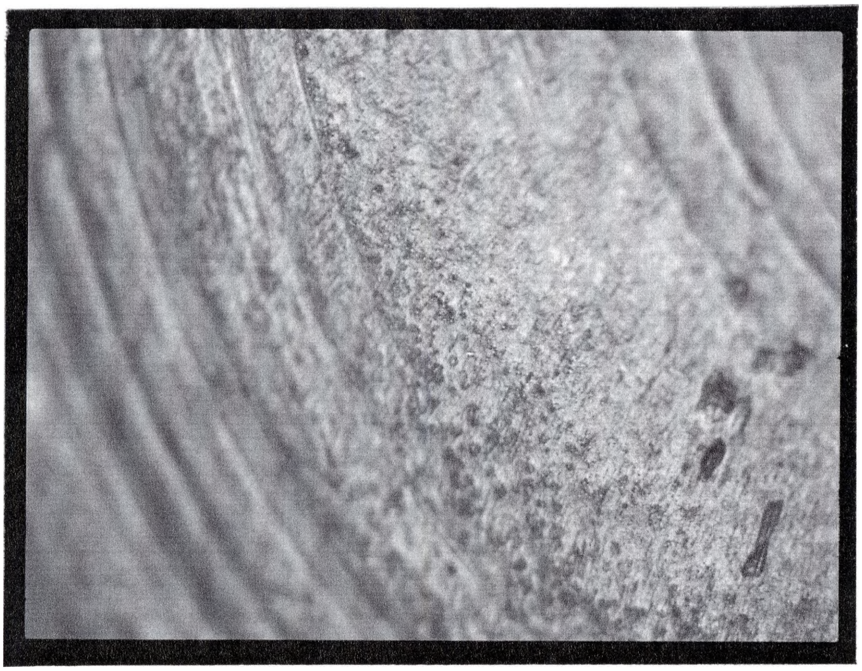

Figure 7.8 Above; Fine scoring of elastomer surface. Photo taken from the flat sheet underside of a 4mm conical featured sample at 160X after 4 million cycles. Note original elastomer surface towards the left and larger cavities to the right. Below; intermediate surface erosion of a 25.4mm hemispherical sample taken at 192X after 2 million cycles.

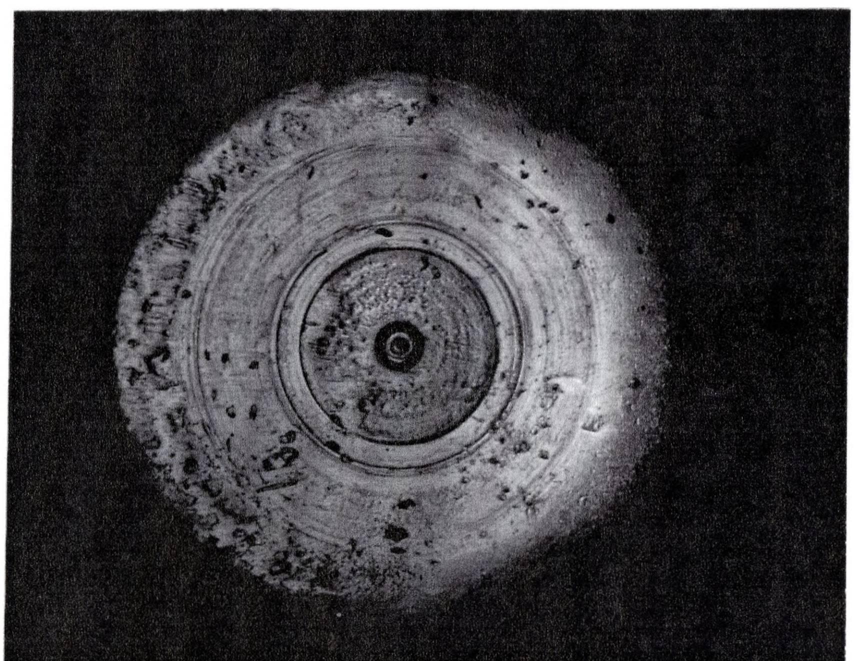

Figure 7.9 Above; severe erosion of elastomer surface. Photo taken from flat underside of a 25.4mm spherical featured sample at 40X after 2 million cycles. Below; flat, top face of a 4mm cone taken at 48X magnification after 2 million cycles. Photo illustrates abrasion pattern on surface to the right and erosion of peripheral regions to left.

conical sample, typical of the eventual erosion seen on smaller samples. The cited references on wear herein, offer no description or mechanisms of three body wear other than the mention that very little attention has been paid to this area.

On the basis of overall observation the general wear pattern for elastomer samples begins with surface abrasion likely by roll formation, and existance of a ridged wear pattern. As more and more detached elastomer particles collect the elastomer surface starts to become slightly scored and a three body wear begins to degrade surfaces further. This process continues and accelerates until eventually the original elastomer surface is worn away in regions of high relative motion. Smoothly eroded regions, ploughing, radial scoring and elastomer debris in various sizes become evident and easily visible under the microscope (more severe surface degradation being visible to the eye). With further cycling the surfaces simply degrade further eroding more severely and in new areas. With all samples tested the ridged abrasion pattern was evident after 2 million compression cycles. Erosion or removal of the initial sample surfaces occurred to varying degrees at various numbers of cycles. The 25.4mm sphere and 12.7mm disc shapes showed severe material removal after 2 million cycles, while smaller samples such as the 4mm conical shape exhibited only very small eroded regions on most cones after 6 million cycles. Overall, cylindrical shapes showed the poorest resistance to wear with spherical shapes wearing intermediately and conical shapes the best. Lastly, it is difficult to estimate the contribution of the water bath to overall wear reduction. Very smooth conforming surfaces tend to impede the ingress of lubricant and flat elastomer surfaces appeared to squeeze out the water almost entirely. For the various featured shapes the water likely provided some degree of boundary lubrication which is the combination of both liquid and solid contact.

7.4.3 Quantitative Wear Assessment

At the outset of fatigue testing the current work was not perceived as a wear study and therefore proper wear test protocols and methods were not recognized. As testing progressed however, it was decided to attempt to quantify some of the wear which was being observed. The assessment of wear can be accomplished by either monitoring the change on some typical test specimen dimension or by gravimetric techniques which monitor test specimen weight loss, or the weight of collected debris. It was decided that the second of these methods (ie measurement of sample weight before and after testing) using a suitably accurate scale might shed some light on sample wear rates.

The recording of specimen weight meant that samples had to be clean both prior to, and after testing. As mentioned in the methods section it was discovered through trial and error that the only simple way to accomplish this and avoid dust, soap or mineral contaminants, was by thorough washing with a soft bristled brush, followed by hot water and distilled water rinses. With a non destructive method of cleaning established, the first attempts at monitoring weight revealed that samples weighed more after testing than prior. This was the result of fluid sorption by samples submerged in the distilled water bath. Attempts to offset the presence of moisture were tried by heating samples prior to weighing. A pilot trial indicated that samples exhibited no further loss in weight after placement in a small oven at 120 °C for three hours. This procedure reduced discrepancy between sample weights before and after testing however, the method of placing warm samples directly into a balance was erroneous since resulting warm air drafts inside the scale are enough to affect the very precise measurements required. Test samples all weighed less than one gram, and the scales used provided readouts to four and five decimal places.

The final method tried to assess weight loss consisted of sample cleaning, placement in a laboratory oven for 3.5 hours at 120 °C, and then cooling to room temperature for 45 minutes in a dessicant jar prior to weighing. Of the five elastomer samples tried with this method before and after the first two million compression cycles, three of the samples showed a net weight loss and the remaining two a weight increase. Further, all of these weight changes were extremely small being less than 0.003%. Therefore, whether through some inconsistency in procedure, the procedure itself, or simply that the amount of weight loss in the first two million cycles is exceedingly small and difficult to determine by any method, these attempts at quantification of wear were considered inconclusive.

In hindsight it is clear that proper wear assessment requires the use of specialized equipment and methods. The problem of weight gain by fluid sorption is also encountered in wear assessment of polyethylene where samples are often heavier after testing than prior. To correct for this researchers have documented fluid sorption and applied correction factors. Test samples have been presoaked prior to testing to minimize fluid sorption during tests, and soak control specimens are used which under go identical procedures as the actual test specimens save wearing itself. Average net gain or loss in weight of the control specimens is corrected for on the wear specimens when weighed. In addition such tests employ very thorough cleaning regimes which include specimen cleaning with water and soap solutions, alcohol, and sonic baths, followed by air jet drying and placement in a vacuum degassing chamber prior to weighing [55]. For future work, some of these above methods might be applied should it be required to determine elastomer wear rates.

7.5 Discussion

The fatigue test machine designed proved to be well suited for the testing done herein. This machine ran successfully without problem to a total of 45 million cycles (including all testing presented in both chapters 7 and 8), which translates into half a year of continuous running time. Overall the machine might have been designed so as to be practically easier to use. Tight space constraints made test set ups and modifications somewhat difficult. In addition a linkage connecting the gear box shaft to the oscillating upper compression plate would have been preferrable to the cam design, thus eliminating the need for an oil bath. Use of multiple test specimens greatly speeded the test proceedure however, owing to sample preparation and observation time, as well as test set up and running time, fatigue testing was by far the most time consuming work undertaken.

During the course of testing no fatigue cracking of elastomer samples was observed. Considering some of the sample surfaces which contained very sharp surface flaws due to molding, this result bodes well for the general resistance to crack propogation. For future work the general importance of sample quality to material assessment and long term durability is emphasized. Swanson and coworkers [4,40], in developing flexible finger joint implants, stressed the importance of design to minimize stresses as well as material and surface quality in creating successful durable implants.

The fatigue testing herein failed in the initial objective of determining a compressive fatigue life for various elastomer shapes. The Dow Corning corporation states the fatigue life of its various Silastic brand flexible elastomer implants to be 260 million movement cycles. It has also been reported that 1 million cycles per year is a reasonably good estimate of the number of loading cycles at the knee joint for active seniors [55]. Thus if the compressive fatigue resistance of elastomer shapes were even 10% of 260 million, a significant potential service life would be realized. Wear of elastomer samples however, has been and continues to be the limiting factor in establishing compressive fatigue resistance. The question of what is acceptable wear may be raised, and the lack of any quantitative data does not permit elastomer wear rates to be compared to polyethylene wear rates found in the literature. Parameters such as different surface textures and the use of bovine serum as a lubricant might improve the wear condition. However, given the smooth conforming nature of elastomer surfaces when flat or pressed flat, as well as a high tendancy to stick to other flat surfaces (through adhesion), it is unlikely that a different lubricant would be able to penetrate between surfaces and impove the wear condition dramatically. On the basis of the wear observed herein, in a relatively low number of compression cycles, it is recommended that situations where relative slippage can occur at the elastomer interface be avoided. The Silastic material does not appear to possess the necessary wear or abrasion resistance to provide long term durability in configurations where relative movement of surfaces can occur. The release of wear debris, whether elastomer or poyethylene, is currently an issue of major concern since resulting biological responses can lead to component loosening, thereby limiting the life of the prosthesis. Future work therefore should focus on minimizing or eliminating slippage and relative movements at the elastomer interface in the hope of removing the wear problem and establishing a compressive fatigue life.

CHAPTER EIGHT

DESIGN AND TESTING OF A NEW ELASTOMER SHAPE

Introduction

Results of tests conducted in previous chapters had revealed that elastomer shapes demonstrated very promising stiffness and shock reduction characteristics, but were susceptible to wear which prevented determination of a compressive fatigue life. To further the current work, and address the problem of wear, a new elastomer sample shape was conceived and fabricated with wear reduction being the primary goal in its design. Design, fabrication, and testing of this new sample shape are presented herein.

8.1 Proposed Design Shape

Radial or lateral expansion of samples when compressed between two parallel plates creates relative movements at the plate interface and subsequent wear. It was recommended at the end of the previous chapter that such movements be eliminated or at least restricted to further fatigue evaluation. To this end, the idea of mechanically constraining samples was considered. As outlined in chapter four complete constraint of a sample is not possible. The material must be left free to deform if it is to act as a compression spring and damper. If however, the sample were constrained at the compression faces only and left free to deform centrally, a useful shape might be achieved.

Following the above rationale a new elastomer shape was conceived which consisted of a right cylindrical shape with flat faced ends pressed into blind holes of equal, or nearly equal, diameters shown in figure 8.1 a). The holes would be shallow enough to leave the central region free to deform, yet restrict lateral movements at each end. In addition, it was decided that the central diameter of the cylinder be reduced to create a tapered or 'hourglass' shape as in figure 8.1 b). This was done for two reasons. First, a taper would prevent a cutting in effect by the edges of the blind holes into the sample sides when samples expanded laterally on compression. Secondly, such a taper would create a least resistance in terms of stiffness at the mid region. This would promote bulging centrally when compressed instead of at the end faces. It was perceived that such a design might significantly reduce the wear problem yet, retain the positive mechanical properties of previous samples, and therefore merited testing.

With the above concept in mind the next step was to select and finalize actual test specimen dimensions. Three sample sizes were chosen for fabriction having largest outer diameters of 4.7mm, 6.3mm, and 7.9mm. To allow for some extra height for end constraint all samples were limited to 5mm in overall height, being slightly higher than the previous test samples. The sections of constant diameter at each of

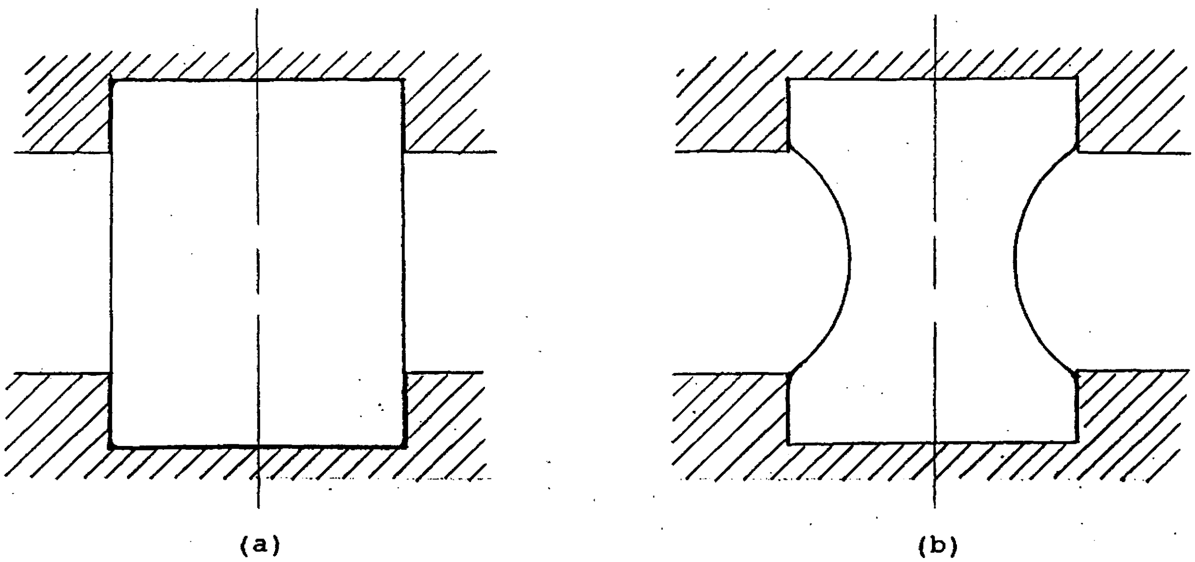

Figure 8.1 (a) Cross section view of a cylindrical elastomer shape with ends constrained in recessed holes. (b) Similar view of a constrained cylindrical shape with tapered mid section.

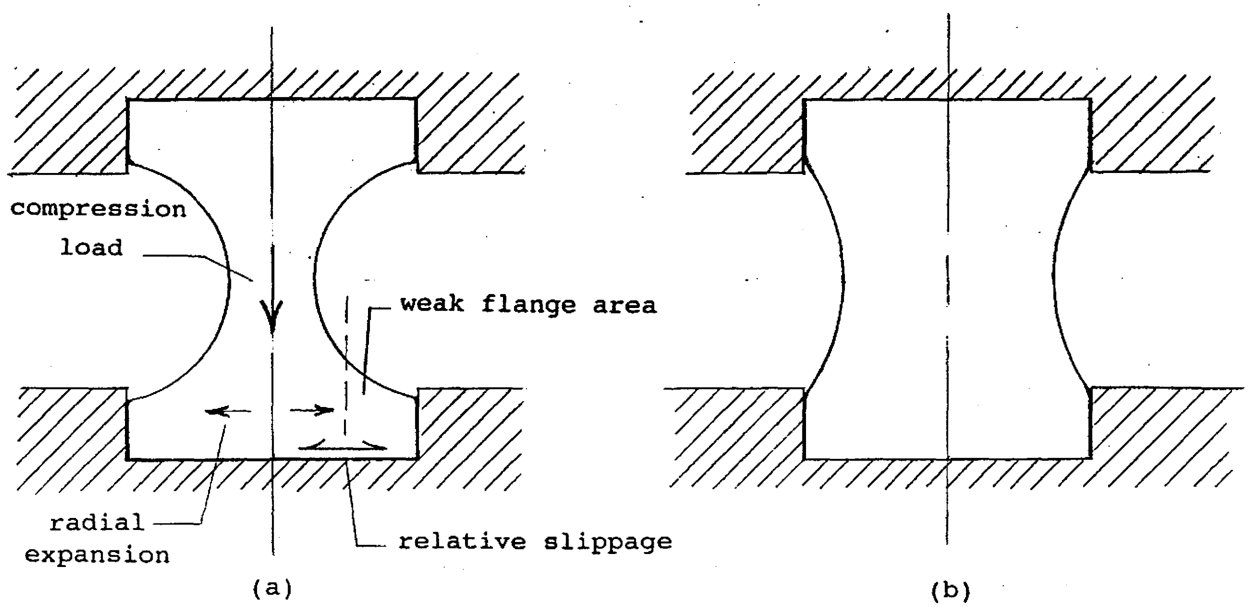

Figure 8.2 (a) Cross section view illustrating relative movement at the compression plate face, resulting from too large a central taper. (b) A more gradual degree of taper, reducing chances of slippage in the contained ends.

the top and bottom ends needed to be substantial enough to offer end constraint, but not so large as to leave inadequate height centrally for sample deformation. These end sections were therefore made 1mm in height each, leaving 3mm of height for the central tapered section. Lastly, the degree of taper at the mid section needed to be determined. For reasons given above, some degree of taper was deemed essential however, too much taper might also prove undesirable. As illustrated in figure 8.2 a) if the central tapered section is too small, a large area of elastomer at the outer periphery of the constrained area would be relatively weak and free to deform, allowing relative movements to occur locally. A more preferable design is illustrated in figure 8.2 b), where local slippage is less likely to occur. The degree of taper was chosen so that the smallest diameter at the mid section was 75% of the largest outer diameter in the constrained regions for each sample. As a result cross sectional area at the mid sections was 56% of that for constrained ends, reducing stiffness considerably and promoting deformation centrally.

8.2 Mold Design

With sample design complete a new mold was required which could practically produce such a shape. The new elastomer shape was much more difficult to mold than previous samples because of the tapered mid section. Once formed into shape by being pressed into a tapered cavity the problem of how to retrieve samples from the mold without damage existed. The tapered samples therefore required some type of split mold which could form the required shape, and then be opened up or taken apart to allow retrieval of the sample.

After consideration of various ideas the technique chosen to fabricate 'hourglass' samples was similar the one used originally. For each sample size, a series of tapered holes were bored into a small aluminum alloy (6061-T6) plate along a straight line using specially fabricated cutting tools. The cross sectional shape of these cavities consisted of the tapered mid section, and one cylindrical end section only. Each plate was then cut along a straight line splitting each of the tapered holes in half, and made to fasten together onto a larger 25.4cm by 25.4cm square aluminum base plate thus creating blind cavities. Small relief channels were cut into the bottom of the split plates to allow for the release of air from the blind cavities, and facilitate the flow of elastomer inward. Using the heated press, uncured elastomer could be pressed into these cavities as with the previous mold. Press height was controlled using four stopping blocks so that in addition to the tapered portion a flat base sheet was also formed on top of the split plates 1mm in thickness. Figure 8.3 a) illustrates the full configuration showing the mold cross section, stopping blocks and resulting elastomer shape. Once the elastomer was pressed into shape, the split plates could be unscrewed from the base plate thus freeing the formed samples. As illustrated in figure 8.3 b) the molded elastomer shape consisted of partial hourglass shapes protruding from a uniform base sheet. By using a circular leather punch of appropriate

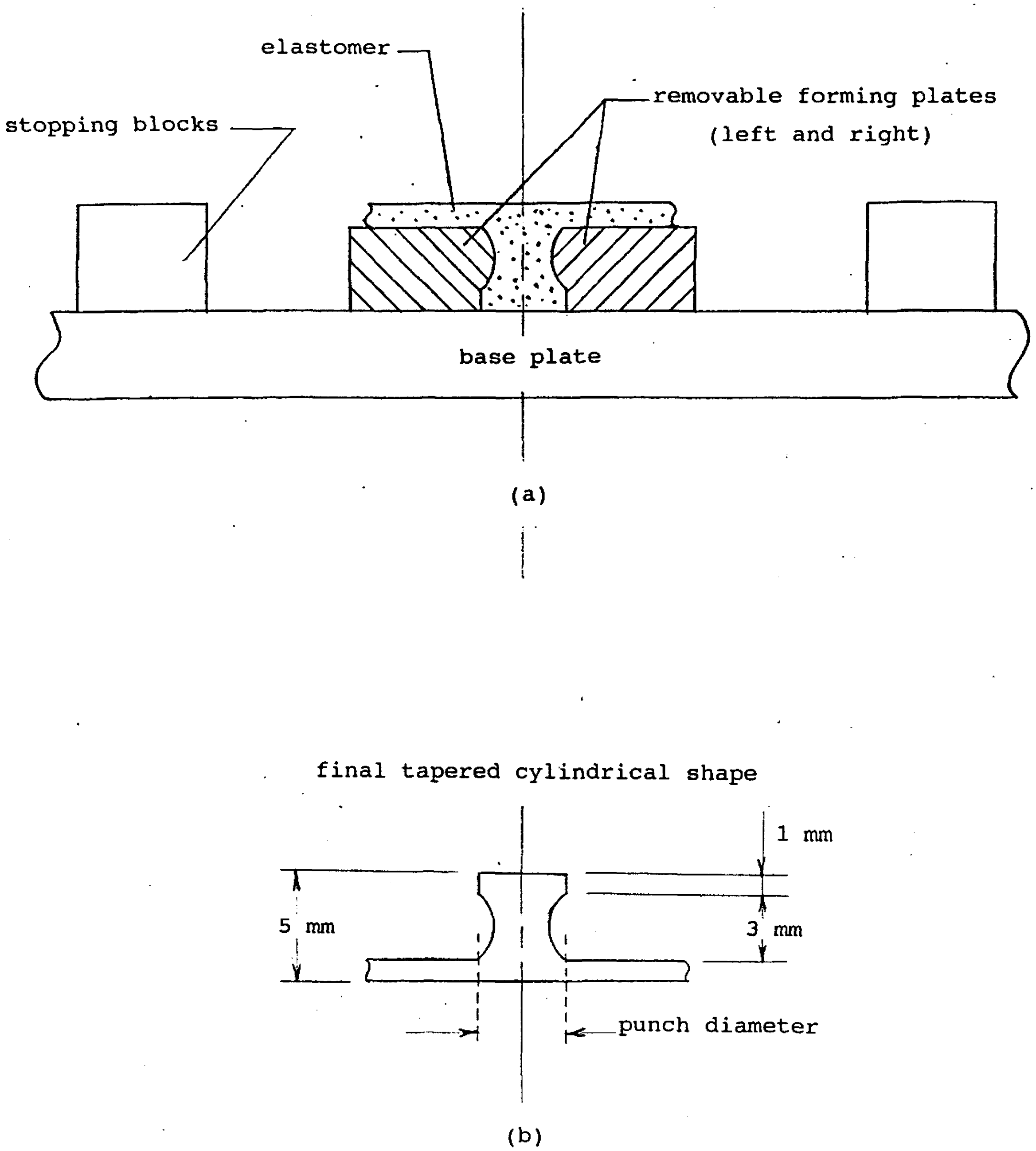

Figure 8.3 (a) Illustration of molding plate cross section showing formed elastomer shape. (b) Final tapered cylindrical shapes were stamped from the base sheet using a leather punch of equal diameter.

diameter individual samples could be easily stamped from the sheet creating the final desired sample shape.

The mold described was fabricated and proved to be very successful. The mold is pictured in figure 8.4. Polishing of the cavity surfaces and use of stopping blocks to control height greatly improved sample quality over the previous mold. Elastomer shapes were more consistent with smooth, much less flawed surfaces.

8.3 Test Sample Configuration

Since design of the new sample shape was based on containment of sample ends in circular holes, the question arose as to what diameter to make the containment holes. If these holes were too large and sample fit loose, the benefit of constraint might be lost. If the fit were too tight samples might become distorted in shape and over stressed. Trial and observation of samples in different sized holes suggested that holes of equal diameter, or zero press fit, were too loose, and that hole diamters 10 thousands of an inch smaller than sample diameters were too tight making sample placement into the cavity difficult. Since several elastomer samples could be tested at once it was decided to try a few different containment hole sizes within the above range, the exact values of which are specified in the method sections to follow.

It was also realized that containment of several samples press fit into

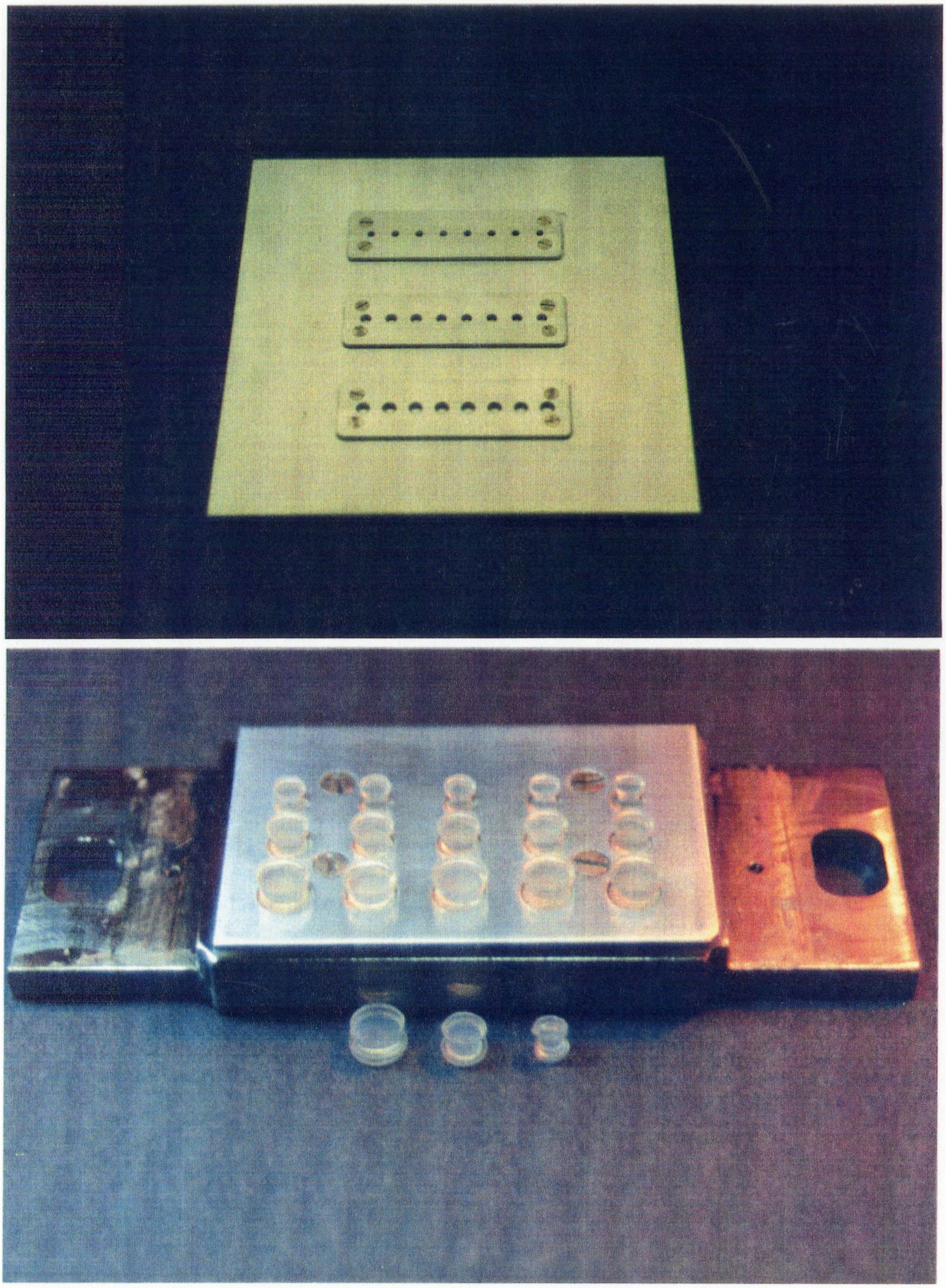

Figure 8.4 Above; molding plate for tapered cylindrical samples. Below; tapered samples stamped from base sheets and mounted in lower compression plate of the fatigue test machine.

blind holes, top and bottom, would be practically difficult to assemble. Therefore, elastomer samples were contained by a series of two plates at each end as illustrated in figure 8.5. A 1.6mm thick aluminum plate with through holes was used to contain sample ends peripherally, while small 3.2mm thick sheets of polyethylene backing served to close the holes and act as the compressing faces. The aluminum plate could be first placed over sample ends making sure all samples fit properly and to the furthest depth. The polyethylene could then be screwed into place pushing back any samples protruding too far through the holes. This idea of using two plates was used for each of the following tests making assembly of test configurations easier, and ensuring samples were seated all the way into each cavity.

8.3.1 Sample Testing

All of the shock testing was completed prior to fabriation of the 'hour glass' shaped samples and therefore no impact testing was conducted with this new shape. Both compression and fatigue tests were carried out for the new sample shape, the methods and results of which are outlined below.

8.4. Force-Deflection Tests

8.4.1. Method

All samples tested were constrained using metal and polyethylene plates as described above. All samples were constrained in holes having diameters approximately 0.1mm (0.004 inches) less than the sample

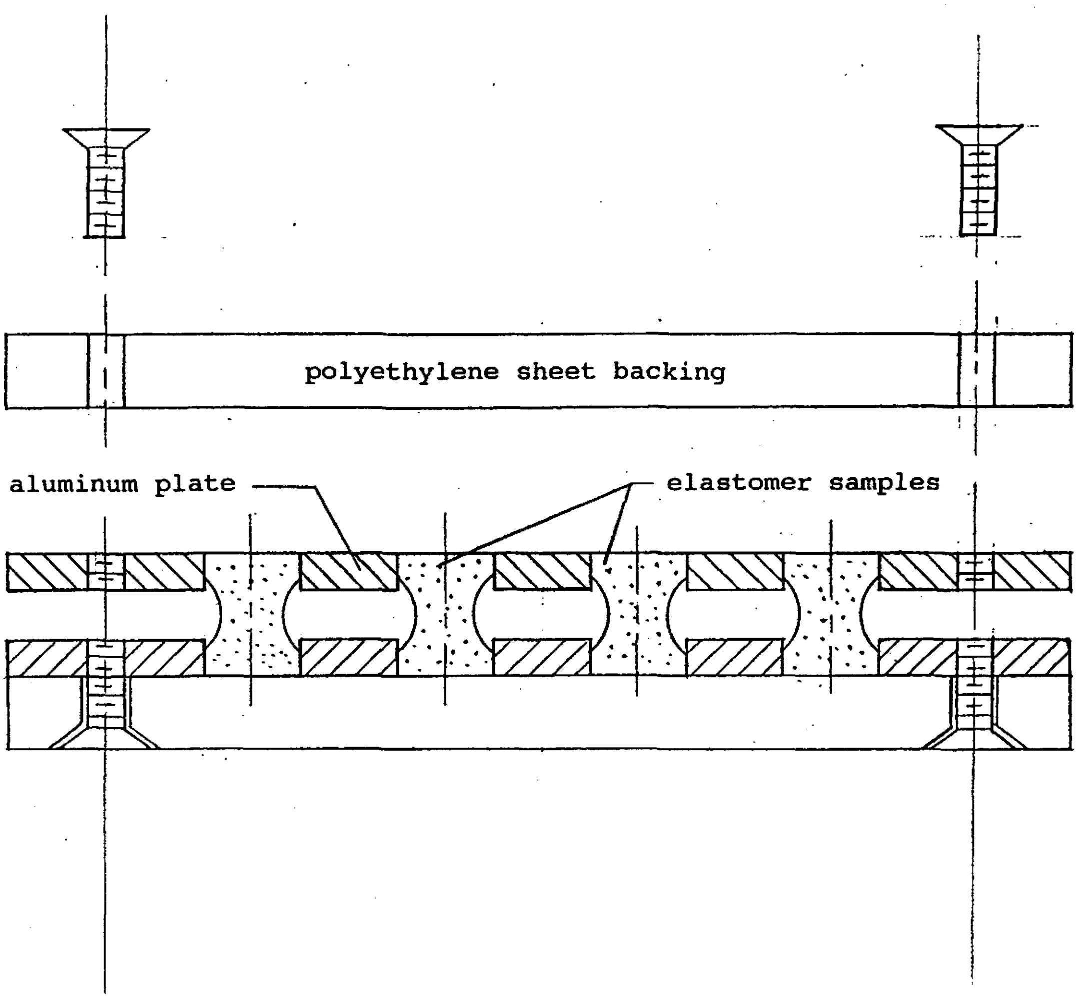

Figure 8.5 Cross section illustrating assembly and constraint of tapered cyindrical shapes for testing. Aluminum plates with spaced holes, and polyethylene sheet were fastened together to contain samples.

diameters, giving a mild press fit. The 7.9mm and 6.3mm diameter samples were tested in groups of five while 4.7mm diameter samples were tested ten at a time.

For test purposes it was assumed that only the tapered central region of each sample was free to deform. Constrained ends were not considered as a functional part of the sample and omitted from the overall height. Test samples were therfore compressed to a strain equalling 20% of the tapered section length of 3mm. Methods used to compress samples were identical to those of section 5.2.1. Preload values were determined by the appropriate fraction of 22N based on the amount of sample surface area occupied at the loaded faces.

8.4.2 Results

Force defection curves for each of the three sample sizes are presented in figures 8.6 to 8.9. Average peak compression forces to 20% strain were 76N, 93N, and 170N for ten 4.7mm diameter samples, five 6.3mm diameter samples, and five 7.9mm diameter samples respectively. Observation of curves in figures 8.6 to 8.9 show that unloading curves tended to follow loading curves more closely than with previous samples. Although areas within these curves were not computed this would indicate low hysteresis and damping characteristics. Compression to 30% strain with the 6.3mm sample showed rapidly increasing stiffness with increased strain as with previous samples. Increasing maximum

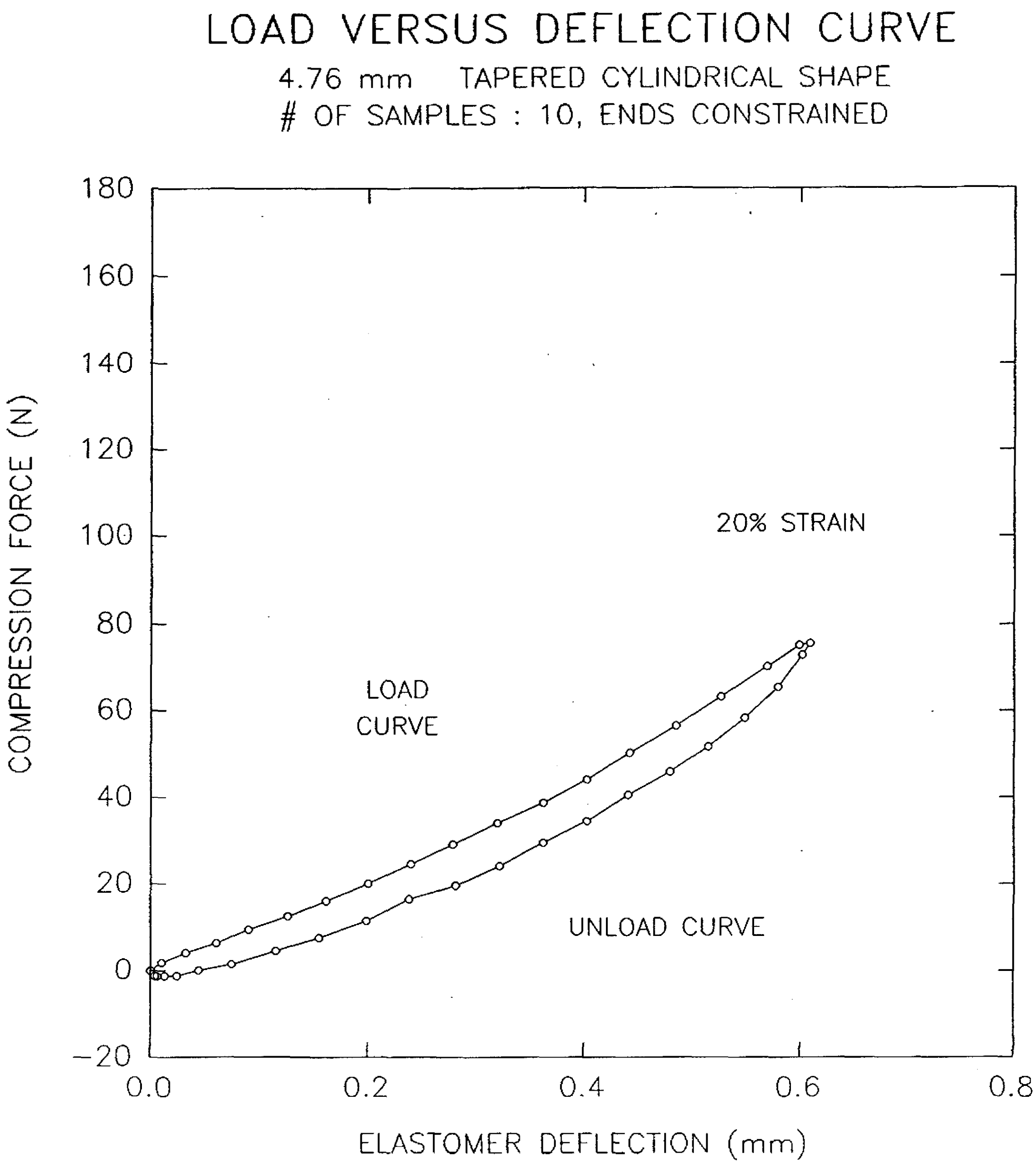

Figure 8.6 Force deflection curve for ten 4.7mm diameter tapered cylindrical shapes compressed to 20% strain at 3 hz.

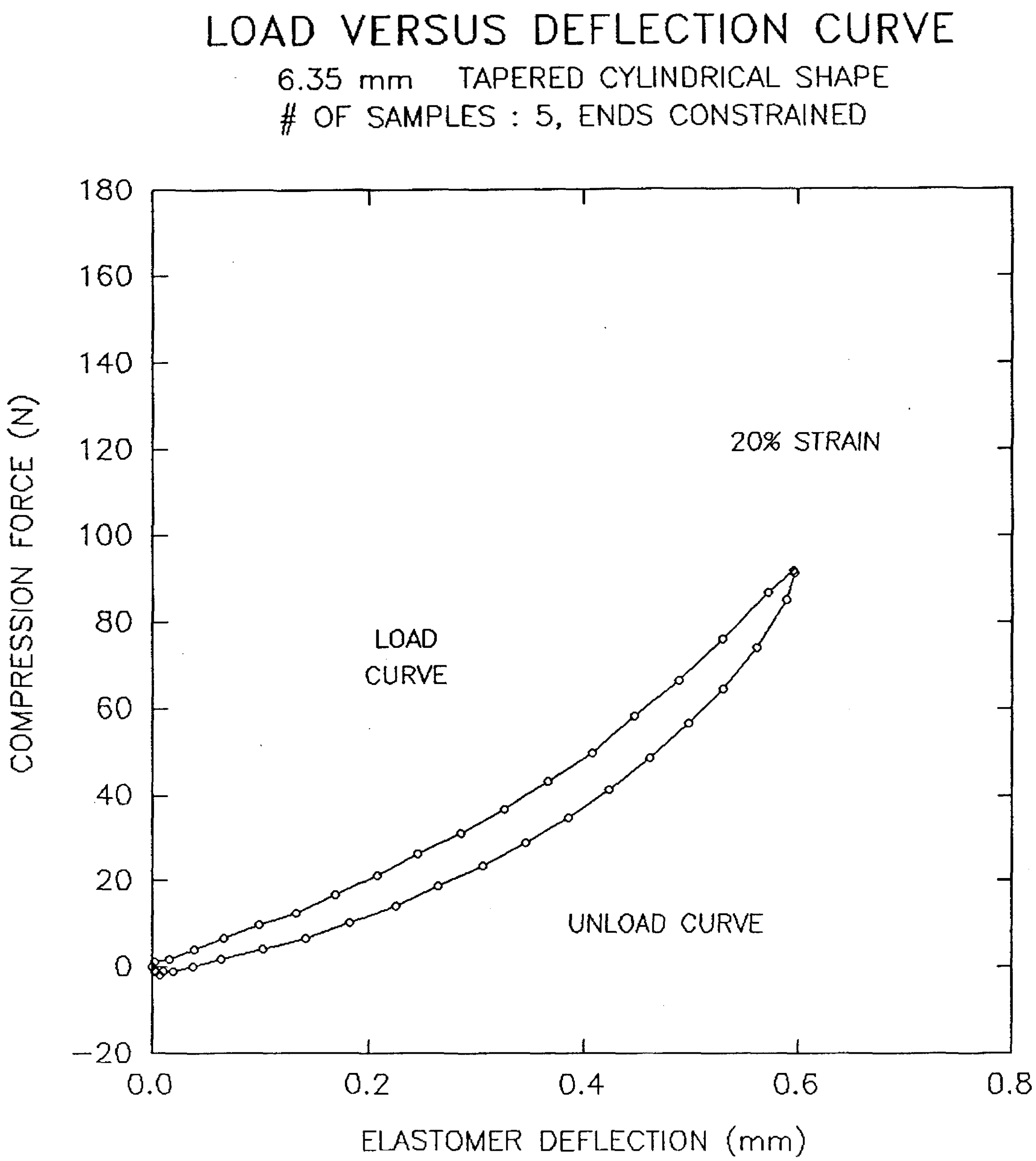

Figure 8.7 Force deflection curve for five 6.3mm diameter tapered cylindrical shapes compressed to 20% strain at 3 hz.

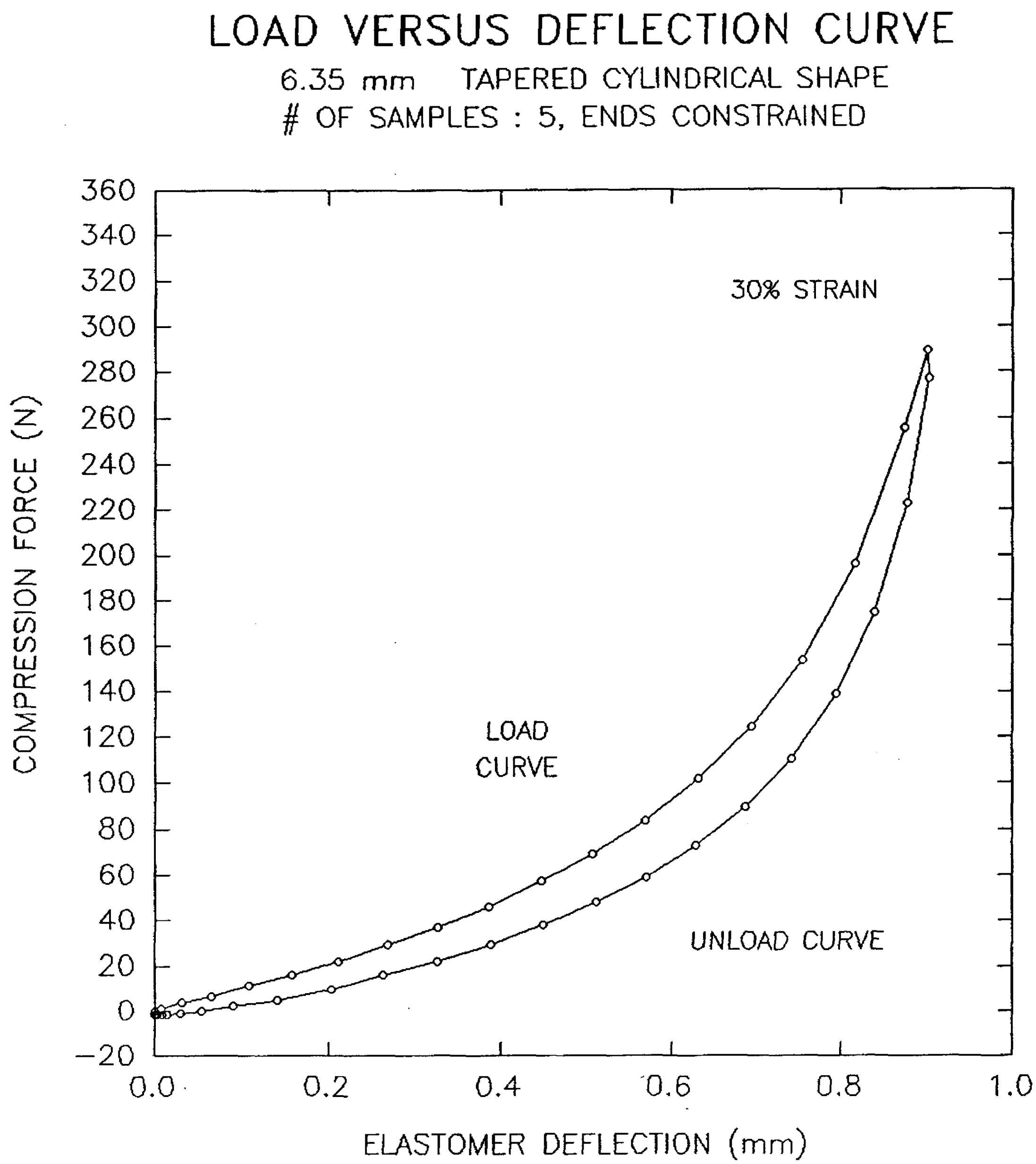

Figure 8.8 Force deflection curve for five 6.3mm diameter tapered cylindrical shapes compressed to 30% strain at 3 hz.

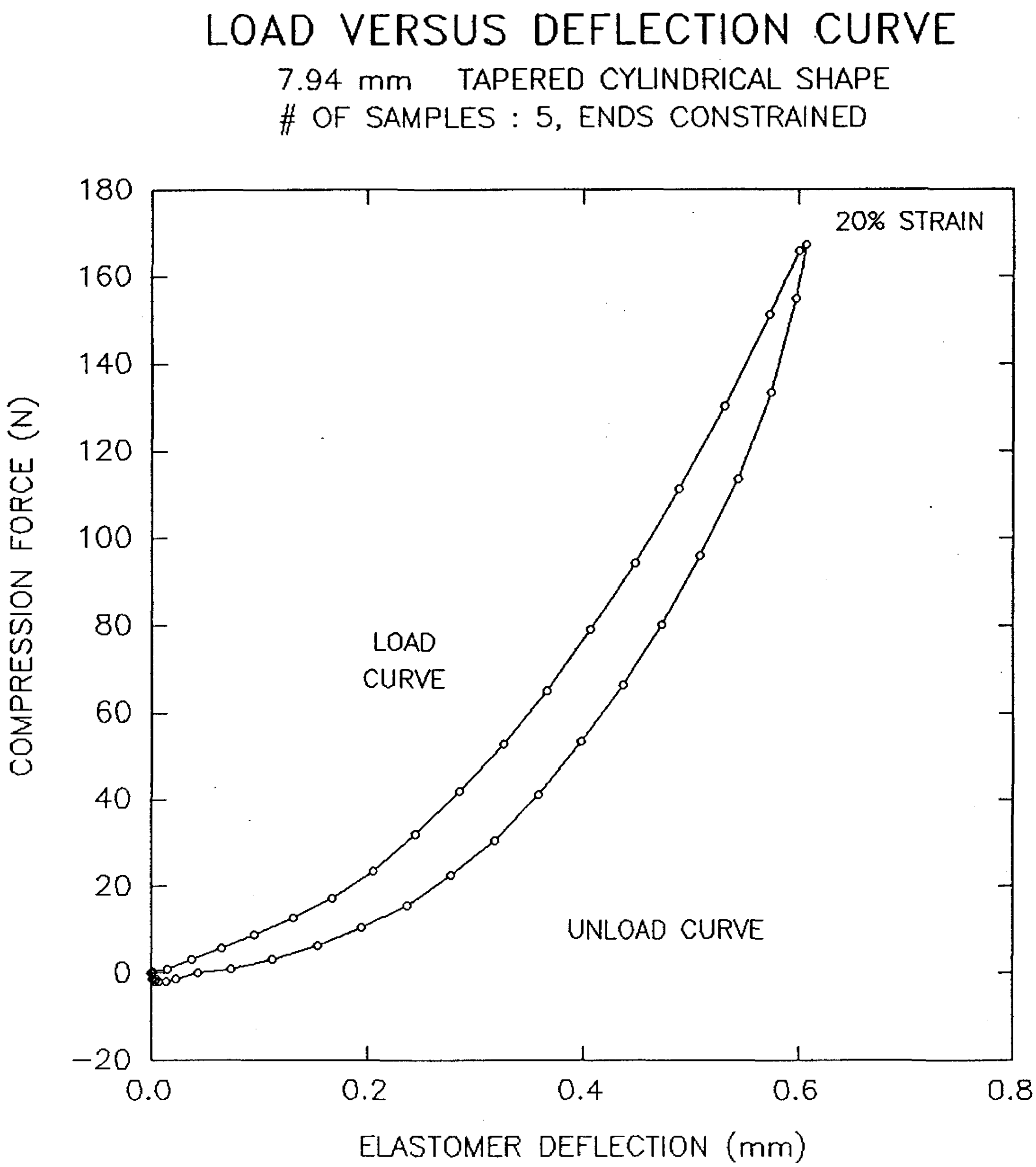

Figure 8.9 Force deflection curve for five 7.9mm diameter tapered cylindrical shapes compressed to 20% strain at 3 hz.

strain from 20 to 30% caused and increase in peak compressive force of 311%.

8.4.3 Discussion

Overall, stiffness of the tapered samples was lower than expected. When test results are extrapolated to the number of samples required to occupy approximately $15cm^2$ of surface area at the load faces, 4.6mm, 6.3mm, and 7.9mm diameter samples would require 632N, 881N, and 1023N respectively to achieve 20% strain. When compared to cylindrical featured sheets where cylinders also occupied approximately $15cm^2$ of surface area, the total stiffness of the tapered shapes is much lower (refer to table 5.1). The most obvious reason for this difference is that the smaller central cross section of the tapered shapes significantly reduces the stiffness of each sample over a right cylindrical shape of equal diameter. Therefore on a per surface area basis, tapered samples will have less compressive resistance. Secondly, the actual height of the individual discs on cylindrically featured sheets was approximately 2.5mm as opposed to the 3mm mid section height of tapered shapes. This contributed to a difference in stiffness via the influence of shape factor. Lastly, there may have been localized deformations in the constrained sample regions similar to that illustrated in figure 8.2 a). Such deformations would reduce the overall stiffness value in comparison to a test sample which was exactly 3mm in height. Thus in hindsight it may not have been strictly correct to assume that samples were effectively 3mm in height with rigid ends.

8.5 Fatigue Testing

8.5.1 Method

Containment of samples for fatigue testing was the same as outlined in section 8.3. Fifteen samples, five of each of the three sizes, were tested simultaneously. All of the containment hole diameters were made smaller than the corresponding sample diameter, creating a degree of press fit to provide tight constraint of the elastomer sample ends. For each sample diameter various amounts of interferance fits were tried. Each test sample diameter is listed below along with differences between the sample diameter, and various containment hole diameters:

Sample Size (dia.)	Interferance Fits
4.7 mm	0.025mm, 0.11mm, 0.14mm, 0.21mm
6.3 mm	0.025mm, 0.1mm , 0.15mm, 0.21mm
7.9 mm	0.08 mm, 0.14mm, 0.24mm

As with force-strain testing the effective sample height, or portion of samples considered free to deform, was taken as 3.0mm. Samples were therefore compression loaded to a deflection equalling 20% of 3.0mm. Test protocol and methods were the same as those outlined in chapter seven.

8.5.2 Results

Tapered cylindrical shapes were fatigue tested to a total of 10.2 million cycles at which point testing was discontinued due to time constraints. Results of wear types, extent of wear, and fatigue cracking observed are summarized in the following sections.

1. *Wear Types*: Types of surface degradation observed on sample compression faces were the same as those observed and outlined in chapter seven, section 7.4. Specific wear types and mechanisms will therefore not be reviewed here.

2. *Sample Wear*: Wear observed on tapered cylindrical shapes after 10.2 million cycles was extremely mild. For all test samples no gross erosion or removal of original surfaces occured. Magnification up to one thousand times revealed that ridged abrasion patterns were only present in an extremely narrow band at the very outer perimeter of samples faces (being less than 1/20 times the sample diameter in width). Remaining central surface regions tended to show either no visible wear, or were slightly scratched and scored by a three body wear. A summary of surface condition according to sample to size is as follows:

i) 4.7mm Diameter: Four of the five samples tested showed no visible surface deterioration save for a slightly dulled appearance, and the narrow region of abrasion at the outer periphery. The remaining sample showed only mild, radially oriented scoring of the surface. This particualar sample was the least constrained, having the smallest interference fit of 0.025mm (.001 inches). Figure 8.10 shows the central and peripheral regions of a 4.9mm diameter sample taken at 50x magnification after 10.2 million cycles. No gross visible wear or abrasion patterns are evident. In comparison, the above photo shows the compression face of 3.2mm diameter cylindrical shaped disc from chapter seven which was tested unconstrained as outlined therein. After 2 million compression cycles this sample face was much more deteriorated showing visible radial scoring, ploughing, and debris at 50x magnification.

ii) 6.3mm Diameter: All five of these samples tested showed some degree of radial scoring and pitting of compression faces centrally, along with an abrasion pattern at the extreme outer peripheries. Samples with the lowest interference fits of 0.025mm, and 0.1mm, showed mild wear over most of their surfaces, and subsequenlty were in the worst condition. Of the remaining two samples having press fits of 0.15mm, and 0.21mm, the former was in the best condition with fine scoring over less than half of its surface area. Visible debris compacted to sample surfaces was observed on the three worst worn samples.

iii) 7.9mm Diameter: As with the 6.3mm diameter case, samples with the lowest press fit suffered the most wear followed by those with the

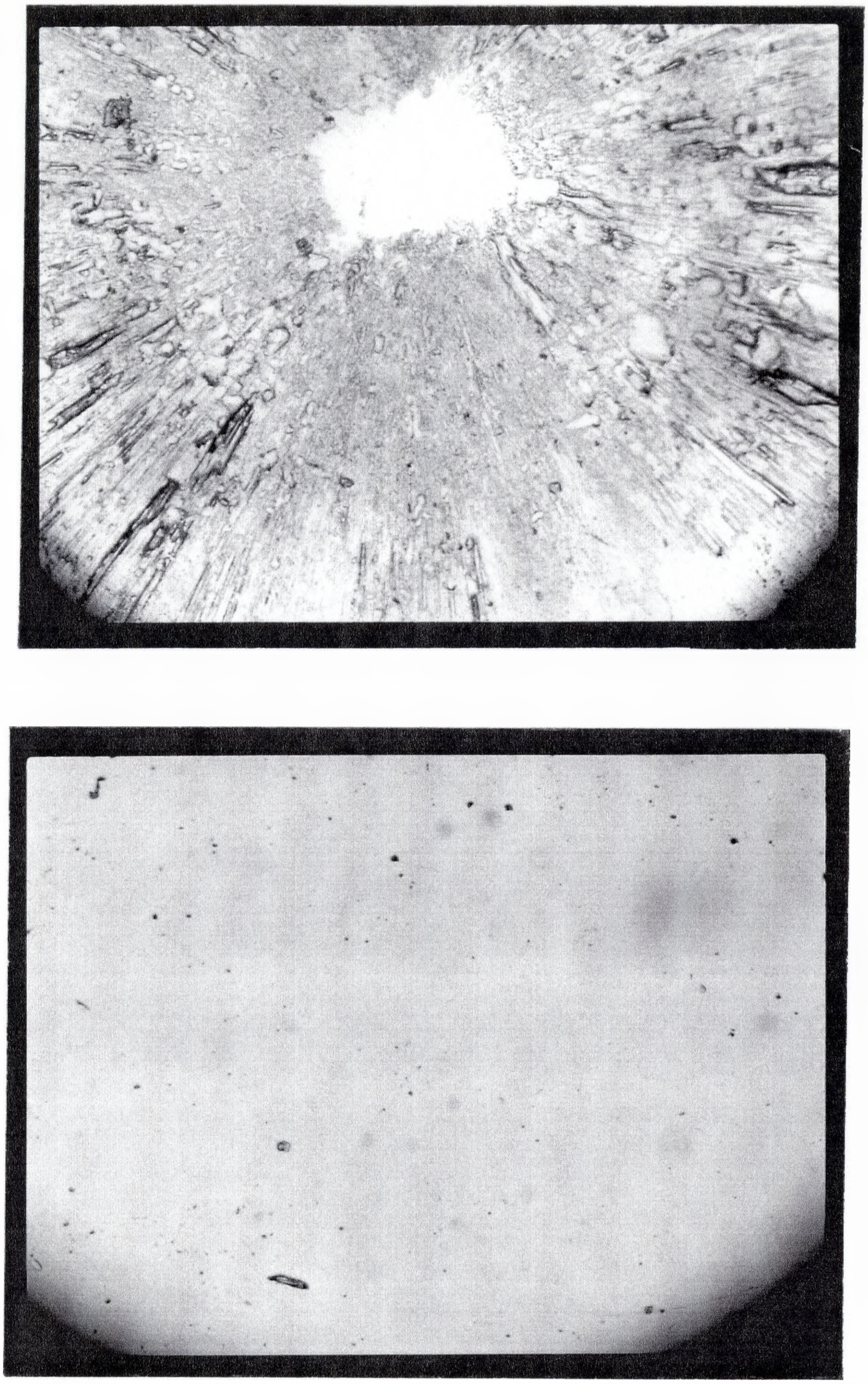

Figure 8.10 Above; surface degradation of a 3.2mm diameter right cylindrical disc, fatigue tested unconstrained to 2 million cycles. Below; surface condition of a constrained 4.7mm diameter tapered cylinder, fatigue tested to 10.2 million cycles.

highest fit. Again wear observed consisted of radial scoring and pitting of surfaces centrally, along with an abrasion pattern at the outer periphery. Elastomer debris was noted on the three worst worn sample surfaces. The remaining two samples, having press fits of 0.14mm, were in near perfect condition with no visible surface deterioration save for the abrasion pattern at the edges.

In total six out of the fifteen samples tested were in near perfect condition after 10.2 million compression cycles. The remaining samples were very mildly worn, particularly in comparison to samples tested in chapter seven. In terms of general wear, the 4.7mm diameter samples were in the best condition followed by the 7.9mm, and then 6.3mm diameter samples.

3. *Fatigue Cracking*: Because of the tapered shape, elastomer samples did not simply bulge outward at the mid section when compressed. It was noted that on loading, surfaces at the very mid section of smallest diameter tended to buckle and fold inward. This action created a visible, sharply defined, crease line around sample mid sections. Examination of samples after 10.2 million cycles showed that most had developed small cracks along this crease line. The development of crease lines and subsequent cracks tended to worsen as sample size increased. Samples with a higher shape factor tended to buckle more. With 4.7mm diameter samples, two of the five tested had at least one crack. Creasing of the surface occured to varying degrees ranging from

none, to creasing around the entire mid section perimeter. With 6.3mm diameter samples most had crease lines around the entire mid section. Four of these five samples had a number of visible cracks, with an average of six per sample. All of the 7.9mm diameter samples had crease lines around the entire mid section and a significant number of visible cracks, the highest number noted being twenty for one sample. Most of the cracks were very small in size requiring magnifications of 100 to 200x to be seen. The largest cracks were observed on 7.9mm diameter samples, ranging up to a maximum of approximately 0.5mm in length. All cracks tended to propogate circumferentially along the line of the crease instead of inward, being larger in length than in depth or width.

8.5.2 Discussion

The containment of elastomer samples greatly reduced surface wear. Several samples showed no visible or gross surface deterioration. On remaining samples the degree of wear observed was very mild in comparison to that observed in chapter seven. Constraint of samples did not eliminate relative movements at the compression interface altogether, but did make existing movements much more localized. Where sufficient movements did occur abrasion patterns, surface scoring, and debris were identifiable as in chapter seven. The existance of an abrasion pattern around sample peripheries indicated greater relative motions at the very edges of the sample face. This may have been due to a squeezing out effect as was illustrated in figure 8.2a). Also, local areas where sample edges did not perfectly fit the constraining cavity existed. Slight out of roundness, and edge flashing from the molding process on samples, left room locally for some relative motion to occur. In regions of minimal relative motion, such as on sample surfaces which showed no visible wear, it is thought that fatigue wear may have occured. If so, its effects were extremely mild leaving no visible marks or debris of distinguishable size at 1000x magnification.

Test results from all three sample sizes indicated that an optimimun degree of constraint existed. Samples with the smallest interference fits all tended to suffer the most wear. Samples which were constrained with the highest press fits tended to wear intermediately. In these cases it was noted that when pressed into the aluminum plate and constrained peripherally, the flat elastomer sample end was constrained tightly so as to bow into a concave shape. As a result the elastomer sample did not tend to rest flatly within the blind hole, likely resulting in relative surface movements when compression loaded. Samples which were fitted intermediately with a press fit of approximately 0.15mm showed the least wear. This worked particularly well with the 7.9mm diameter samples where the two samples with this fit were not visibly worn.

Results of testing showed that the amount of diametral taper chosen was too much, causing a wrinkling and subsequent cracking of sample surfaces centrally. It is believed that increasing the mid section diameter would cause samples to bulge instead of buckle, alleviating this problem. This increase in diameter would have the added benefit of stiffening samples making them more feasible for knee joint application. It is important however, that some degree of taper at the mid section be maintained. It has been reported that for right cylindrical shapes, if a crack forms along the straight sides it tends to propogate inward towards the sample center leading to ultimate failure of the specimen [47]. If the walls are gradually curved or tapered inward however, cracks tend to propogate along the surface, and only result in eventual removal of a small portion of the surface itself. This later case is far more preferable since the specimen does not ultimately fail and can still perform its function.

Thus, initial testing with tapered or hourglass shapes has illuminated several points. This basic shape and concept of constraint significantly reduces wearing at the compression plate interface. A specific or optimum amount of constraint appears to exist which minimizes the tendancy for relative movements at the interface. Although samples proved susceptible to cracking, this was considered a design flaw. Redimensioning of samples along the same basic shape should greatly improve both resistance to cracking, and sample stiffness necessary for knee application.

While the constrained hourglass sample shape provided a significant improvement in terms of wear, it might be improved significantly more if samples were bonded into place using an adhesive. The combination of bonding with mechanical constraint would eliminate relative movements, and hence wear, at the compression plate interface altogether. Mechanical containment would provide most of the constraining force, minimizing shear forces at the bonded interface and thereby, improving bond durability. In addition, adhering samples would ensure that they stayed seated in place, particularly under loads which were not entirely compressive. Overall, the idea of bonded tapered discs appears attractive for prosthetic knee joint design incorporating an elastomer cushion. Such a design of course depends upon the availability of a suitable, durable and biocompatible bonding material. To this end, the author is aware of at least one potential adhesive material. The Dow Corning Medical division has developed a silicone material known as Silastic brand Medical Adhesive Type A. This adhesive is used for bonding silicone elastomers to each other and to some synthetics or metals. The material comes in a paste form which can be applied and shaped as desired, and cures into a solid form much like conventional silicone elastomers. This material is also currently available in sterile form and is biocompatible once cured. Further work therefore, might first focus on the general availability and proper use of such adhesives. Using one or more candidate adhesives, the durability of elastomer discs bonded and constrained to both metal and polyethylene surfaces could be evaluated under repeated loading.

CHAPTER NINE

CONCLUSIONS AND RECOMMENDATIONS

9.1 Conclusions

A hypothesis has been formulated which states that the introduction of a compliant shock absorbing material into a total knee prosthesis would serve to moderate high stresses and strain rates, protecting the bone-cement-metal interface, and thereby, extend joint life. An abundance of evidence exists indicating that current knee joint prostheses remain undesirably limited in service life due to mechanical overloading. However, very limited research to date has addressed the idea of compliancy in artificial joints.

Four criteria were established for any compliant material considered for prosthetic application namely, biocompatibility, fatigue resistance, shock reduction, and appropriate stiffness and elasticity. Based on preliminary investigation results, and proven biocompatibility, Dow Corning's Silastic brand HP100 elastomer was selected for experimental evaluation as a compliant interface material.

A flat space located between metal and polyethylene tibial components was chosen as the most feasible location to incorporate a compliant shock absorbing material into a prosthetic knee joint. Elastomeric test specimens were designed and fabricated in a flat sheet form with various geometrically shaped surface features on top to act as load bearing supports. To provide cushioning effects when compressed along one axis, surface features had to be left unconstrained to deform along the remaining two ordinate axes. A maximum design strain limit of 20% was recommended in the interest of maximizing elastomer cushion fatigue life.

When loaded in compression the elastomer demonstrated a distinct non linear stress strain behavior, becoming increasingly stiff with increasing strain. Hysteresis losses for the material ranged from 28 to 92% at 20% compression strain and 3hz loading frequency, depending strongly on test sample shape. Testing also verified the influence of shape factor. Samples with higher shape factors demonstrated a higher unit compression resistance. Of the elastomer shapes tested, only cylindrically featured sheets and flat smooth sheets possess suitable stiffness to withstand physiological knee joint loads without exceeding 20% compression strain. Adequate surface area is not available in a prosthetic knee joint to produce spherical or conical featured sheet samples which can support physiological loads and remain under 20% compression strain.

Elastomer shapes demonstrated a stiffening tendancy with increasing rate of strain. As compression times increased from 4.5 seconds to 19 millisiconds, compression resistance of three different test shapes increased by as much as 34%. This increase paralleled the amount of sample hysteresis. That is, samples with the greatest hysteresis showed the greatest stiffness increases in response to higher strain rates.

Repetitive loading of three different elastomer shapes demonstrated that samples were able to maintain a continuous, repeatable, dynamic response equal in frequency to the loading cycle frequencies of 3hz and 5hz. This response indicates that these shapes are able to recover to a sufficiently undeformed state after loading, so as to cushion subsequent and repeated physiological impacts occurring during normal gait.

When added to a human bone-prosthesis configuration, and subjected to physiological impacts, elastomer samples demonstrated significant shock reduction benefits. Cylindrical, spherical, and conical featured shapes provided consistent peak force attenuation in the range of 56 to 70%, as well as pulse duration increases of 119 to 327% over three different impact loads. Flat smooth sheet samples provided lower force reductions in the range of 5 to 29%, and pulse duration increases of 8 to 37%. Under impact loads having a duration of 14 milliseconds or less, elastomer samples exhibited a highly elastic behavior with little material damping evident. Samples also exhibited a large increase in compressive stiffness over the results of controlled force-strain tests. These results further demonstrated a viscous, strain rate sensitive property of the material. The range of different geometrically featured shapes tested, as well as variations of surface area in the range of 18 to 30cm^2, provided little difference in peak force attenuation over the three impact loads tested.

Satisfactory fatigue evaluation of silicone elastomer samples has been prevented thus far due to wearing of elastomer surfaces. Lateral expansion of samples when compressed creates relative movements at the compression plate interface, causing wear of the elastomer surfaces through abrasion, roll formation, and three body wear. Although attempts at wear quantification were unsuccessfull, it is believed that the elastomer does not possess the necessary wear resistance to provide long term durability under conditions of relative movement. The release of wear debris is highly undesirable in prosthestic joints due to resulting inflammatory biological responses. A new elastomer sample design incorporating mechanical constraint to minimize relative movements, greatly reduced wear at the compression plate interface. This tapered cylindrical shape proved susceptible to fatigue cracking however, redimensioning to increase the mid section diameter should alleviate this problem.

Mechanical tests herein demonstrate that a suitably stiff and dynamically responsive elastomer cushion, capable of providing significant force and strain rate reductions, can be designed for prosthetic knee joint use. The problems preventing ultimate use of such a cushion are insufficient compressive fatigue evalution, wear of the material, and subsequently, lack of a practical method to incorporate the elastomer successfully into a prosthetic joint.

9.2 Recommendations

Testing has indicated that cylindrical elastomer shapes are preferred as load bearing supports, and that sample constraint at the compression faces is necessary to eliminate the wear problem. To this end, the idea of bonding, coupled with mechanical constraint of cylindrical shapes, appears as an attractive and feasible method to solve not only wear and fatigue evaluation problems, but to produce a practical final joint design. At least one candidate biocompatible adhesive material called Silastic Type A Medical Adhesive is known to be currently available from the Dow Corning Corporation. The following are therefore recommended for future work:

1. A general investigation of biocompatible bonding materials potentially available, and their proper use.

2. Further testing with one or more candidate adhesive materials to include;
    i) compressive testing of bonded cylindrical shaped discs to evaluate fatigue life of both the elastomer, and bonded interface.

ii) further mechanical evaluation of bonded discs to assess stiffness and ultimate strength in both shear and tension.

3. Pending completion of the above recommendations and favourable experimental results, various compliant knee joint designs could be considered for application.

REFERENCES

1. Ghista, D.N., Roaf, R. (ed) (1978) Orthopaedic mechanics and procedures, Academic Press Inc., 111 Fifth Av. New York, U.S.

2. Laskin, R.S., Denham, R.A., Apley, A.G. (1984) Replacement of the knee., Springer-Verlag Berlin, Printed in Great Britain, 1984.

3. Moskowitz, R.W., Howell, P.S., Goldberg, V.M., Mankin, H.J. (1984) Osteoarthritis, diagnosis and management., W.B. Saunders Company, 1 Goldthorne Ave., Toronto, Canada.

4. Swanson, A.B. (1973) Flexible implant arthroplasty in the hand and extremities., C.V. Mosby Company, St. Louis, U.S.

5. Inman, U.T., Ralston, H.J., Todd, F. (1981) Human walking, Williams and Wilkins, 428 Preston St., Baltimore, U.S.

6. Perry, J. (1985) Normal and pathologic gait, American Academy of Orthopaedic Surgeons Atlas of Orthotics, 2nd Edition, C.V. Mosby Company, St. Louis, U.S.

7. Winter, D.A. (1988) The biomechanics and motor control of human gait, University of Waterloo Press, Dana Porter Library, Waterloo, Ontario, Canada.

8. Bresler, B., Frankel, I.P. (1950) The forces and moments in the leg during level walking, Transactions of the American Society of Mechanical Engineers, Vol. 72, 27.

9. Morrison, J.B. (1970) The mechanics of the knee joint in relation to normal walking, Journal of Biomechanics, Vol. 3, 51.

10. Morrison, J.B. (1969) The function of the knee joint in various activities, Biomedical Engineering, Vol. 4, 573.

11. Rohrle, H., Scholten, R., Sigolotto, C., Sollbach, W. (1981) Joint forces during walking, Proceedings of the Eighth Canadian Congress of Applied Mechanics, Moncton N.B., Canada, June 7-12.

12. Harrington, I.J. (1976) A bioengineering analysis of force actions at the knee in normal and pathological gait, Biomedical Engineering, Vol. 11, 167.

13. Seireg, A., Arvikar, R.J. (1975) The preciction of muscular load sharing and joint forces in the lower extremities during walking, Journal of Biomechanics, Vol. 8, 89.

14. Light, L.H., McLellan, G.E., Klenerman, L. (1980) Skeletal transients on heel strike in normal walking with different footwear, Journal of Biomechanics, Vol. 13, 477.

15. Folman, Y., Wosk, J., Voloshin, A., Liberty, S. (1986) Cyclic impacts on heel strike : A possible biomechanical factor in the etiology of degenerative disease of the human locomotor system, Archives of Orthopaedic Trauma Surgery, Vol. 104, 363.

16. Voloshin, A., Wosk, J., Brull, M. (1981) Force wave transmission through the human locomotor system, Journal of Biomechanical Engineering, Vol. 103, 48.

17. Simon, S.R., Paul, I.L., Mansour, J., Munro, M., Abernetty, P.J., Radin, E.L. (1981) Peak dynamic force in human gait, Journal of Biomechanics, Vol. 14, 817.

18. Voloshin, A.S. (1984) Shock absorbtion of running shoes with resilient midsoles, 37th ACEMB, Los Angeles Cal., Sept. 1984.

19. Voloshin, A., Wosk, J. (1980) Shock absorbtion of menisectomized and painfull knees : a comparative in-vivo study, Journal of Biomedical Engineering, Vol. 5, 157.

20. Jorgensen, U., Bojsen-Moller, F. (1989) Shock absorbancy factors in the shoe/heel interaction, with focus on the role of the heel pad, Foot and Ankle, Vol. 9, No. 11, 294.

21. Jorgensen, U. (1985) Achillodynia and loss of heel pad shock absorbency, Journal of Sports Medicine, Vol. 13, No. 2, 128.

22. Radin, E.L., Parker, H.G., Pugh, J.W., Steinberg, R.S., Paul, I.L., Rose, R.M. (1973) Response of joints to impact loading III, Journal of Biomechanics, Vol. 6, 51.

23. Radin, E.L., Paul, I.L. (1971) Importance of bone in sparing articular cartilage from impact, Clinical Orthopaedics and Related Research, Vol. 78, 342.

24. Radin, E.L., Orr, R.B., Kelman, J.L., Paul, I.L., Rose, R.M. (1982) Effect of prolonged walking on concrete on the knees of sheep, Journal of Biomechanics, Vol. 15, No. 7, 487.

25. Chu, M.L., Yuzdani-Ardakani, S. (1986) An in-vitro simulation study of impulsive force transmission along the lower skeletal extremity, Journal of Biomechanics, Vol. 19, No. 12, 979.

26. Hoshino, A., Wallace, W.A. (1987) Impact absorbing properties of the human knee, Journal of Bone and Joint Surgery, Vol. 69-B, 807.

27. Wright, T.M., Bartel, D.L. (1986) The problem of surface damage in polyethylene total knee components, Clinical Orthopaedics and Related Research, Vol. 205, 67.

28. Rose, R.M., Ries, M.D., Paul, I.L., Crugnola, A.M., Ellis, E. (1984) On the true wear rate of ultrahigh molecular weight polyethylene in total knee prostheses, Journal of Biomedical Materials Research, Vol. 8, 207.

29. Mina, J.M., Marcler, R.A., Amstutz, H.A. (1982) The pathology of failed total knee arthroplasty, Clinical Orthopaedics and Related Research, Vol. 170, 175.

30. Wosk, J., Voloshin, A. (1981) Wave attenuation in skeletons of young healthy persons, Journal of Biomechanics, Vol. 14, No. 4,261.

31. Chao, E.Y., Mullen, J. (1976) Closed Loop, MTS Systems Corp., p4-7.

32. Garg, A., Walker, P.S. (1986) The effect of the interface on the bone stresses beneath tibial components, Journal of Biomechanics, Vol. 19, No. 12, 957.

33. Goldstein, S.A., Kuhn, J.L., Hollister, S.J., Goulet, R.W., Loubert, P.V. (1988) The relationship between experimentally controlled loads and trabecular bone remodeling, Abstracts of 34th Annual Meeting of the Orthopaedic Research Society, Feb 1988, Atlanta Georgia, U.S.

34. Walker, P.S., Miegel, R.E., Rodger, R.F., Onchi, K., Kurosawa, H., Granholm, J. (1984) A compliant interface for total knee replacement, Proceedings of the First International Conference on Engineering and Clinical Aspects of Endoprosthetic Fixation, I Mech E Publication, London England, June, 1984.

35. Pillar, R.M., Lee, J.M., Maniatopoulos, C. (1986) Observations on the effect of movement on bone ingrowth into porous surfaced implants, Clinical Orthopaedics and Related Research, Vol. 208, 108.

36. Bartel, D.L., Bicknell, V.L., Wright, T.M. (1986) The effect of conformity, thickness, and material on stresses in ultra high molecular weight components for total joint replacement, Journal of Bone and Joint Surgery, Vol. 68-A, No. 7, 1041.

37. Abbott, K. (1977) Mechanical causes of loosening in knee joint replacement, Journal of Biomechanics, Vol. 10, 387.

38. Laskin, R.S., (1990) Total condylar knee replacement in patients who have rheumatoid arthritis, Journal of Bone and Joint Surgery, Vol. 72-A, No. 4, 529.

39. Frich, E.E. (1983) Technology of silicones in biomedical applications, In: Rubin, L.R. (ed), Biomaterials in reconstructive surgery, Mosby, St. Louis, Missouri, pp.73-90.

40. Swanson, A.B., deGroot-Swanson, G., Frich, E.E. (1982) Flexible (silicone) implant arthroplasty in the small joints of extremeties: Concepts, physical and biological considerations, experiments and clinical results, In: Rubin, L.R. (ed), Biomaterials in reconsuctive surgery, Mosby, St. Louis, Missouri, 595.

41. Kelly, B.P., Kilby, M.J., Newcombe, W.R., Repo, R.U. (1987) Preliminary data on the use of an elastomeric material to extend joint life in knee prostheses, An undergraduate thesis report, Dept. of Mechanical Engineering, McMaster University, Ont. Canada.

42. Repo, R.U., Newcombe, W.R., Kelly, B.P., Kilby, M.J. (1988) Moderating regional bone stress under tibial prosthetic components, 22nd Annual Meeting of the Canadian Orthopaedic Research Society, Ottawa, Canada, June 6, 1988.

43. Kimmich, E.G. (1956) General engineering properties of rubber, In: McPherson, A.T., Klemin, A. (ed), Engineering uses of rubber, Reinhold Publishing Corp., New York, U.S.

44. Lynch, W. (1978) Handbook of silicone rubber fabrication, Van Nostrand Reinhold Publishers, West 33rd St. New York, U.S.

45. Evans, F.G. (1973) Mechanical properties of bone, Charles C. Thomas Publishers, 301-327 East Lawrence Ave. Springfield Illinois, U.S.

46. Greenburg, S.W., Gonzalez, D., Gurdjian, E.S., Thomas, L.M. (1968) Changes in physical properties of bone between the in vivo, freshly dead, and embalmed conditions, Proceedings of the Twelfth Stapp Car Crash Conference, New York, pp271-279.

47. Freakly, P.K., Payne, A.R., (1978) Theory and practice of engineering with rubber, Applied Science Publishers , Ripple Road, Essex, England.

48. Downie Smith, J.F., (1956) The design of rubber mountings, In: McPherson, A.T., Klemin, A. (ed), Engineering uses of rubber, Reinhold Publishing Corp., New York, U.S.,p104.

49. Bombelli, R., Mathys, R. (1982) Cementless isoelastic RM total hip prosthesis, Journal of the Royal Society of Medicine, Vol.75, 588.

50. Leidholt, J.D., Gorman, H.A. (1968) Use of silastic cushions on a metalic hip prosthesis in dogs, Clinical Orthopaedics, Vol.61, 164.

51. Price, G.F.W. (1978) Interim report on a modification of methylmethacrylate fixation of prosthesis into bone, Journal of Bone and Joint Surgery, Vol. 60-B, 293.

52. Repo, R.U., Newcombe, W.R., Belbeck, L., Winfield, D. (1981) Interface studies of an elastic canine femoral replacement prosthesis, Orthopaedic Transactions, Vol. 5, 471.

53. Repo, R.U., Newcombe, W.R., Winfield, D. (1983) An elastic canine total hip-an alternative method of total joint attachment to bone, Orthopaedic Transactions, Vol. 7, 307.

54. Newcombe, W.R., Repo, R.U., Eaton, N.B., Occhionorelli, J. (1987) A mechanical evaluation of an elastic femoral prosthetic stem, Journal of Biomechanics, Vol. 20, No. 2, 179.

55. Clarke, I.C., (1982) Wear screening and joint simulation studies versus materials selection and prosthesis design, CRC Critical Reviews in Biomedical Engineering, Vol. 8, No. 1.

56. Sarkar, A.D., (1980) Friction and wear, Academic Press London Ltd., 24/28 Oval Rd., London NW1.

57. Moore, D.F., (1972) Friction and lubrication of elastomers, Pergamon Press Ltd., 207 Queens Quay West, Toronto, Canada.

58. Marshall, J.W., (1956) Rubber in automobiles, In: McPherson, A.T., Klemin, A., (ed), Engineering uses of rubber, Reinhold Publishing Corp., New York, U.S., p342.

APPENDIX A

LOAD VERSUS DEFLECTION CURVES FOR ELASTOMER SHAPES

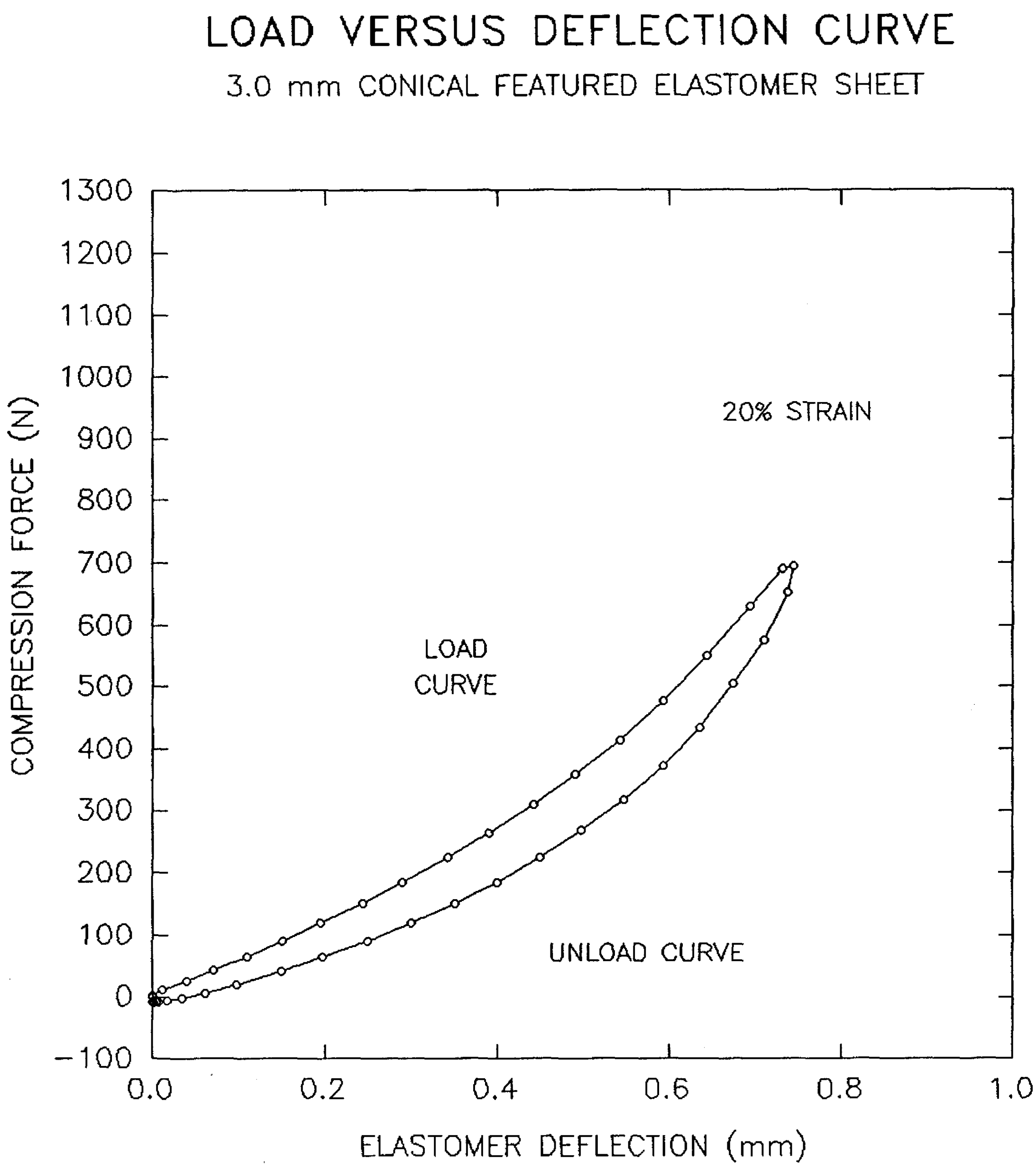

Figure A.1 Force deflection curve for $30cm^2$ conical featured elastomer sheet loaded to 20% strain at 3 hz.

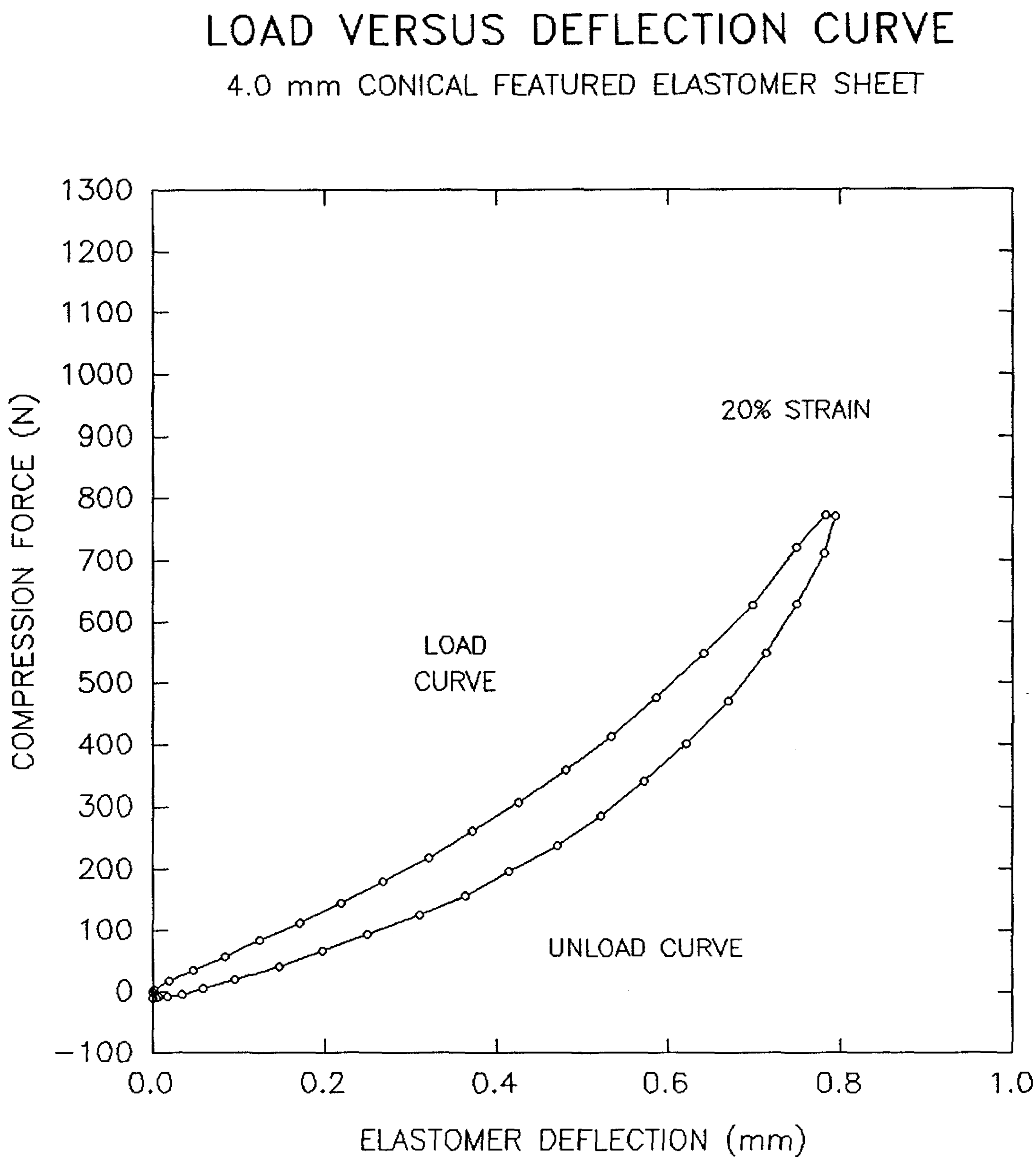

Figure A.2 Force deflection curve for $30cm^2$ conical featured elastomer sheet loaded to 20% strain at 3 hz.

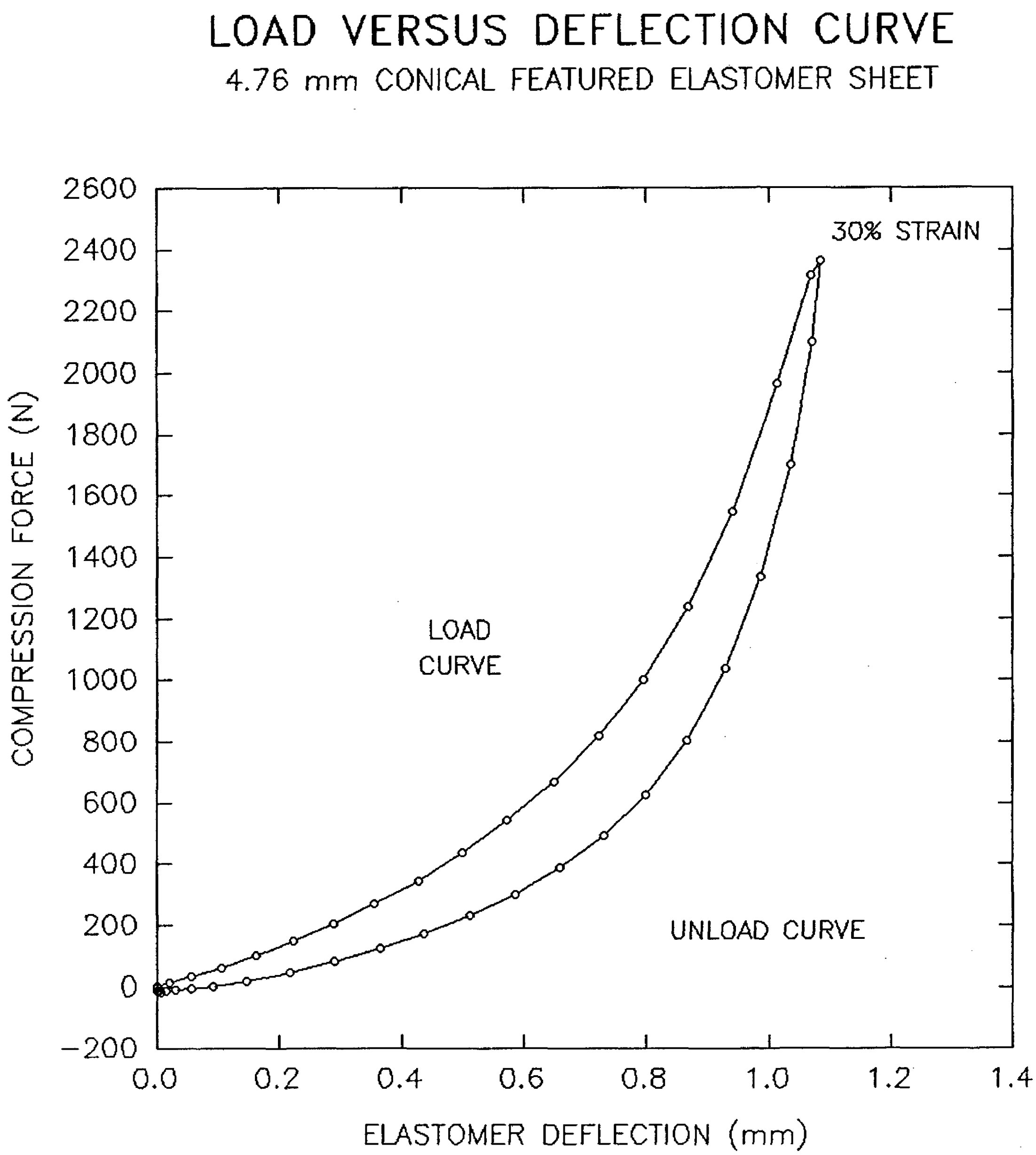

Figure A.3 Force deflection curve for $30cm^2$ conical featured elastomer sheet loaded to 30% strain at 3 hz.

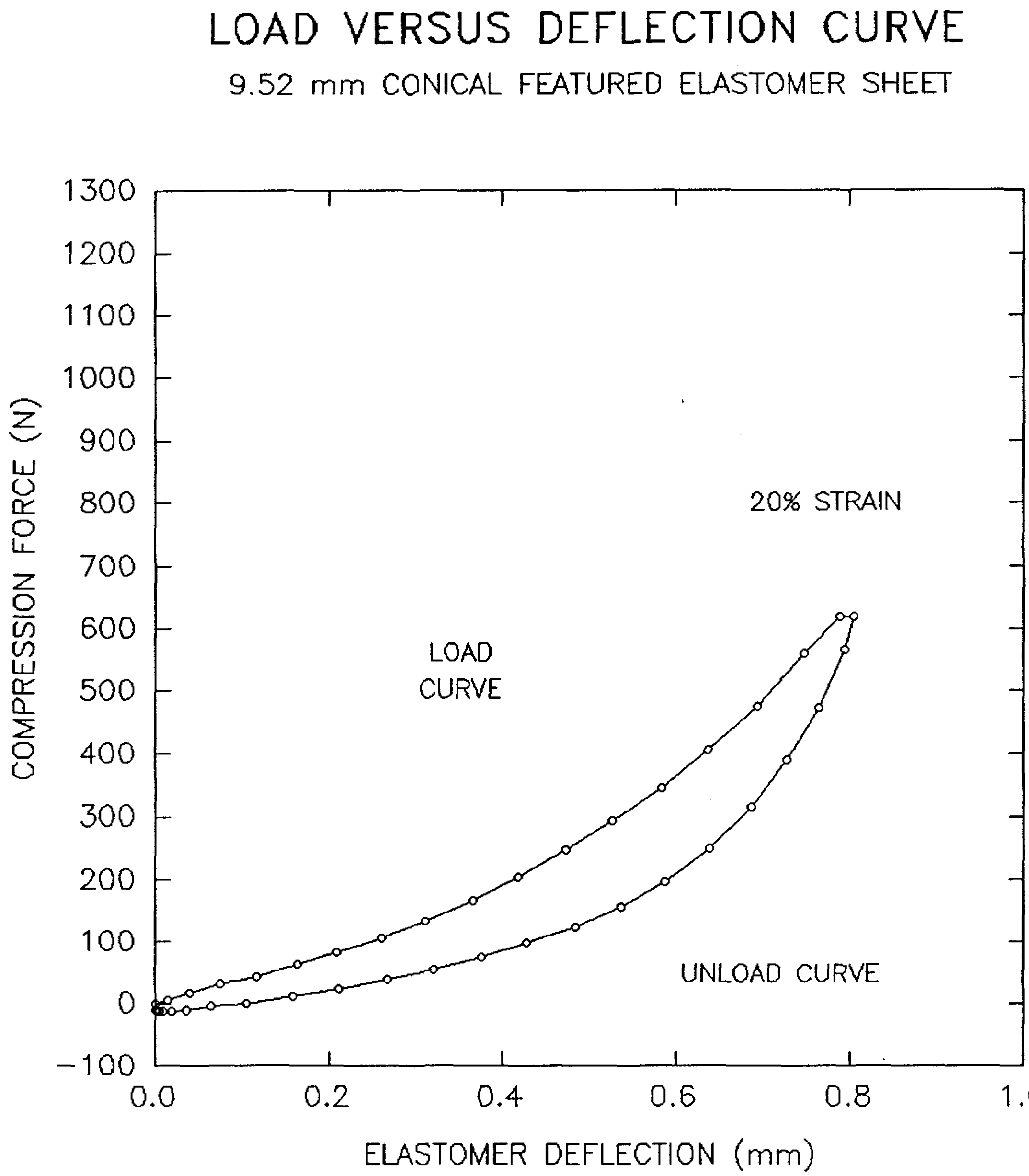

Figure A.4 Force deflection curve for $30cm^2$ conical featured elastomer sheet loaded to 20% strain at 3 hz.

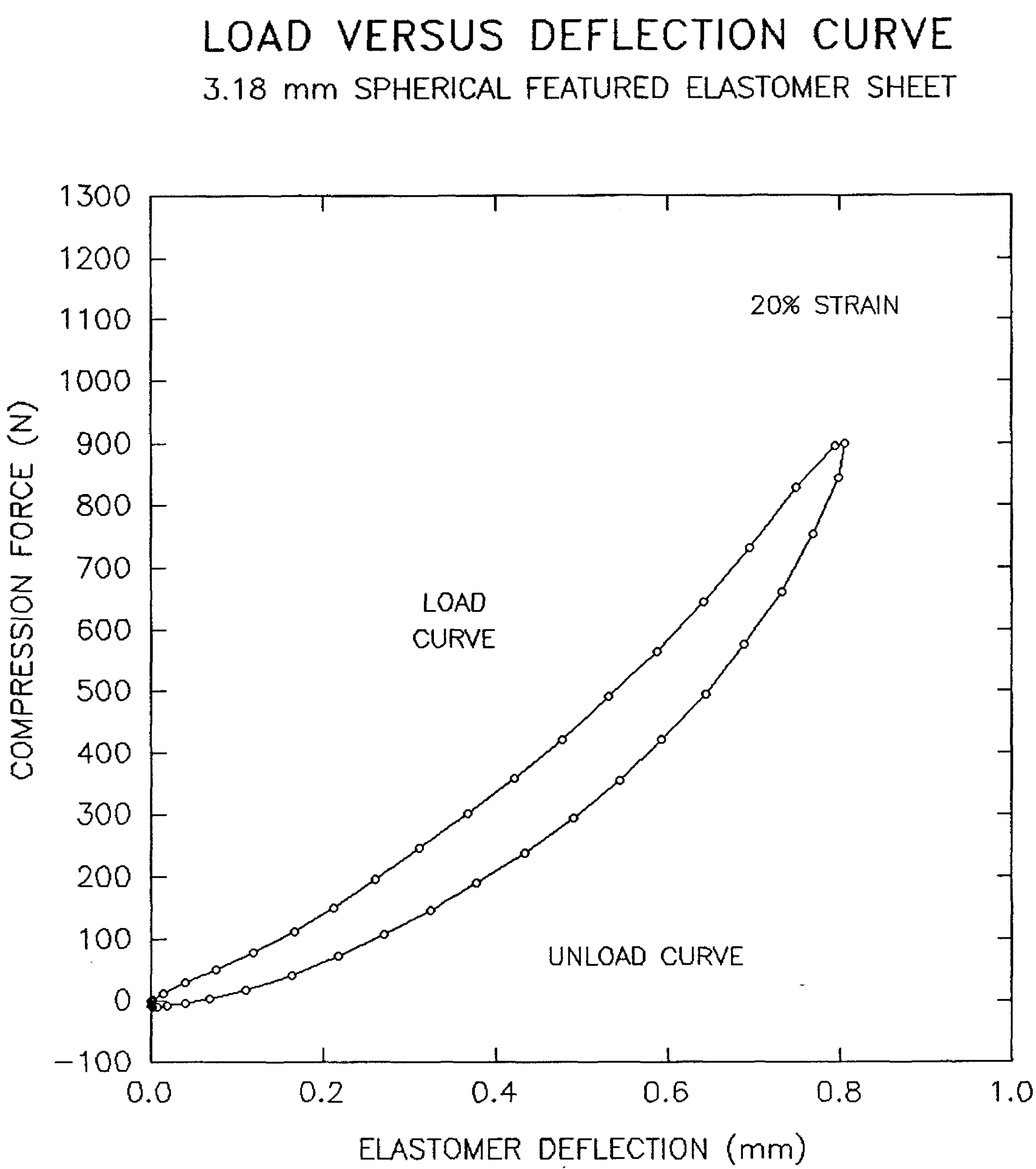

Figure A.5 Force deflection curve for $30cm^2$ spherical featured elastomer sheet loaded to 20% strain at 3 hz.

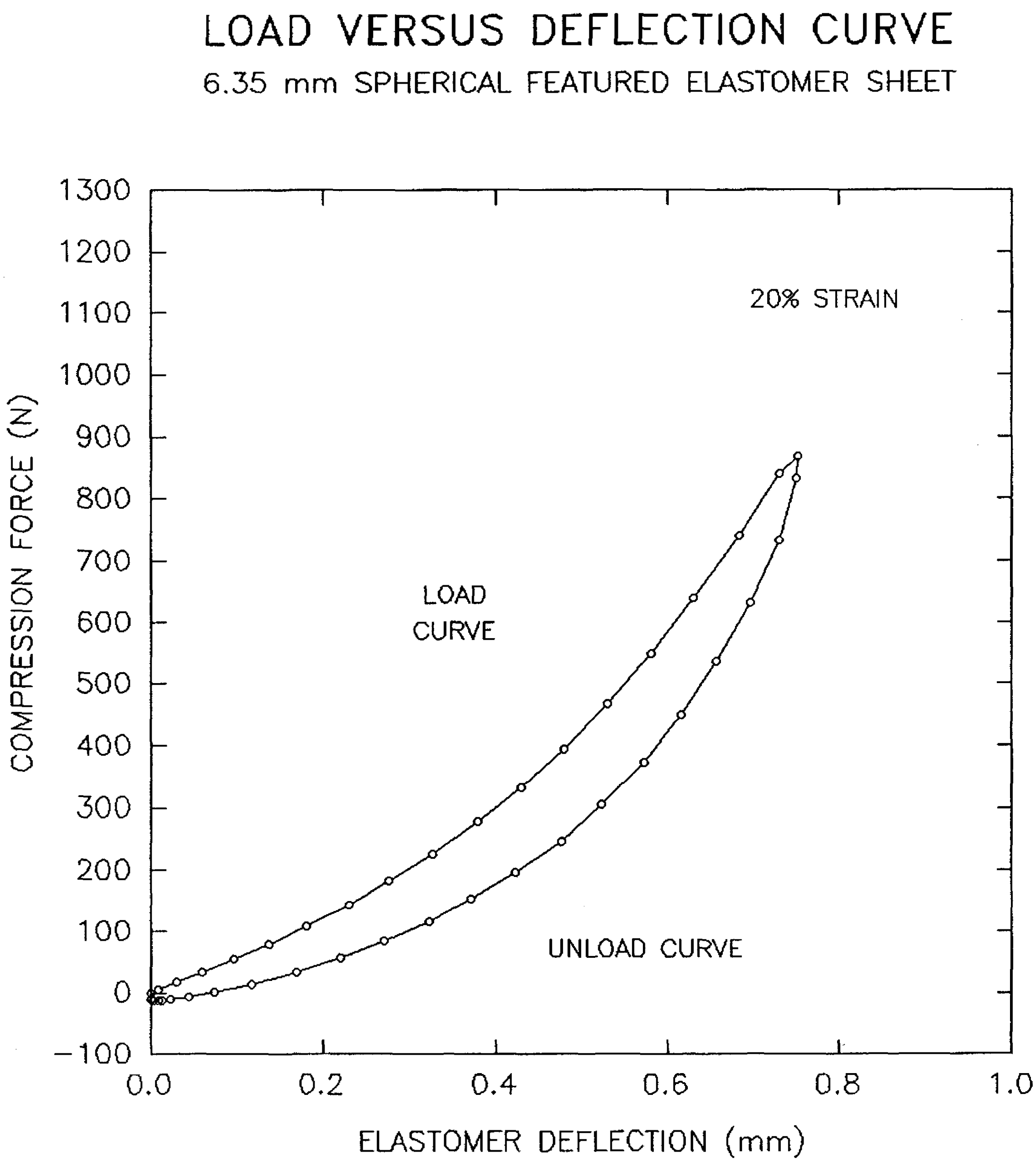

Figure A.6 Force deflection curve for $30cm^2$ spherical featured elastomer sheet loaded to 20% strain at 3 hz.

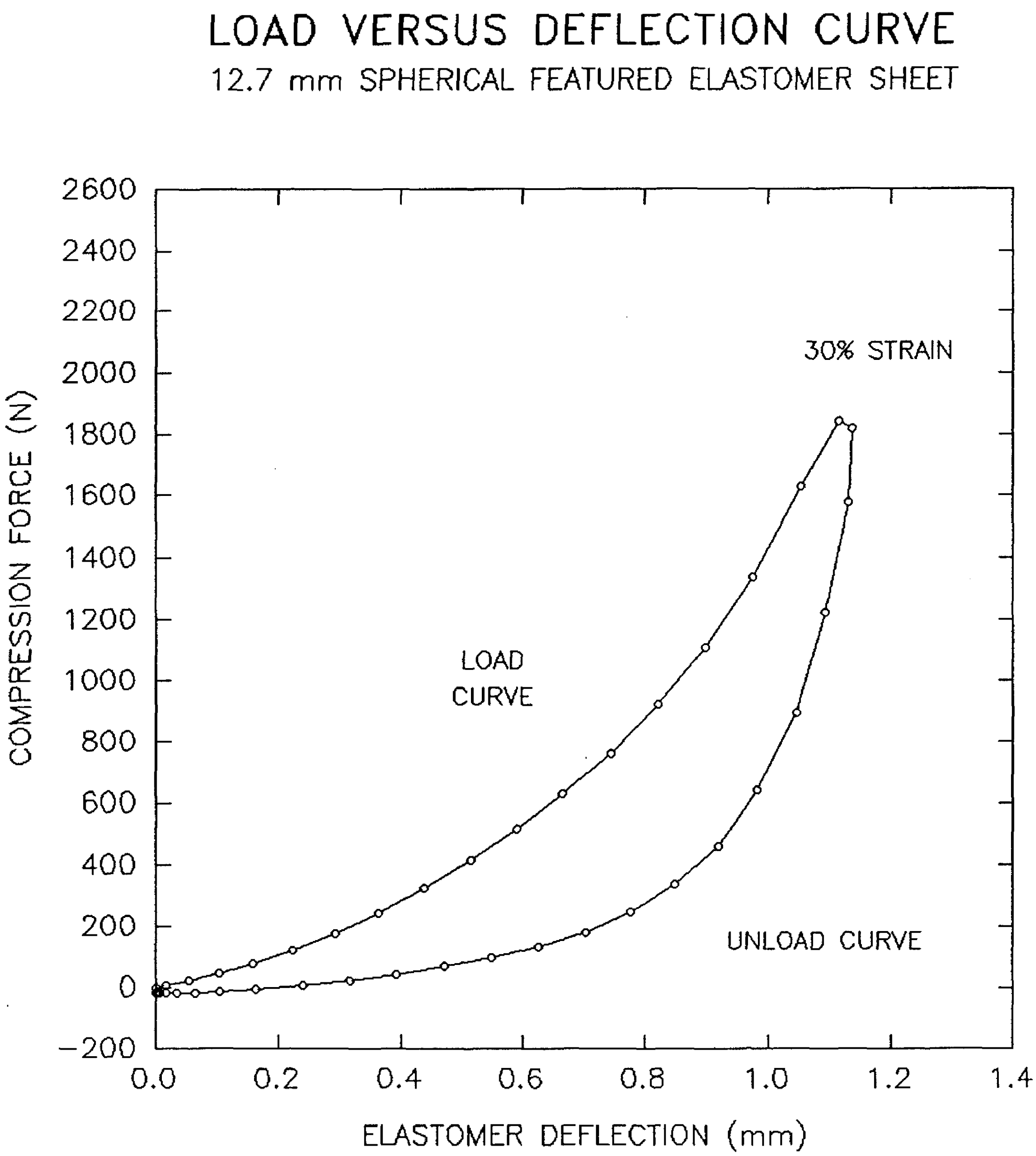

Figure A.7 Force deflection curve for 30cm^2 spherical featured elastomer sheet loaded to 30% strain at 3 hz.

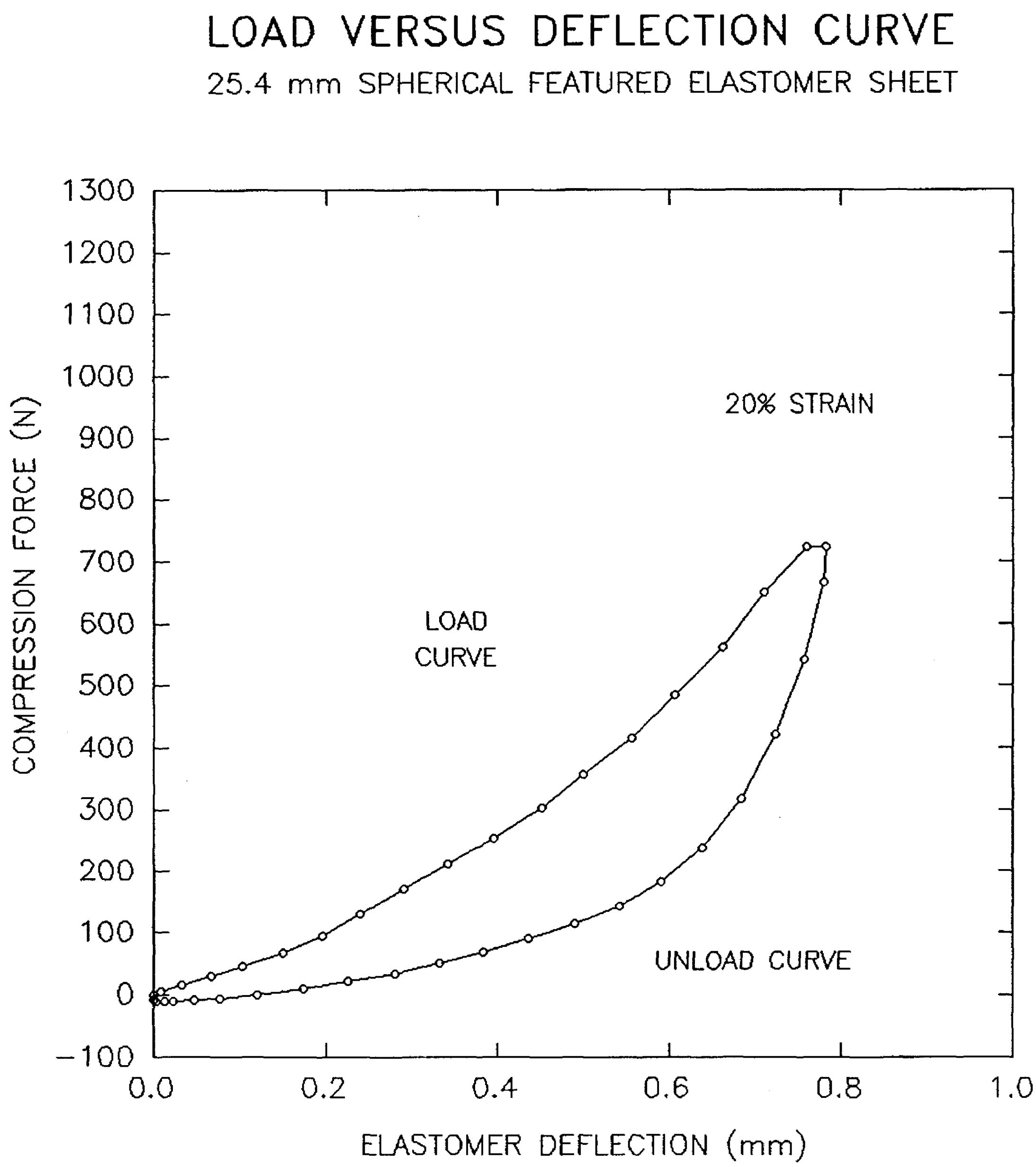

Figure A.8 Force deflection curve for $30cm^2$ spherical featured elastomer sheet loaded to 20% strain at 3 hz.

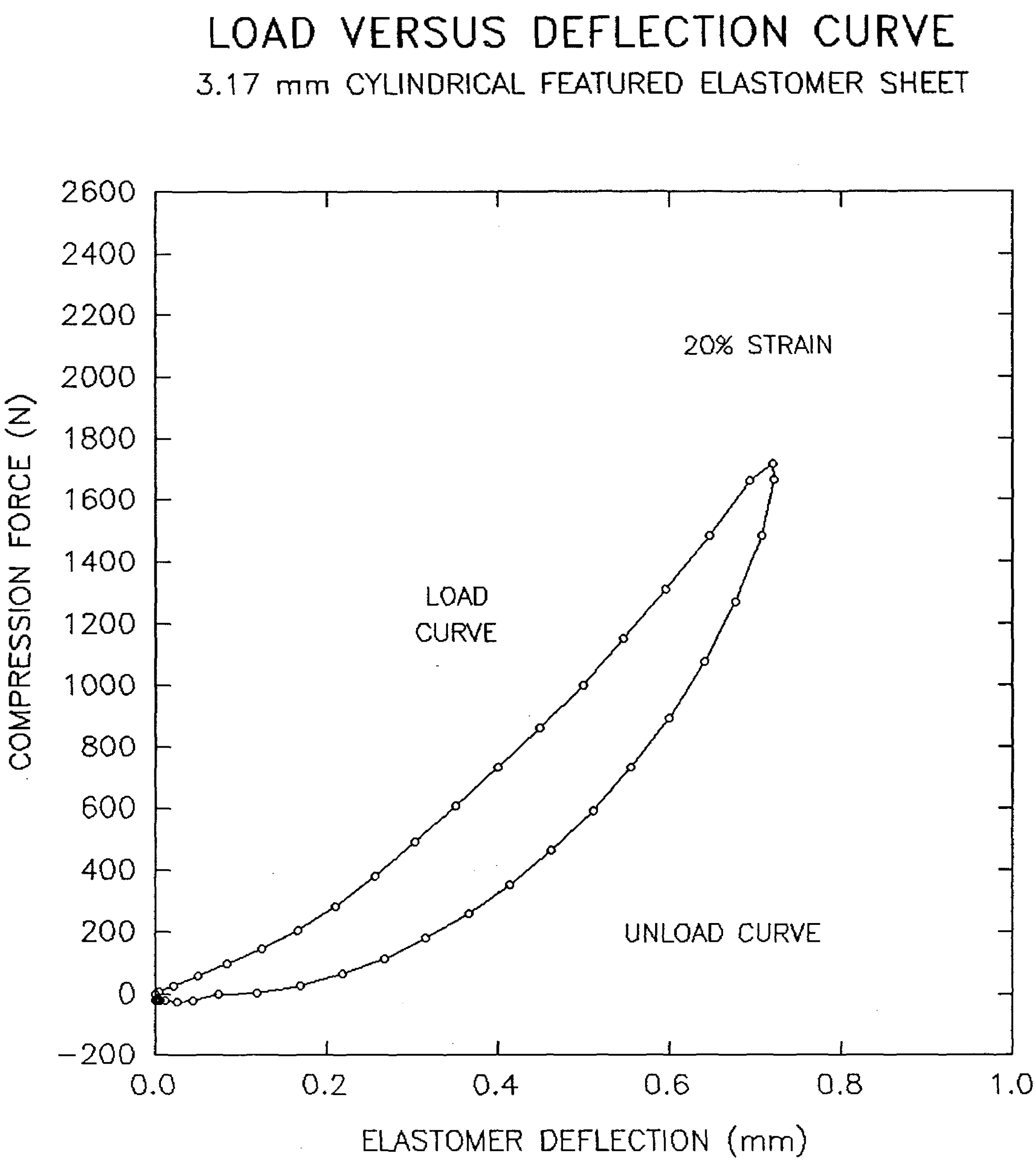

Figure A.9 Force deflection curve for $30cm^2$ cylindrical featured elastomer sheet loaded to 20% stain at 3 hz.

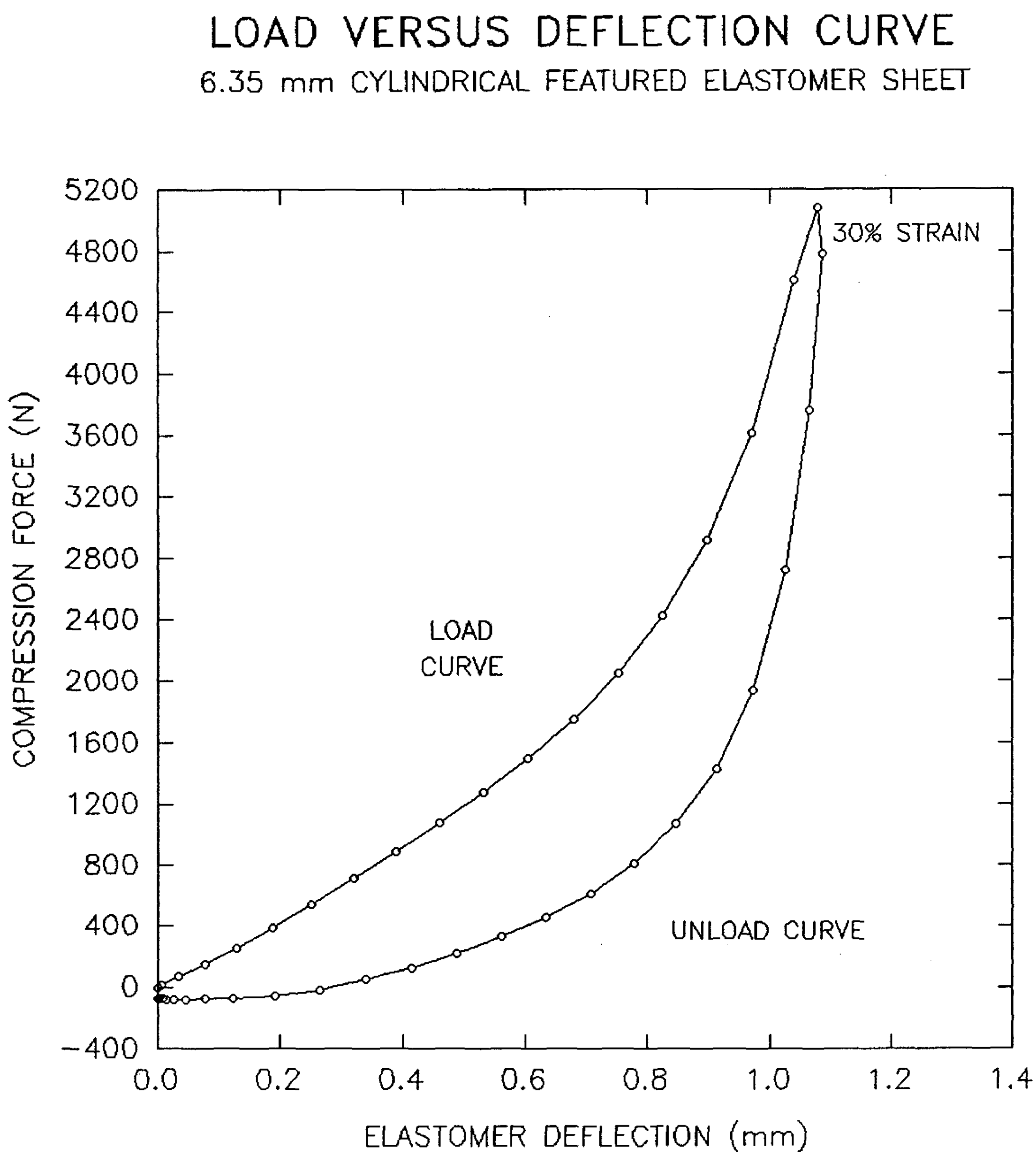

Figure A.10 Force deflection curve for $30cm^2$ cylindrical featured elastomer sheet loaded to 30% stain at 3 hz.

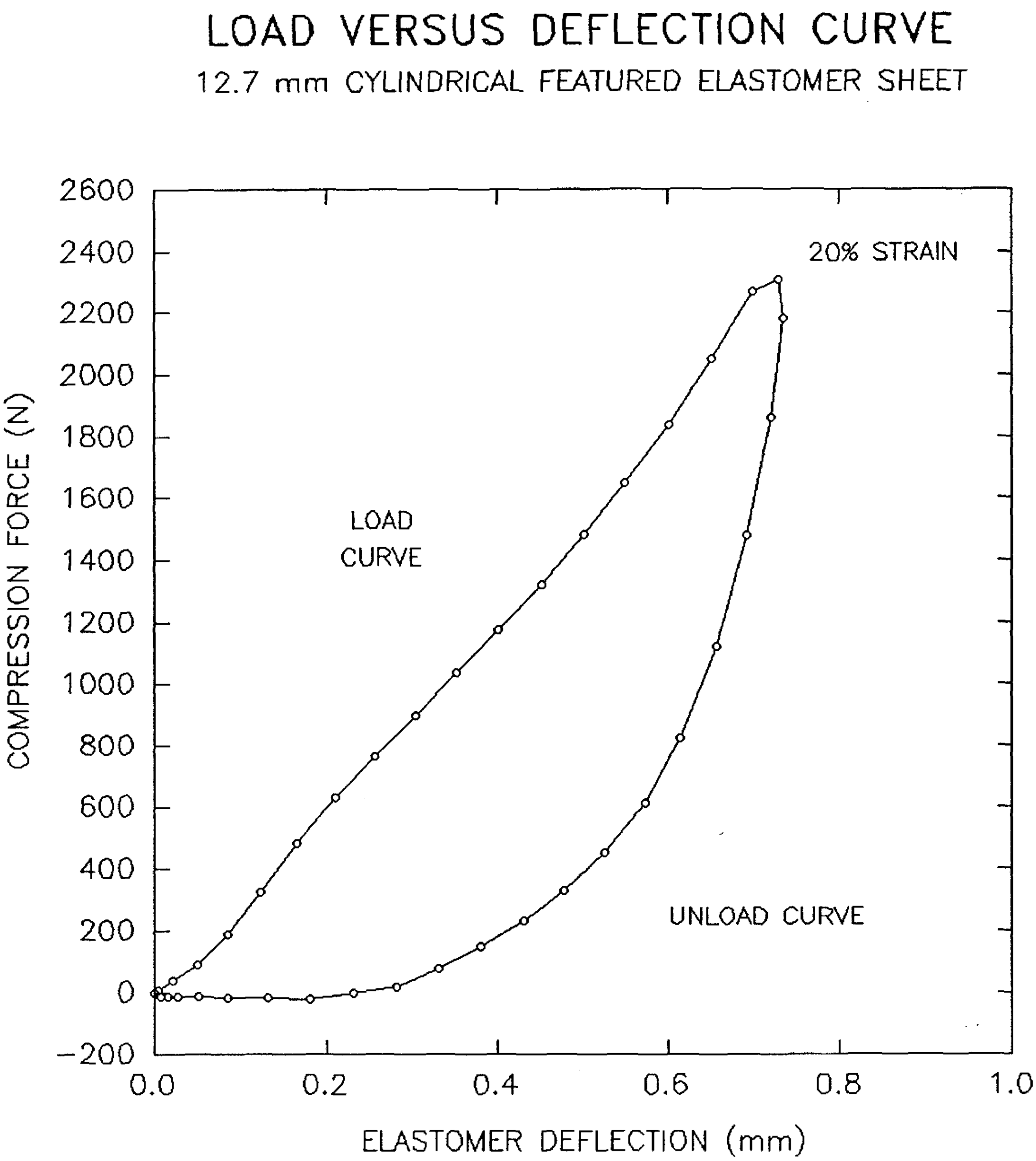

Figure A.11 Force deflection curve for $30cm^2$ cylindrical featured elastomer sheet loaded to 20% stain at 3 hz.

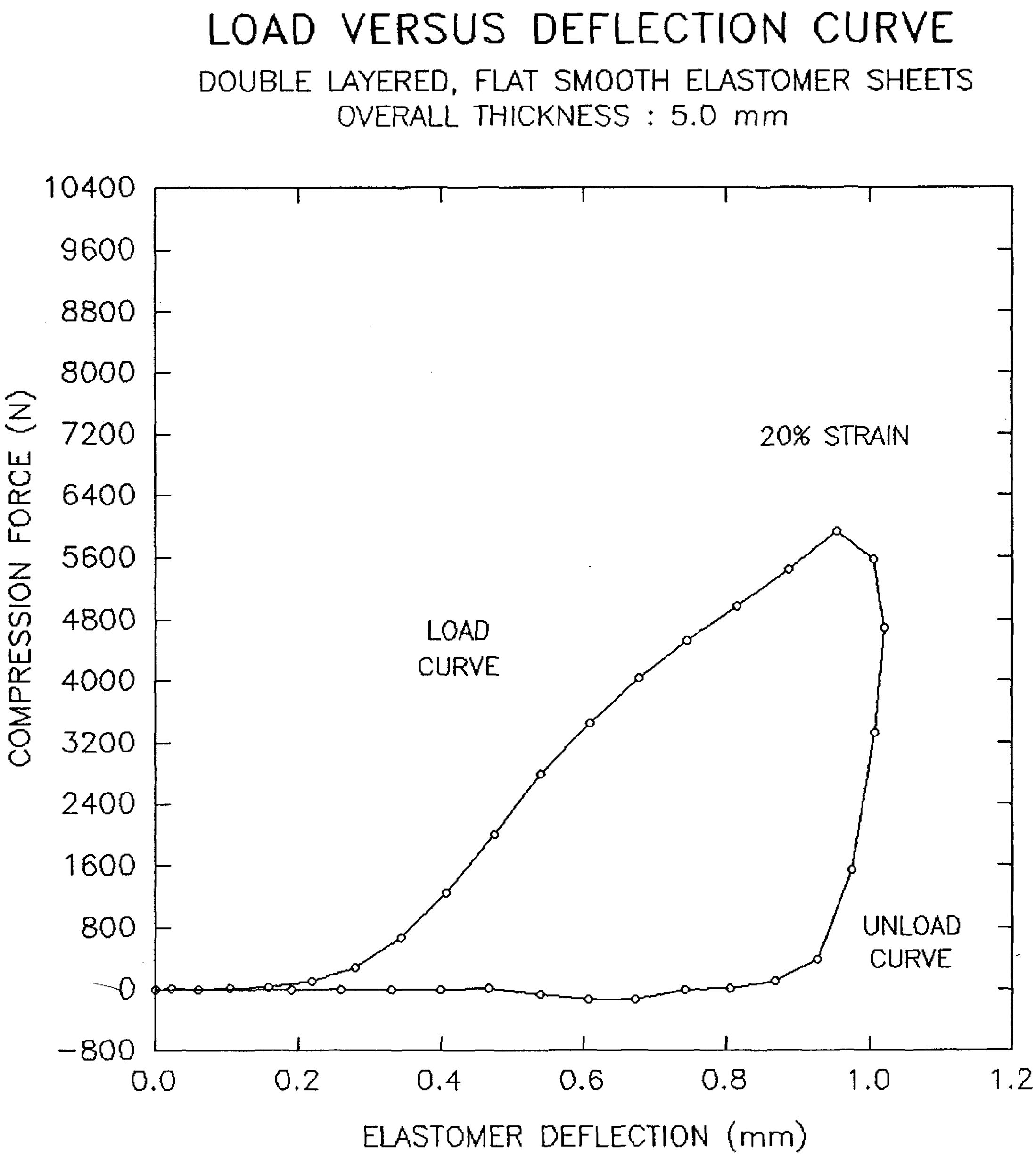

Figure A.12 Force deflection curve for $30cm^2$ flat elastomer sheet loaded to 20% strain at 3 hz.